AD-A150 876 MILLIMETER-WAVE DIFFRACTION DEVICES AND MATERIALS(U) 1/2
BATTELLE COLUMBUS LABS OH M R SEILER ET AL. 28 DEC 84
AFOSR-TR-85-0131 F49620-82-C-0099

UNCLASSIFIED F/G 20/8 NL

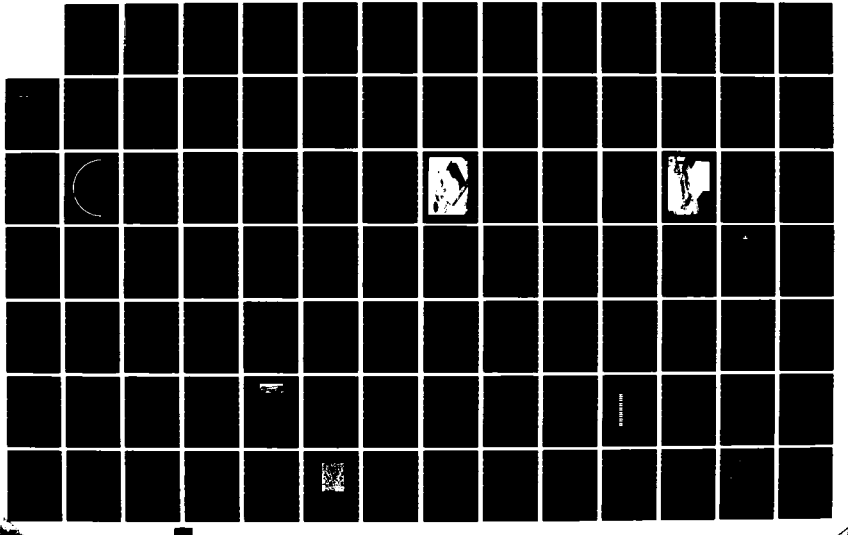

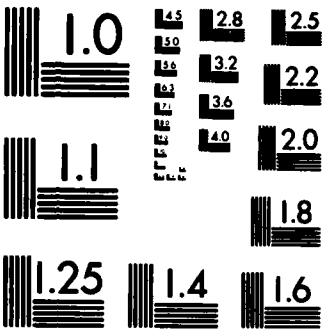

~~STUDIES OF~~ MILLIMETER-WAVE DIFFRACTION DEVICES AND MATERIALS

MILTON R. SEILER
RICHARD W. RIDGWAY
BATTELLE
COLUMBUS LABORATORIES
505 KING AVENUE
COLUMBUS, OHIO 43201

28 DECEMBER 1984

FINAL REPORT FOR PERIOD 1 SEPTEMBER 1982 - 31 OCTOBER 1984

PREPARED FOR

AIR FORCE OFFICE OF SCIENTIFIC RESEARCH
BOLLING AIR FORCE BASE, D.C. 20332

DECLASSIFICATION/DOWNGRADING SCHEDULE	UNLIMITED
ERFORMING ORGANIZATION REPORT NUMBER(S)	5. MONITORING ORGANIZATION REPORT NUMBER(S) AFOSR-TR- 85-0131
NAME OF PERFORMING ORGANIZATION: TTELLE COLUMBUS LABORATORIES 6b. OFFICE SYMBOL (If applicable)	7a. NAME OF MONITORING ORGANIZATION AIR FORCE OFFICE OF SCIENTIFIC RESEARCH
ADDRESS (City, State and ZIP Code) lumbus, Ohio 43201	7b. ADDRESS (City, State and ZIP Code) Bolling AFB, D.C. 20332
NAME OF FUNDING/SPONSORING ORGANIZATION 8b. OFFICE SYMBOL (If applicable)	9. PROCUREMENT INSTRUMENT IDENTIFICATION NUMBER F49620-82-C-0099
ADDRESS (City, State and ZIP Code)	10. SOURCE OF FUNDING NOS. PROGRAM ELEMENT NO.: 61102F PROJECT NO.: 2306 TASK NO.: B2 WORK UNIT NO.
TITLE (Include Security Classification) llimeter-Wave Diffraction Devices and Materials (U)	
PERSONAL AUTHOR(S) R. Seiler, R. W. Ridgway	
TYPE OF REPORT nal	13b. TIME COVERED FROM 9/1/82 TO 10/31/84
14. DATE OF REPORT (Yr., Mo., Day) 1984 December 28	15. PAGE COUNT 133
SUPPLEMENTARY NOTATION	

COSATI CODES		
ELD	GROUP	SUB. GR.

18. SUBJECT TERMS (Continue on reverse if necessary and identify by block number)
Millimeter-Wave Dielectric Beam-Steering Silicon Diffraction Ferrofluid Varistor Cadmium Sulfide Ferrites Antenna Waveguide Semiconductor Grating Gallium Arsenide

TABLE OF CONTENTS

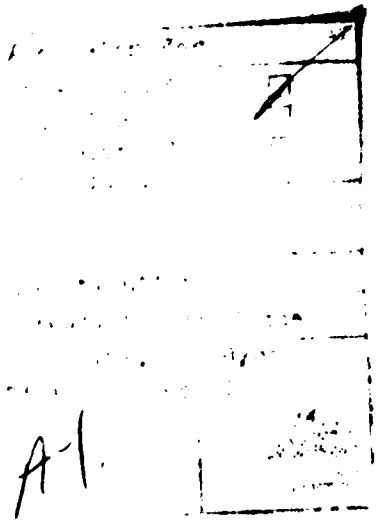

LIST OF FIGURES

LIST OF FIGURES (Continued)

LIST OF TABLES

PREFACE

This research was supported by the Air Force Office of Scientific Research, Bolling AFB, D.C., 20332, under Contract No. F49620-82-C-0099. Lt. Col. Harry Winsor served as the AFOSR program manager during the period September, 1982 through August, 1983 and Capt. Kevin Malloy served in the same capacity from September, 1983 to December, 1984.

STUDIES OF MILLIMETER-WAVE DIFFRACTION DEVICES AND MATERIALS

by

Milton R. Seiler and Richard W. Ridgway

1.0 INTRODUCTION

This is the final technical report on "Millimeter-Wave Diffraction Devices and Materials" prepared under Contract F49620-82-C-0099 for the Air Force Office of Scientific Research. The period covered is September, 1982 through October, 1984.

This study has been concerned with the interaction of dielectric waveguides and a nearby periodic structure or grating. The broad objective is to make gratings of controlled spacing to achieve beam-steerable antenna structures or signal processing devices. There is significant literature in SOVIET publications which calls these effects "diffraction electronics". U.S. literature would classify the subject as "leaky wave" or "surface wave" antennas.

The center frequency of interest was 94 GHz for the present work, although the concepts are applicable at any wavelength as long as periodic structures may be fabricated with spacings comparable to the wavelength. At millimeter-wave frequencies or above these structures potentially offer a mechanism for beam steering that eliminates the difficulty of assembling discrete phase shifters such as PIN diodes. Hence, cost-effective solutions to millimeter-wave beam steering or null steering seem to be available.

The present study examined a variety of periodic structures that could easily give an adjustable period. Among the structures were coiled springs, ripples in fluids, dielectric constant and conductivity variations. In accordance with the program objective, no device or effect was optimized. Instead, the preliminary examination or data collection was designed only to provide an indication of potential feasibility and effectiveness. The devices for future optimization will be selected at a later date.

The following sections of this report discuss the program objectives, the "diffraction electronics" effect, experimental results, potential device applications and conclusions. Additional sections of the report give inventions and publications and a list of professional personnel associated with the research.

2.0 SUMMARY

Millimeter-wave phased arrays present challenges to the antenna designer who wishes to accomplish beam steering or null steering by conventional techniques. PIN diode or ferrite phase shifters become difficult and expensive to fabricate to millimeter-wave specifications.

The study presented in this report deals with simplified antenna structures using the interaction of dielectric waveguides and periodic structures or gratings. The nominal operating frequency was 94 GHz.

Polystyrene waveguides were the most successful type used on the program. They were fabricated with the same cross-sectional dimensions as the inside dimensions of standard WR-10 hollow metallic waveguide (0.05" x 0.1"). Gratings brought within about 1 mm of the waveguide are coupled by an evanescent mode. Radiation from the combined waveguide-grating structure occurs at an angle which is dictated by the period of the grating. Beam steering was achieved by varying the grating period.

Gratings were successfully fabricated from grooved metallic blocks, coiled springs, conductive strips on insulating substrates, periodic variations in dielectric constant and ripples in ferrofluid. Preliminary attempts to use bulk acoustic wave gratings in semiconductors were unsuccessful.

A pulsed Nd:YAG laser was used to "write" conductive regions on a thin film of amorphous silicon. This technique shows promise for photoconductive gratings which may allow high-speed scanning or the creation of short bursts of millimeter-wave radiation.

No optimization was performed during this present study. Successful as well as unsuccessful experiments are explained for the benefit of future researchers in this area.

3.0 RESEARCH OBJECTIVES

OVERALL OBJECTIVE

The overall objective of the proposed program is to investigate new technology for two related applications that occur in millimeter-wave devices: (1) antenna beam steering and (2) signal processing and millimeter-wave computer applications.

Antenna Beam Steering Area (Objective I)

Provide an early demonstration of new phenomena allowing non-optimized antenna beam steering at 94 GHz. Continue with a longer term demonstration of efficient antenna beam steering by modulation of a periodic semiconductor structure in proximity to a dielectric waveguide.

Signal Processing Area (Objective II)

Conduct initial research and development of a millimeter-wave signal processing/computer device that employs diffraction principles in a semiconductor periodic structure. The device will involve piezo-electrically generated electron density waves, photo-induced conductivity changes or other semiconductor modulation techniques. Basic computer or signal processing capability involving Fourier transform, spectrum analysis, digital logic or signal correlation will be demonstrated.

3.1 DISCUSSION AND ANALYSIS

3.1.1 Background

There is a current trend toward military electronics applications in the millimeter-wave region of the spectrum. Millimeter-wave antenna and signal processing devices present challenging opportunities for the design engineer. Discrete components for phase shifting or control, commonly used in the micro-wave region, are difficult to fabricate to size and performance specifications of millimeter-waves. Propagation losses in conventional "single-mode" hollow waveguide become more severe as operating frequency is increased.

One option that is sometimes attractive is the use of optical rather than microwave techniques. The use of microwave and millimeter-wave lenses has been one example. Another example is the optical diffraction grating, which is closely analogous in theory and application to the antenna array. However, most antenna systems desire a well-defined main-lobe, with low side-lobes, and the absence of grating lobes. Hence a simple diffraction grating does not necessarily solve the millimeter-wave antenna design problem. If gratings or similar periodic structures are to be used as components in a millimeter-wave antenna, they must be associated with an excitation method that produces either a single dominant lobe or a controlled number of lobes, both in angular position and relative power. Null steering is also a critically desired characteristic.

The Soviet open literature contains a number of experimental papers on a class of millimeter-wave antennas employing "diffraction electronics".[1,2,*] A periodic structure consisting of a metallic reflection grating is brought in proximity to a dielectric waveguide which is excited by a mm-wave source. (See Figure 1.) Coupling by the evanescent mode causes an excitation of the grating conducting elements. The phase velocity of the excitation is identical to that in the waveguide. The direction of the radiated volume wave is given by Floquet's theorem[5]:

$$\cos \theta_n = \frac{c}{v_p} + n \frac{\lambda}{\ell} \quad ,$$

*References are listed at the end of this report.

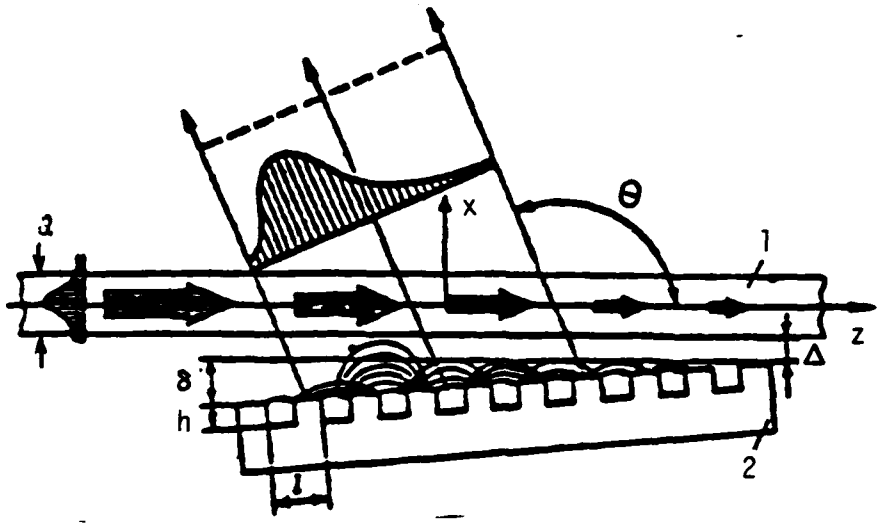

[From Ref. 1]

1 = Dielectric Waveguide

2 = Diffraction Grating

λ = 4.30 mm

FIGURE 1. ANTENNA ARRAY DIAGRAM

(75% Efficiency)

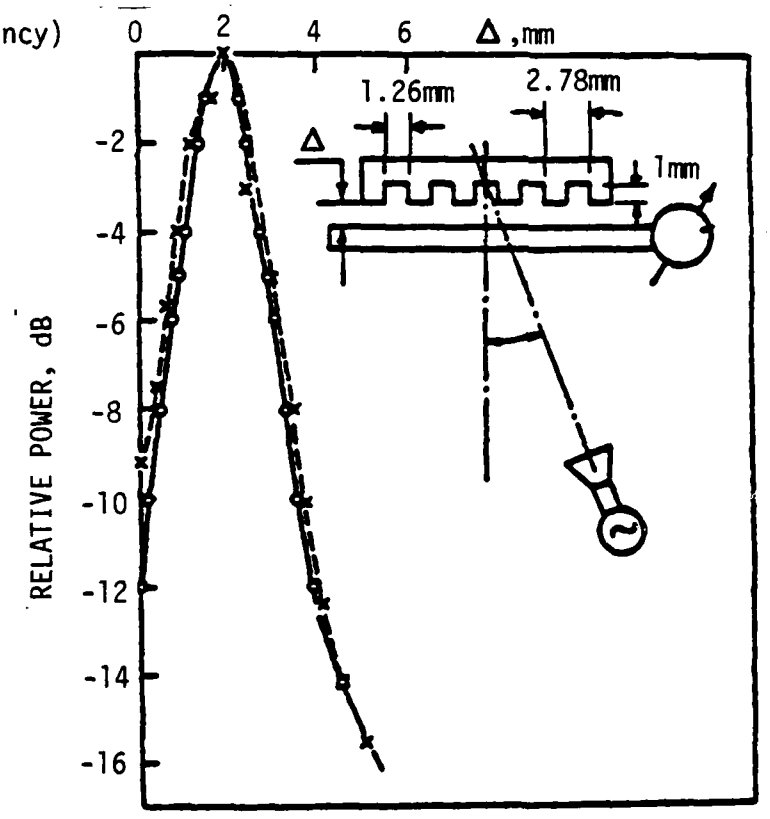

[From Ref. 2]

λ = 5.78 mm

FIGURE 2. DIAGRAM OF MEASURING APPARATUS

Power induced in waveguide as a function of impact parameter.

where

$n = -1, -2, -3, \ldots$ harmonic number

v_p = phase velocity of surface wave on periodic structure

c = velocity of light in vacuum

λ = free space wavelength

ℓ = period of grating .

Hence the grating period effectively controls the direction of radiation.

Typical values used in the Soviet experiments are:

h = depth of grooves = 0.85 mm

$\lambda = 4.3$ mm

$\ell = 3.0$ mm

$n = -1$

$v_p/c = 0.82$

$\cos \theta \cong -0.21$

The relative aperture distribution along the periodic structure may be varied by mechanically controlling the tilt angle between dielectric waveguide and the grating. The aperture distribution in turn affects the side-lobe level. Reported side-lobe levels were below -20 dB.

Figure 2 shows another experiment where the waveguide-periodic structure is acting in the receiving mode. The coupling efficiency is strongly dependent upon the spacing between the waveguide and the grating (impact parameter).

There is no real advancement in the state-of-the-art in the above experiments. All of the antenna characteristics associated with such fixed periodic structures are well known or easily measured. There are a number of related results reported in the U.S. literature.[6] However, there is one important consideration in all of these experiments; namely, the achievement of a single dominant lobe controlled in direction by the grating period. All that is needed is the ability to steer the beam by a variable grating.

3.1.2 Analysis

Consider a dielectric waveguide in air with a dominant TM mode propagating in the z-direction (Figure 3.) The waveguide is coupled to a periodic conducting structure through an evanescent mode. If the waveguide potential function is ψ, then the transverse magnetic odd mode* is

$$\begin{aligned} \psi &= A \sin(ux) e^{-j k_z z} && |x| < a/2 \quad , \\ &= B e^{-vx} e^{-j k_z z} && x > a/2 \quad , \\ &= -B e^{vw} e^{-j k_z z} && x < -a/2 \quad , \end{aligned} \tag{1}$$

where a = thickness of waveguide in the x direction. The corresponding E and H fields are

$$E_x = \frac{-k_z}{\omega\epsilon} \frac{\partial\psi}{\partial x} \qquad E_z = \frac{1}{j\omega\epsilon} (k^2 - k_z^2)\psi \quad ,$$

$$H_y = \frac{\partial\psi}{\partial x} \quad , \tag{2}$$

*The notation is that of Harrington "Time Harmonic Electromagnetic Fields", McGraw-Hill (1961) pp 163-165.

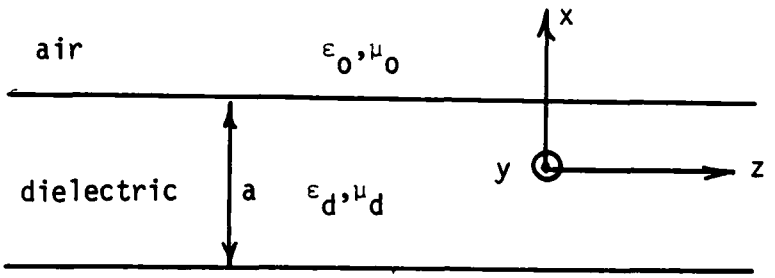

ε_o = permittivity of air

ε_d = permittivity of dielectric

μ_o = permeability of air

μ_d = permeability of dielectric

FIGURE 3. GEOMETRY OF THE WAVEGUIDE

where k_z = guide propagation constant

$$\varepsilon = \varepsilon_d \qquad |x| \leq a/2 \quad ,$$

$$\varepsilon = \varepsilon_o \qquad |x| > a/2 \quad , \tag{3}$$

where ε_o and ε_d are the permittivities of free space and the dielectric, respectively. The separation parameters obey the relation

$$u^2 + k_z^2 = \omega^2 \varepsilon_d \mu_d \qquad |x| \leq a/2 \quad ,$$

$$-v^2 + k_z^2 = k_o^2 = \omega^2 \varepsilon_o \mu_o \qquad |x| > a/2 \quad . \tag{4}$$

(The problem has been assumed to be two-dimensional; that is, there is no variation in the y-dimension). Evaluation of the fields leads to

$$E_x = \frac{k_z A u}{\omega \varepsilon_d} \cos u x \, e^{-jk_z z} \qquad |x| < a/2 \quad ,$$

$$E_z = \frac{A}{j\omega \varepsilon_d} u^2 \sin u x \, e^{-jk_z z} \qquad |x| < a/2 \quad ,$$

$$E_z = \frac{-B}{j\omega \varepsilon_o} v^2 e^{-vx} e^{-jk_z z} \qquad x > a/2 \quad ,$$

$$= \frac{B}{j\omega \varepsilon_o} v^2 e^{vx} e^{-jk_z z} \qquad x < -a/2 \quad ,$$

$$H_y = -Au \cos ux e^{-jk_z z} \qquad |x| < a/2 \quad ,$$

$$= Bve^{-v|x|}_{\varepsilon}{}^{-jk_z z} \qquad |x| > a/2 \quad . \tag{5}$$

At the conducting strips, there will be a z-directed induced sheet current J_s given by

$$J_z = J_s = \hat{n}x\, H_y = Bve^{-v|x|}{}_e{}^{-jk_z z} \quad , \tag{6}$$

where $\hat{n}$ = local normal to the conducting strips. The sheet currents represent an excitation to a series array of strips that radiate in the direction θ, given by

$$\cos\theta = \frac{c}{v_g} - n\frac{\lambda}{\ell} \quad , \tag{7}$$

where n = mode number $0, \pm 1, \pm 2 \ldots$

λ = free space wavelength

ℓ = period of structure

c = free space velocity of light

v_g = propagation velocity in the waveguide

$= \frac{\omega}{k_z}$

The surface excitation travels at the same phase velocity as the wave in the dielectric. Alternatively, the array antenna may be treated as a series of E-field excitations (z-directed) in the gap between the strips.

The power in the waveguide will progressively decrease in the z-direction because of this radiation loss. If the radiation loss is considered to be the dominant loss mechanism, then we have the following normalized power expression:

$$r\, e^{-\alpha x(z)}\, P(z) = \rho(z) = \frac{-dP}{dz} \quad , \tag{8}$$

where $\alpha = 2v$ = power attenuation coefficient in evanescent mode

r = radiation efficiency per unit length

$P(z)$ = normalized power in waveguide

$x(z)$ = distance from waveguide to periodic structure

$\rho(z)$ = power radiated per unit length (or, alternatively, the normalized excitation per unit length).

Two cases will be considered below. The first will be a discussion of the optimum shape $x(z)$ for the grating. The second case will be a discussion of a non-optimized shape - specifically a straight periodic structure that is held at a constant distance from the waveguide. The implicit assumption in all of the analysis is that the presence of the grating does not alter the mode structure in the waveguide.

3.1.3 Optimum Grating Shape

It is known that for maximum power received in the direction θ, the excitation $\rho(z)$ should be uniform.

Hence,

$$\frac{-dP}{dz} = \rho_o = \text{constant} \quad . \tag{9}$$

Substitution of equation (9) into equation (8) yields

$$P(z) = 1 - \rho_o z \quad , \tag{10}$$

which is a linear relationship. Also, from this result we obtain

the following:

$$r\, e^{-\alpha x(z)}(1 - \rho_o z) = \rho_o \quad ,$$

or

$$x(z) = -\frac{1}{\alpha}\left[\ln \frac{\rho_o}{r} - \ln\,(1 - \rho_o z)\right] \quad ,$$

$$= x_o + \frac{1}{\alpha}\ln(1-\rho_o z) \quad , \tag{11}$$

where

$$x_o = -\frac{1}{\alpha}\ln \frac{\rho_o}{r} \qquad \left(\frac{\rho_o}{r} < 1\right) \tag{12}$$

Equation (11) shows that the optimum grating shape is slightly curved. If we were to assume that $x(L) << x_o$ then approximately

$$x_o + \frac{1}{\alpha}\ln\,(1-\rho_o L) \cong 0 \quad ,$$

or

$$x_o \cong -\frac{1}{\alpha}\ln\,(1-\rho_o L) \quad , \tag{13}$$

where L = total length of the grating.

By using equation (12) in equation (13), we obtain

$$\frac{\rho_o}{r} \cong (1-\rho_o L) \quad ,$$

or

$$\rho_o = \frac{r}{1 + rL} \quad . \tag{14}$$

It is clear that all of the waveguide power can not be radiated because we require

$$(1-\rho_o L) > 0 \quad ,$$

so that x(z) is always positive in equation (11).

The value of r may be estimated by examining the radiation resistance of a slot. Harrington[7] has treated a ribbon of current and shown that the radiation resistance is

$$Z = \frac{\eta_o^2}{2} \gamma_{apert} \quad , \tag{15}$$

where η_o^2 = (impedance of free space)^2

γ_{apert} = G + jB = admittance of a capacitive slot radiation aperture.

A case that has been examined experimentally involves equal gap and strip lengths (50% duty cycle), each .35λ in length. Then the real part of γ_{apert} is approximately [8]

$$G_a = \frac{2.7b}{\eta_o \lambda} \text{mhos} \quad , \tag{16}$$

where b = y-width of grating = width of waveguide. Hence, the radiation impedance of the current ribbon is

$$Z \cong \frac{\eta_o^2}{2} \frac{2.7b}{\eta_o .35\ell\lambda} = \frac{1.35\eta_o b}{\lambda\ell} \text{ ohms per unit length} \quad , \tag{17}$$

where ℓ = period of grating.

The radiation efficiency per unit length is then

$$r = \frac{(J_s^2 \cdot Z)\ \text{grating}}{(E_x \times H_y^*)\ \text{guide}} e^{-2vx} = \frac{(Bv)^2 Z}{(Au)^2} \frac{\omega\varepsilon_d}{k_z} \tag{18}$$

Matching E_z and H_y at the dielectric boundary, $x = \pm a/2$, leads to

$$B_v = -Aue^{+va/2} \cos \frac{ua}{2} \quad . \tag{19}$$

Substitution of equation (18) into equation (17) leads to

$$r = \frac{Z\, e^{va} \cos^2 \frac{ua}{2}}{k_z/\omega\varepsilon_d} \quad . \tag{20}$$

The theory of Marcatili[9] has been used with excellent success to predict the mode constants in the guide. Agreement between theoretical guide wavelengths and experimental probe measurements are within experimental error. The results for a polystyrene guide ($\varepsilon_r = 2.54$) with a = 1.25 mm, b = 2.5 mm and λ = 3.2 mm are:

$$k_z = 1.21\ k_o \text{ (Theory and experiment)}$$

$$u = 2.314\ \text{mm}^{-1} \text{ (Theory)}$$
$$v = 1.63\ \text{mm}^{-1} \text{ (Theory)}$$

Hence,

$$r = \frac{1.35\ b}{\lambda \ell} \quad \frac{e^{2.04}\ \cos^2(1.44)}{1.21}\ 2.54 \cong \frac{.35\ b}{\lambda \ell} \quad . \tag{21}$$

Using the value $r = .35b/\lambda\ell$ in equation (14), we obtain

$$\rho_o = \frac{.35\frac{b}{\lambda \ell}}{1+.35\ \frac{Lb}{\lambda \ell}} \tag{22}$$

The total fraction of the waveguide power radiated in a length L is then

$$\text{Efficiency} = \rho_o L$$

$$= \frac{.35\ \frac{bL}{\lambda}}{1+.35\ \frac{bL}{\lambda \ell}} \quad . \tag{23}$$

Theoretical results for a grating with $\ell = 2.2$ mm, $L/\lambda = 20$ and $b = 2.5$ mm are then

$$\text{Efficiency} = \frac{8}{9} = .89 \quad .$$

This is within experimental error of values obtained by measurement using straight gratings. (The above value does not consider reflection losses at the dielectric-metallic waveguide interface.)

The estimated initial value, x_o, for locating the grating is from equations (12) and (14)

$$x_o = \frac{-1}{\alpha} \ln \frac{\rho_o}{r} \quad ,$$

$$= \frac{-1}{2v}\left(\ln \frac{1}{1+rL}\right) \quad ,$$

$$= \frac{-1}{3.26} \ln \frac{1}{1 + .35\ bL/\lambda\ell} = .67 \text{ mm} \quad .$$

Values of $x_o \cong 1$ mm were observed experimentally. (The optimum slope of a straight grating would be approximately x_o/L. For $L = 20\lambda$, $\lambda = 3.2$ mm, the slope is approximately 0.01 (0.57^o), which closely agrees with observation.)

3.1.4 The Straight Grating with Constant Separation

When a non-optimum, straight section is used for the grating, the excitation becomes

$$\rho(z) = r\, e^{-\alpha x_o} \quad P(z) = \frac{-dP}{dz} \quad . \tag{24}$$

The solution for P(z) is

$$\ln P(z) = e^{-rX_o z} \quad . \tag{25}$$

where

$$X_o = e^{-\alpha x_o} \quad .$$

Hence, the waveguide power and the excitation are exponential as given below:

$$\rho(z) = \frac{-dP}{dz} = r\, X_o e^{-rX_o z} \tag{26}$$

We seek the optimized value of x_o or X_o which produces maximum radiated power in a given direction θ. This condition will be achieved when the mean square deviation from the uniform excitation, ρ_o, is minimized. That is, we seek to minimize the integral

$$I\,(X_o,\, L) = \int_o^L (\rho(z) - \rho_o)^2\, dz \quad , \tag{27}$$

with respect to X_o. Substitution of equation (26) into equation (27) yields

$$I = \frac{rX_o}{2}\,(1 - e^{-2rX_oL}) - 2\rho_o(1-e^{-rX_oL}) + \rho_o^2 L \quad . \tag{28}$$

Differentiation of equation (28) with respect to X_o leads to the minimizing condition

$$0 = w\, e^{-2w} + \frac{1}{2}(1-e^{-2w}) - 2\rho_o L\, e^{-w} \quad , \tag{29}$$

where

$$w = rX_oL \quad .$$

Rearranging gives

$$(\frac{1}{2} - w)e^{-2w} = \frac{1}{2} - 2\rho_o Le^{-w} \quad . \tag{30}$$

The maximum efficiency for which a solution exists is $\rho_o L \cong .84$.

Then the approximate solution is

$$w_{optimum} \cong 1.1 = rX_o L \quad .$$

The corresponding value of X_o is

$$x_o = \frac{-1}{\alpha} \ln \left(X_o\right) = \frac{-1}{\alpha} \ln \left(\frac{1.1}{rL}\right)$$

$$= \frac{-1}{3.26} \ln \left(.138\right) = .61 \text{ mm} \quad ,$$

where $r = .35b/\lambda\ell$, $b = 2.5$mm, $\ell = 2.2$mm and $L/\lambda = 20$.
Experimental results are usually within the range of .5 to 1 mm depending upon L and the type of grating. The optimum separation x_o has been shown theoretically to depend upon the following parameters

L/λ. Increased L/λ increases overall radiation efficiency and increases x_o.

Grating period ℓ. Assuming the period is equally divided between air-gap and conducting strip, the effect of increasing ℓ should be to decrease the elemental radiation resistance and to require a reduction in x_o to improve coupling.

3.2 EXPERIMENTAL ARRANGEMENT

The basic experimental setup used to investigate radiation patterns of a diffraction antenna system is illustrated in Figure 4. The experiment was designed to operate at a center frequency of 94 GHz. A listing of the test equipment is provided in Table 1. At this frequency, the wavelength (λ) in free space is 3.19 mm. The arc radius of approximately 2 ft. (23.5 inches) was chosen to ensure that the horn antenna is in the far field of the radiating sample. The far field range was calculated from the standard formula normally used in the layout of antenna pattern test ranges--i.e., far field range $R_{ff} \geq \frac{2D^2}{\lambda}$, where D is the diameter of the aperture. In this case, the length of the dielectric waveguide was used for D. For a nominal (arbitrary) value of 2 cm, $R_{ff} \geq 250$ mm. The 600 mm arc radius is more than twice this value. The brass structure used in initial testing is about 6.6 cm long. This could theoretically require $R_{ff} \geq 8.9$ feet, which would be impractical for this project. Measurements taken at R = 1 ft. and R = 2 ft. indicate a $1/R^2$ variation in power. The 2 ft. radius was, therefore, deemed acceptable.

The RF power source used is a CW klystron having an operating range of 91 to 98 GHz, and a nominal power output of 300 mw. The actual power output was measured at various frequency settings when the unit was new, and also after several months of use. The values are shown in Figure 5. The degradation with operating time is evident from the two curves.

The standard gain horn used to measure the radiated power has a nominal gain of 25 dB. The parameters of the horn are listed in Table 2. The data shown here were provided by the manufacturer, Baytron.

Calibrated thermistors manufactured by Hughes EDD were used in conjunction with an HP 432A to measure radiated power as well as power transmitted through the dielectric waveguide to the termination. The thermistors are accurate to within 0.2 dB (5%) over the frequency range 91-98 GHz. The thermistors are rated at 10mw maximum. Thus a 20 dB coupler was used at the waveguide load termination to reduce the power applied to the thermistor by a factor of 100. Power levels at the horn antenna were less than 10 mw, so additional attenuation was not necessary when measuring radiated power.

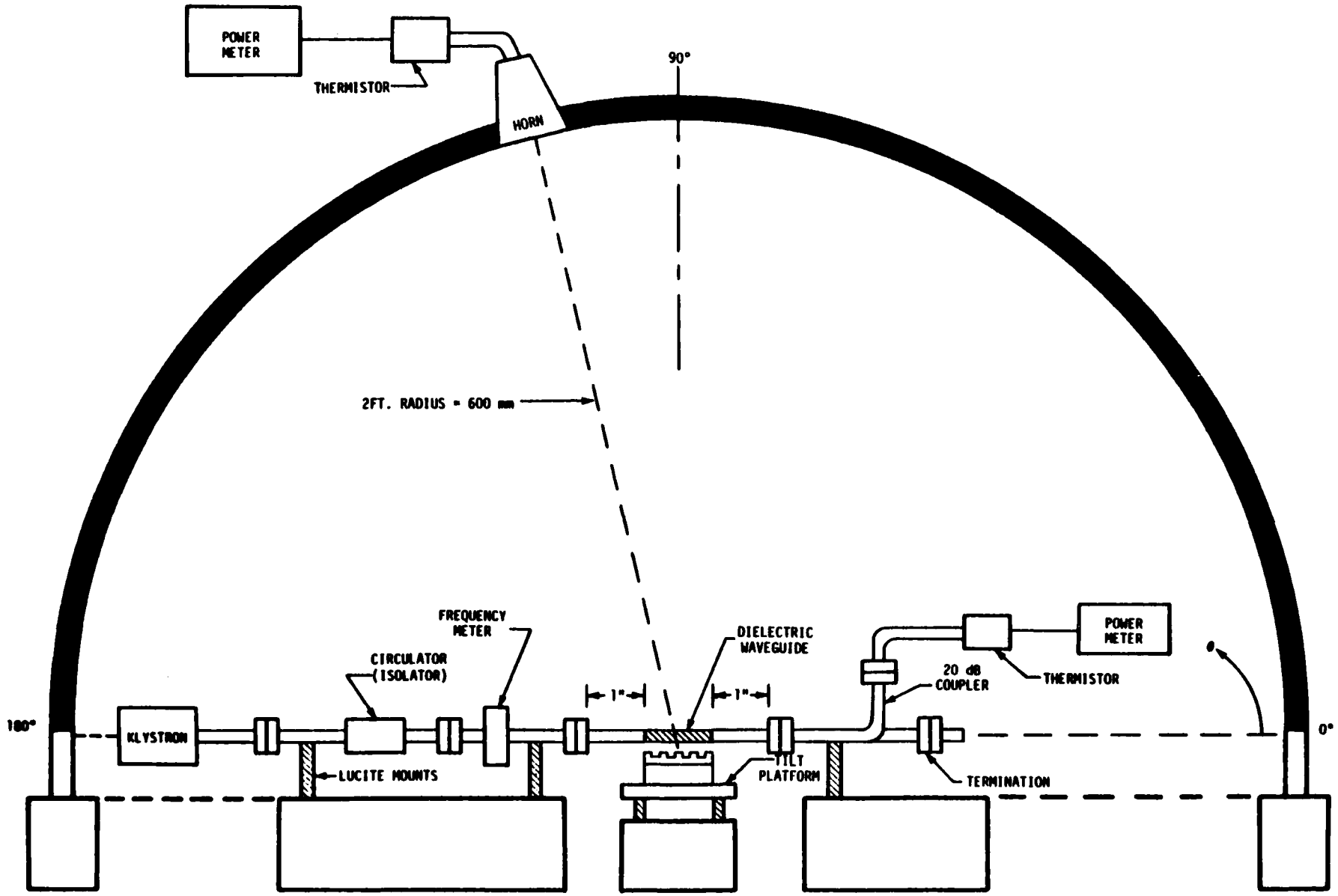

FIGURE 4. BASELINE EQUIPMENT ARRANGEMENT

TABLE 1.

LIST OF MAJOR ITEMS OF TEST EQUIPMENT

ITEM NO.	DESCRIPTION	MFG.	PART NO.
1	KLYSTRON,CW, 91-98 GHz, 300 mw max	VARIAN	VRBZ113B23
2	FERRITE ISOLATOR	BAYTRON	2R-10
3	FREQUENCY METER	BAYTRON	3R-48
4	METAL WAVEGUIDE, COIN SILVER, WR-10 (W-BAND)	BAYTRON	3R-60/* * = 2 INCH OR 4 INCH
5	STANDARD GAIN HORN	BAYTRON	7R-67/25
6	THERMISTOR MOUNT	HUGHES	45776H-1000
7	POWER METER COMPATIBLE WITH ITEM 6	HEWLETT-PACKARD	HP 432A
8	CRYSTAL MOUNT	BATYRON	4-10-200
9	CRYSTAL VIDEO DETECTOR, IN53	BAYTRON	4-10-30X
10	SWR METER COMPATIBLE WITH ITEM 9	HEWLETT-PACKARD	HP 415E
11	COUPLER, 20dB, WR-10 WAVEGUIDE	BAYTRON	3-10-302/20
12	PHASE SHIFTER	BAYTRON	3-10-111

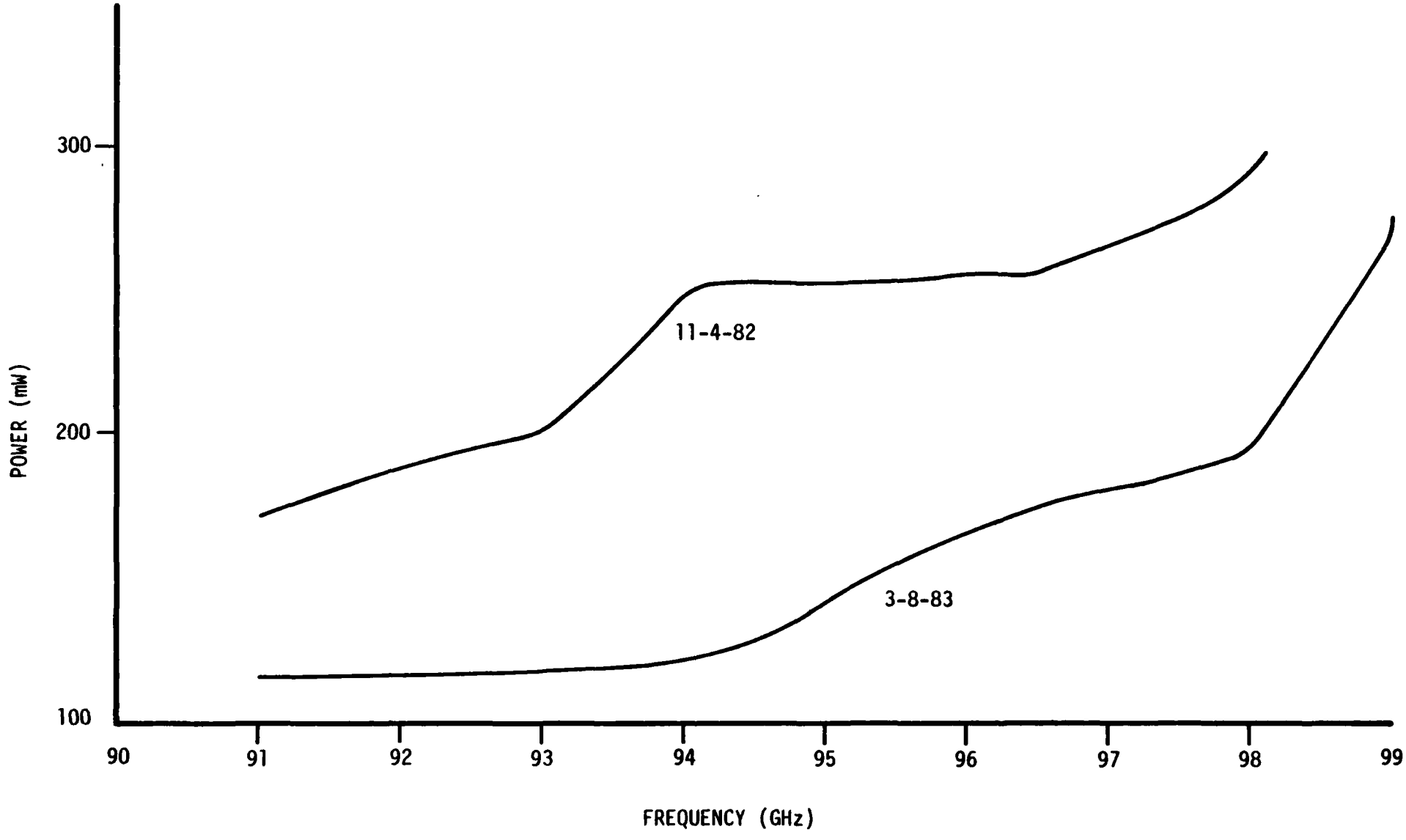

FIGURE 5. KLYSTRON POWER VS. FREQUENCY MEASURED AT TWO DIFFERENT TIMES

TABLE 2.

PARAMETERS OF STANDARD GAIN HORN

FREQUENCY	$1.25f_c$ (73.8 GHz)	$1.57f_c$ (92.7 GHz)	$1.9f_c$ (112.2GHz)
GAIN	23.8 dB	25.86dB	27.50
E-PLANE BEAMWIDTH			
@ 3dB	12^o	10^o	8.0^o
10dB	21^o	17^o	14.6^o
20dB	50^o	40^o	34.0^o
H-PLANE BEAMWIDTH			
@ 3dB	12.8^o	10.2^o	8.6^o
10dB	22.4^o	18.8^o	16.8^o
20dB	40.8^o	33.8^o	29.2^o

Commercially available WR-10 metal waveguide and components were used to make all connections. A ferrite circulator was used to prevent any load mismatches from affecting the klystron. An in-line, reactive type of frequency meter was used to measure the source frequency.

The setup was verified by duplicating the Soviets' experiment. Polystyrene was used as the dielectric waveguide, and was cut to the size and shape indicated in Figure 6. The length was chosen to accommodate a periodic structure 20 wavelenths long. This represents a fairly large aperture. (At X-Band, for comparison, an aperture of 20λ would be about 2.1 feet long.) The ends of the polystyrene were tapered as shown to ease the transition from the metal waveguide. The amount of tapering did not appear to be critical to achieve satisfactory matching. The cross-section of the sample was cut to the same size as the slot in WR-10 waveguide. The tapered ends were inserted into open-ended sections of metal waveguide as indicated in Figure 4. The depth of insertion at either end was adjusted to maximize the power delivered to the load (in the absence of the periodic structure). Typical values of load power at 94 GHz were in the range of 70-110 mw.

The cross-section of the polystyrene waveguide--i.e., 0.1 inch by 0.05 inch, is such as to give a "snug" fit when inserted into the WR-10 slot. According to Ramo and Whinnery[10] the cutoff frequency f_c for a 1^{st} order mode in a dielectric slab of thickness a is given by

$$f_c = \frac{c}{2a\sqrt{\mu_d \varepsilon_d - 1}}$$

where

c = speed of light in air = 3×10^{11} mm/sec

ε_d = relative dielectric constant = 2.54 for polystyrene

μ_d = permeability of dielectric $\cong 1$.

Using these values,

f_c = 95.2 GHz.

Therefore, we are operating slightly below cutoff when using polystyrene of this thickness. This means that there will be a slight attenuation loss from the guide (without a grating) and the propagation constant is complex $\left(k_z = \beta_1 - j\,\beta_2\right)$.

An electric field probe was constructed to measure the guide wavelength. A photograph of the probe and transport is given in Figure 7.

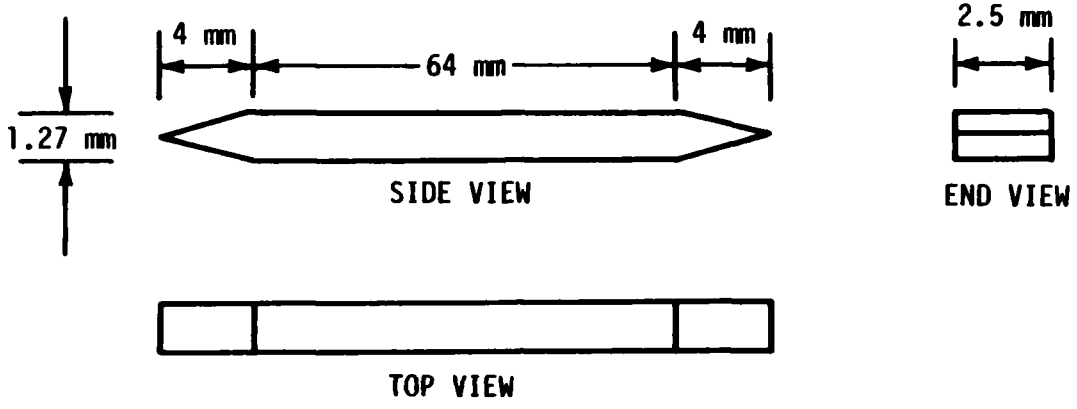

FIGURE 6. POLYSTYRENE USED FOR DIELECTRIC WAVEGUIDE
(NOT TO SCALE)

FIGURE 7. ELECTRIC FIELD PROBE

The electric fields were measured along the length of the dielectric (without a periodic structure in place). The variation is shown in Figure 8.

The electric field variation across the dielectric was also measured, as shown in Figure 9. These patterns show that the dielectric is predominantly in a single mode of operation, as desired.

The baseline periodic structure was milled from brass stock. A photograph of the unit is given in Figure 10. The period (ℓ) of 2.2 mm was selected to produce a beam angle in the vicinity of 100° at 94 GHz.

The peak of the beam as calculated from equation (7) is located at $\vartheta = 103.3^{\circ}$, if it is assumed that $c/V_g = 1.22$. During initial testing, measurements of θ indicated a value of 107° at 94 GHz. It was later found that the sample was not quite at the geometric center. After realignment, θ was found to be 103.75°. The ratio c/V_g can be determined from data taken using the electric probe shown in Figure 8, which indicate that the wavelength (λ_g) in the dielectric, averaged over the length from $x = 4.3$ to $x = 14.8$ mm, is 2.62 mm. The corresponding value of c/V_g is

$$c/V_g = \lambda/\lambda_g$$

$$= 3.191/2.62$$

$$= 1.218.$$

A value of 1.22 was calculated by using Marcatili's equations (See Section V.) The 1.22 value was reported by the Soviets[1] for an operating frequency of 69.8 GHz. It is concluded that c/V_g for polystyrene is 1.22, and that this ratio is not a strong function of frequency for identical waveguide modes. The notches in the structure were cut to a depth of about 0.7 mm, which corresponds to a value used by the Soviets[1], $h = (V_g/c)\sqrt{\lambda/4}$. Other notch depths were not investigated with the brass structure since it was determined from the literature that this value was near optimum.

The experimental results obtained with the baseline structure are presented in Section 3.3. The results obtained with other gratings are presented in Section 3.4.

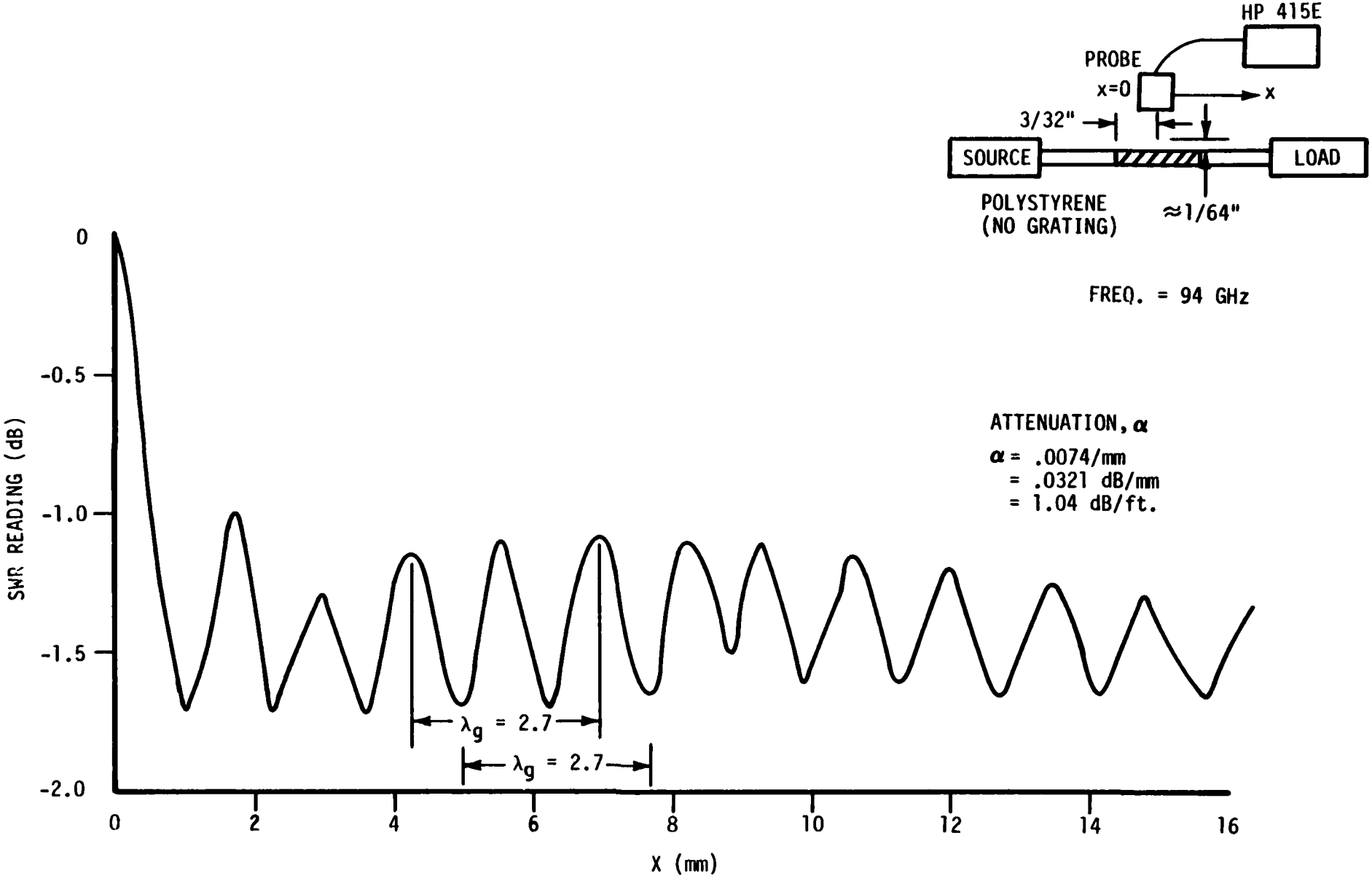

FIGURE 3. ELECTRIC FIELD VARIATION ALONG LENGTH OF DIELECTRIC WAVEGUIDE

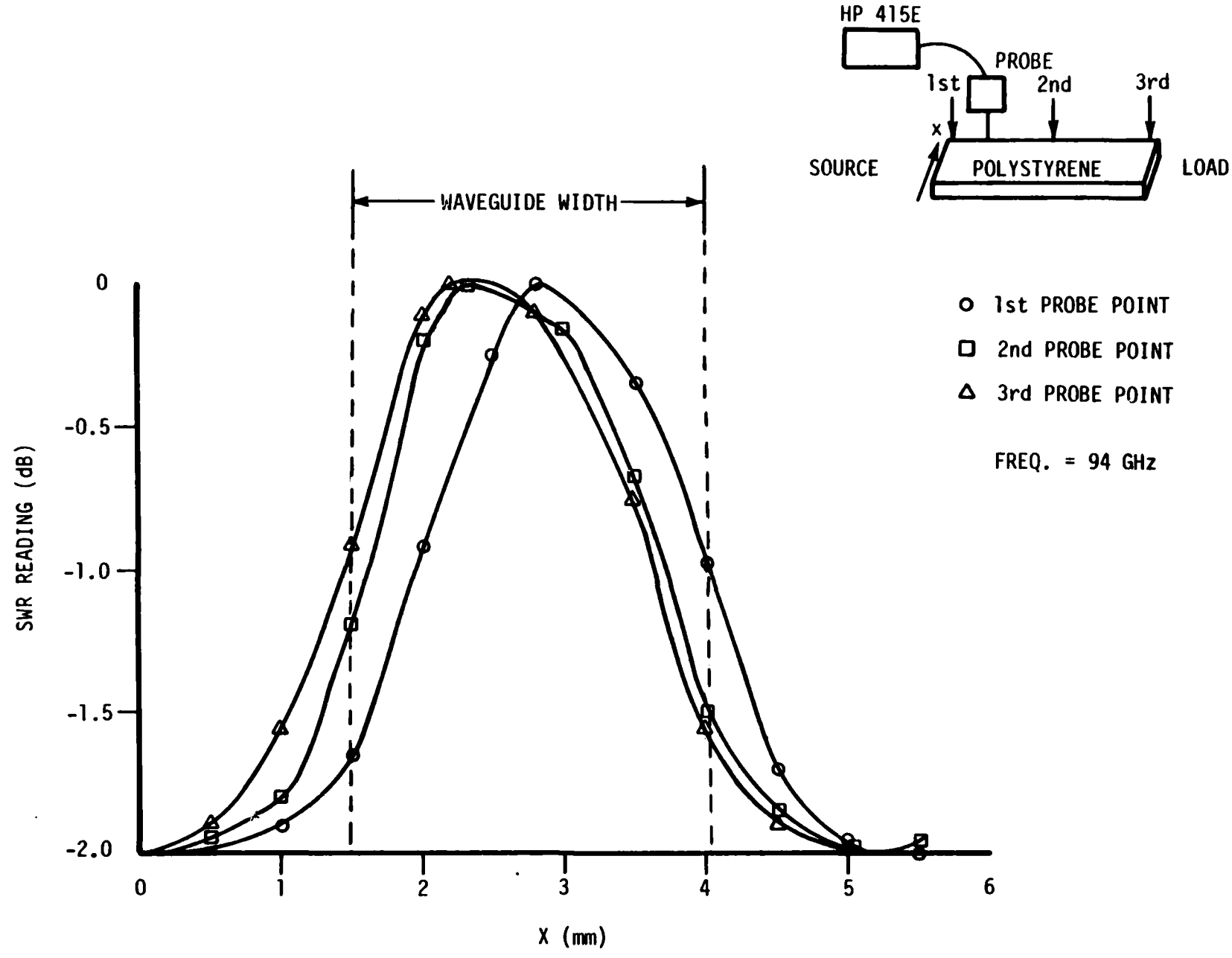

FIGURE 9. ELECTRIC FIELD VARIATION ACROSS DIELECTRIC WAVEGUIDE

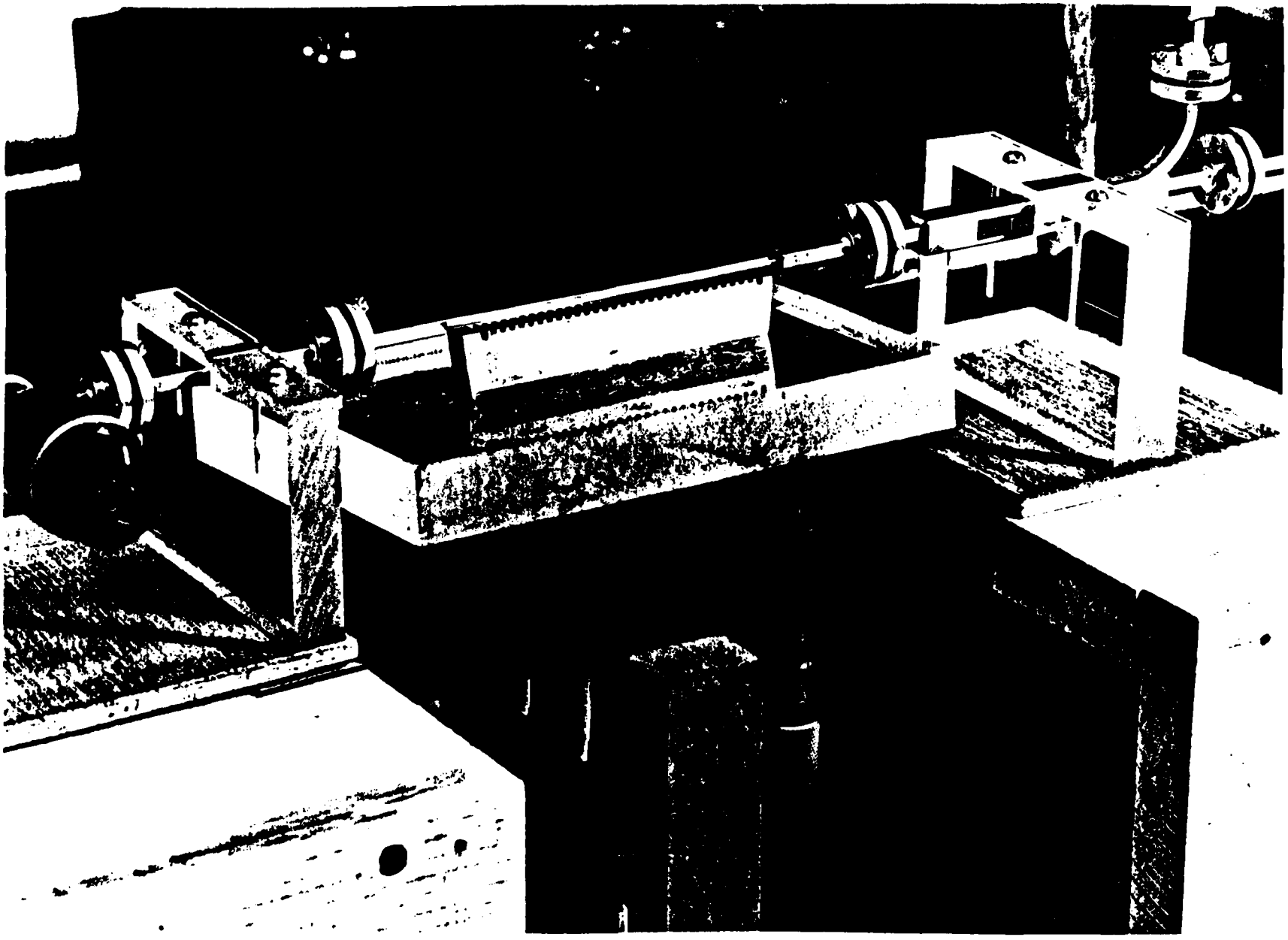

FIGURE 10. BASELINE CORRUGATED BLOCK

3.3 EXPERIMENTAL RESULTS FOR RIGID CONDUCTIVE GRATINGS

3.3.1 Baseline Corrugated Block

The arrangement indicated schematically in the sketch of Figure 11 was used to verify the basic test setup, and to establish a reference with which to compare the performance of various gratings.

A corrugated brass structure was used for the baseline grating. The tilt (Δ of Figure 11) was adjusted for maximum received power at 94 GHz. The radiation pattern was measured at three frequencies--91, 94, and 98 GHz. Tilt was not changed from the setting used at 94 GHz. Results are presented in Figure 12 and show the frequency scanning potential of the device.

It was of interest to measure the power gain of the dielectric--brass structure system at 94 GHz. If the dielectric antenna has a gain G_D and radiates P_T watts, the power intercepted by a standard gain horn of effective aperture A_H, location at a range R_H, is

$$P_{HORN} = \frac{P_T G_D}{4\pi R_H^2} \cdot A_H \quad . \tag{31}$$

In this experiment, the power transmitted was determined by measuring the power delivered to the dielectric termination with and without the structure in place. This was found to be about 24 mw. The power received by the horn was .74 mw . The effective aperture of the horn, as calculated from its specified gain of 26.1 dB, is $A_H = 330$ mm^2. G_D is then calculated as

$$G_D = \frac{P_{HORN}}{P_T} \cdot \frac{4\pi R^2}{A_{HORN}}$$

$$= \frac{.74}{42} \times \frac{4\pi(510)^2}{330}$$

$$= 22.4 \text{ dB} = \text{gain of dielectric antenna.} \tag{32}$$

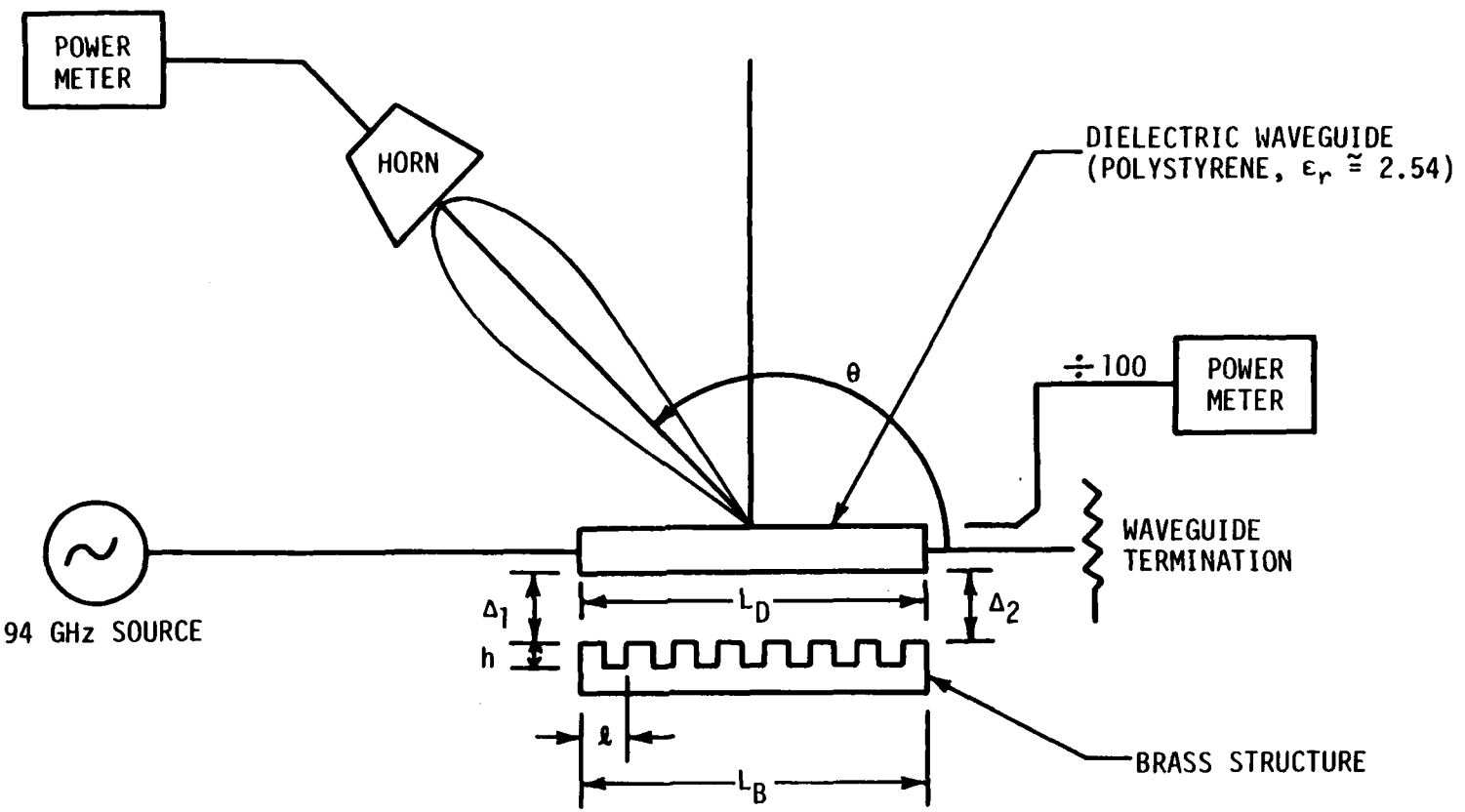

SYMBOL	PARAMETER	VALUE
ℓ	Grating Period	2.2 mm
L_B	Length of Grating	66 mm
N	Number of Periods in Grating	30
h	Grating Notch Depth	0.67 mm
L_D	Length of Dielectric Waveguide	78 mm
Δ_1, Δ_2	Impact Parameter	$\Delta_1 \cong 1.1$ mm, $\Delta_2 \cong 0.5$ mm

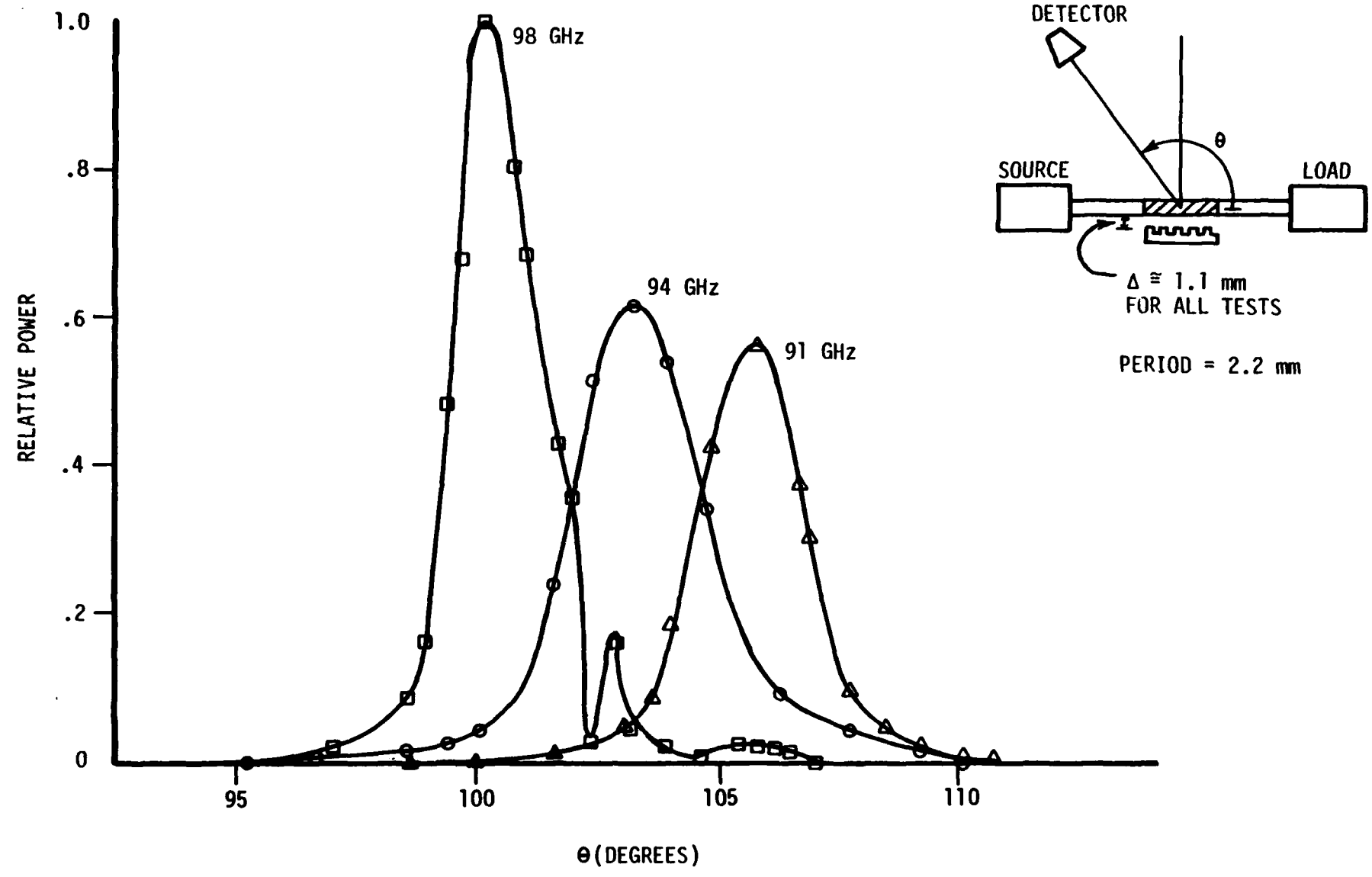

FIGURE 12. BRASS STRUCTURE AT 3 FREQUENCIES

3.3.2 Foil Grating

The ultimate goal of this research is to develop an electronically controllable grating, possibly through conductive bands positioned periodically on the surface of a photoconductive or semiconducting substrate.

To simulate a "surface effect" grating, 1.1 mm wide strips of self-adhesive lead foil of .0015 inch thickness were placed on a clear quartz microscope slide. The width and spacing of the strips were chosen to simulate the brass grating.

The radiation pattern was measured at a frequency of 98 Hz. It was found that the beam pointing angle was at the same angle (102.5^{o}) as that obtained with the brass structure. The peak power was 0.3 mw, which is about 9 dB down from that of the brass grating. The pattern data were normalized to the beam peak. The results are shown on Figure 13. The foil grating exhibited higher sidelobes. The sidelobes could be reduced by more careful construction of the grating.

Although the foil grating is not as efficient as the solid brass grating, these results are believed to indicate the following features:

(1) The grating strips do not have to be connected together electrically.

(2) A "deep" conducting notch between the strips is not necessary.

(3) A ground plane under the grating is not necessary.

(4) The foil strips had an average resistance of .064 Ω. Based on the volume of the strips (1.1 mm wide x 9.525 mm long and .0381 mm thickness) its resistivity of

$$\rho = R \frac{WXT}{L} = .064 \frac{1.1 \times .0381}{9.525}$$

$$= 282 \times 10^{-6} \ \Omega\text{-mm} = 28.2 \text{ microhm-cm.} \qquad (33)$$

will support radiation.

It is noted that published data[11] for lead indicates $\rho \cong 20$ microhm -cm.

The resistivity of brass is 9.1 microhm -cm, about one-third that of lead. Subsequent tests were preformed using even higher values of ρ. These results will be presented in a subsequent paragraph.

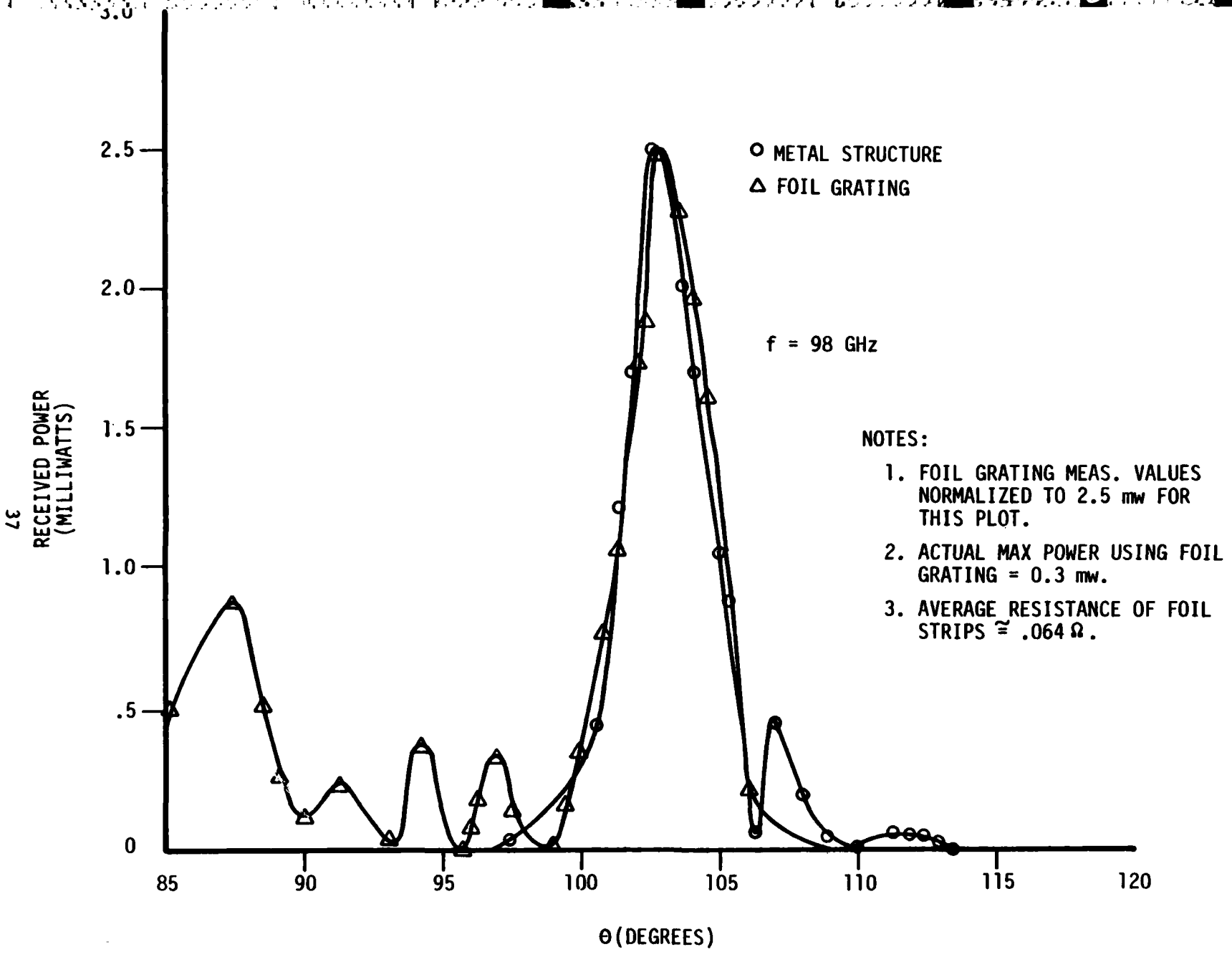

FIGURE 13. COMPARISON OF FOIL GRATING WITH BRASS STRUCTURE

It is noted that the positioning of the foil grating to achieve a detectable radiated beam appeared to be very critical, not only in the tilt and proximity to the dielectric, but also in the orientation along the length of the dielectric. It is expected that the same criticality in orientation would apply to a solid state or all-electronic grating.

3.3.3 Verification of Beam Steering Equation

The position of the beam maximum, as described in an earlier section, is repeated here for reference:

$$\cos \theta = \frac{\lambda}{\lambda_g} - n \frac{\lambda}{\ell} \quad , \tag{34}$$

(since $c = f\lambda$ and $V_g = f \lambda_g$),
where

λ_g is the wavelength in the dielectric waveguide. It was felt necessary to determine λ_g in some manner in order to verify the grating equation.

Close attention was paid to the geometrical alignment of the center of the grating with the 90° mark on the arc. The resulting pattern is shown on Figure 14. The beam maximum occurs at $\theta = 103.3^\circ$. The corresponding value for λ_g is

$$\lambda_g = \frac{\lambda}{\cos \theta + \frac{\lambda}{\ell}}$$

$$= \frac{3.191}{\cos 103.3^\circ + \frac{3.191}{2.2}}$$

$$= 2.61 \text{ mm} \quad . \tag{35}$$

The brass grating was removed, and the electric field variation along the length of the dielectric was measured. The result is given in Figure 15. Since 1-1/2 cyclic variations occur in 4 mm, the corresponding value for λ_g is found to be 2.67 mm. This value of λ_g would produce a beam at 104.9°. These values are within the accuracy tolerances of the test setup.

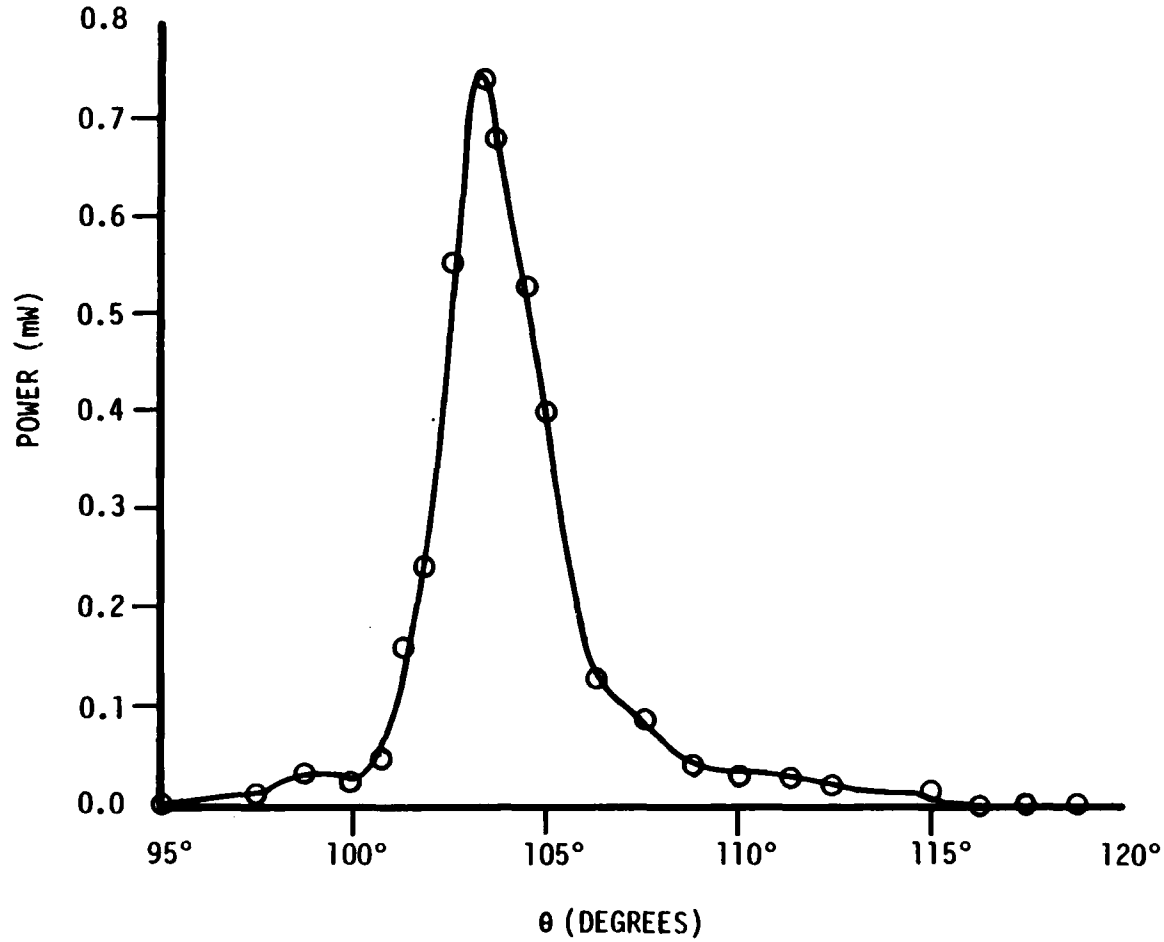

FIGURE 14. BRASS STRUCTURE AFTER KLYSTRON DEGRADATION

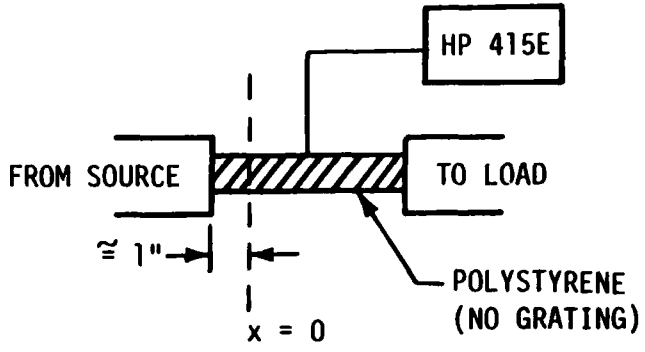

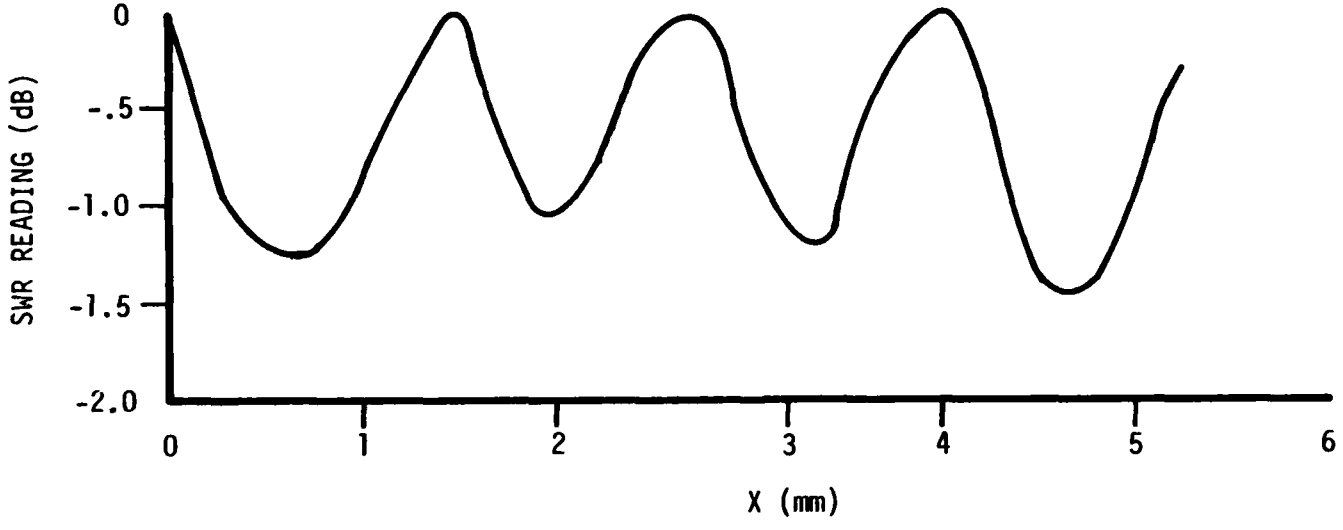

FIGURE 15. ELECTRIC FIELD VARIATION ALONG LENGTH OF DIELECTRIC WAVEGUIDE

Another factor that affects the actual beam angle is that the effective center of the dielectric/grating system does not coincide with the geometric center. This is illustrated in the sketch of Figure 16. The electric fields leaking from the dielectric decrease in amplitude as the wave progresses toward the load end (see Figure 16). Thus the effective array center is shifted toward the source end of the dielectric. This sketch also illustrates the qualitative effect of tilting the structure, which improves the efficiency of the structure by obtaining more uniform "illumination" of the structure along its full length.

> (It is apparent that precise absolute measurements of the beam pointing angle would require determination of the location of the effective center, and then moving the entire waveguide-grating assembly along the z-axis to align it with the 90^{o} mark on the measurement arc.)

Finally, the dielectric guide wavelength was calculated using equations formulated by Marcatili (Ref. 9) following the procedure outlined by Klohn (Ref. 12). The calculations were performed for dielectric waveguide widths of 0.1, 0.2 and 0.4 inch (x1, x2 and x4). The same thickness (.05 inch) was used throughout. The results are listed in Table 3, along with measured values of θ and beam power P at the horn. The measured value of θ was used to derive the quantity c/V_g for comparison with the value calculated from Marcatili's equations.

Also shown in the table are values measured (and calculated) for a so-called "dual beam" structure. This structure was machined from the same type of brass stock as the baseline "single beam" structure. The period was chosen so that two values of n would satisfy the grating equation. Figure 17 is a normalized plot showing the relationship of θ to grating period ℓ. This plot is for polystyrene 0.1 inch wide by .05 inch thick. A period of 3.96 mm (1.24 normalized) was chosen. The theoretical beam angles are 65.4^{o} and 112.82^{o} at 94 GHz.

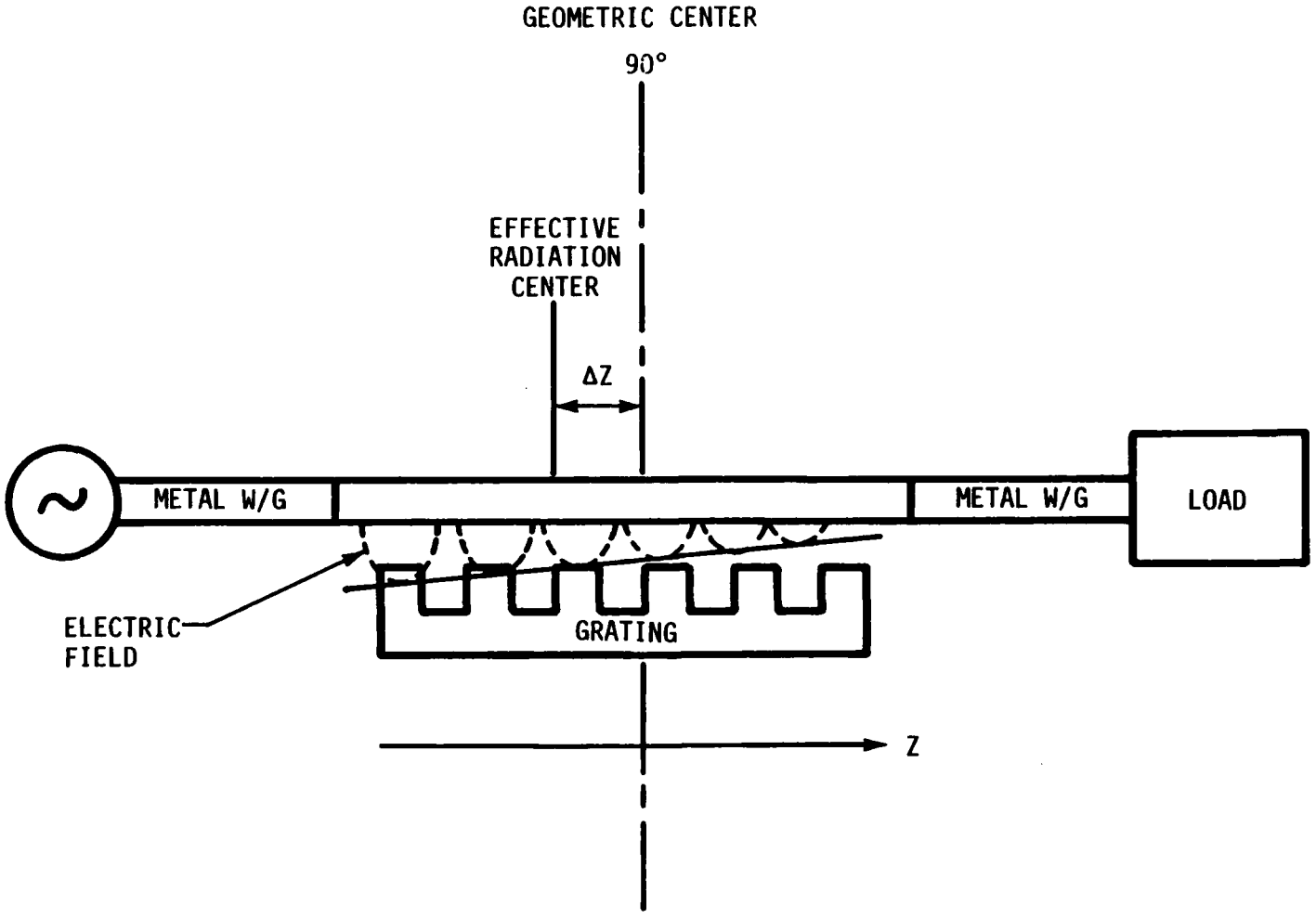

ΔZ = Displacement Of Effective Center of Radiation
From Geomentric Center (Exaggerated in Sketch)

FIGURE 16. DISPLACEMENT OF EFFECTIVE RADIATION CENTER FROM GEOMETRIC CENTER

TABLE 3.

COMPARISON OF MEASURED VALUES WITH VALUES CALCULATED FROM MARCATILI'S EQUATIONS

DIELECTRIC WAVEGUIDE WIDTH	MEASURED DATA			CALCULATED AFTER MARCATILI		
	θ	P	C/V_g	λ_g	$C/V_g = \frac{\lambda_o}{\lambda_g}$	θ
SINGLE-BEAM GRATING(ℓ = 2.2mm)						
x1 = .1 inch	104^o	.78mw	1.21	2.61mm	1.22	103.3^o
x2 = .2 inch	99.75^o	.90mw	1.28	2.50mm	1.275	100.1^o
x4 = .4 inch	96^o	.48mw	1.345	2.46mm	1.2975	98.8^o
DUAL-BEAM GRATING(ℓ = 3.96mm)						
x1 = .1 inch						
	$\theta_1 = 64.4^o$	.89mw	1.24	2.61mm	1.22	65.4^o
	$\theta_2 = 114^o$	.42mw	1.20	2.61mm	1.22	112.8^o
x4 = .4 inch	$\theta_1 = 59^o$	.28mw	1.32	2.46mm	1.2975	60.7^o
	$\theta_2 = 108^o$	.25mw	1.30	2.46mm	1.2975	108.4^o

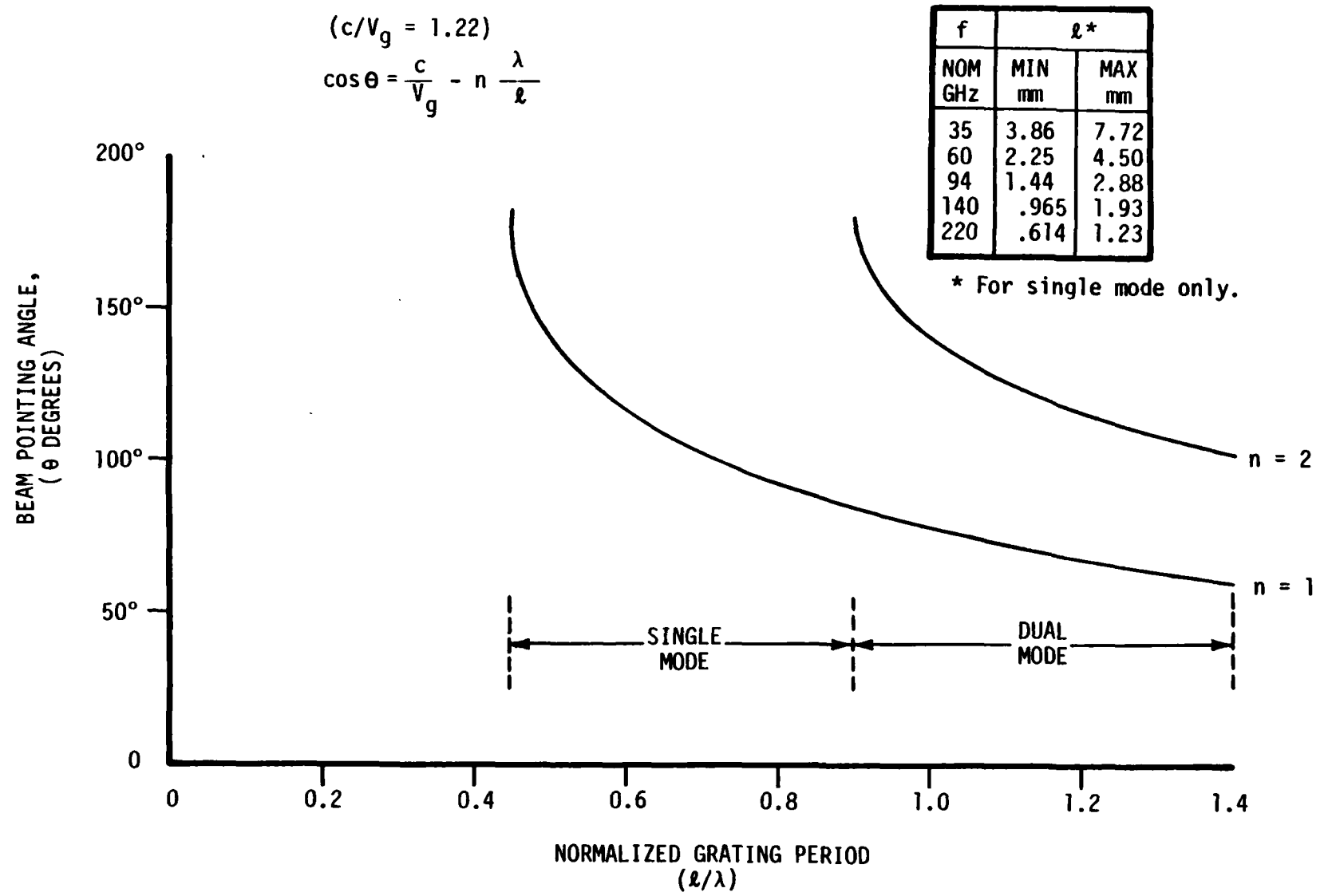

FIGURE 17. BEAM ANGLE (θ) VS. GRATING PERIOD (ℓ)

Some observations can be drawn from these results:

(a) The velocity of propagation in a dielectric material can be conveniently determined by accurately measuring θ, and computing V_g from the grating equation.

(b) If the dielectric constant of the waveguide is known, Marcatili's equations can be used with good accuracy to calculate the velocity of propagation in the guide.

(c) The dielectric constant of a material could be determined from measurements of θ.

3.3.4 Baseline System Used in Receive Mode

The diffraction system has potential applications as a receiver or as a signal processor. Basic experiments were performed to investigate the behavior of the sytem in response to incident radiation. When used for reception, a detector can be readily connected to each end of the dielectric waveguide. As would be expected, the incident radiation must arrive at the angle θ given by the grating equation, if best efficiency is to be obtained.

For the single-beam grating, radiation incident at the angle $\theta = 103.5^{\circ}$ causes received energy to appear primarily at the left (source) end of the dielectric. If the incident radiation falls at the complementary angle--i.e., 76.5°, the received energy is maximum at the right (load) end of the dielectric. Thus, the diffraction antenna is a reciprocal device. If incident radiation of equal power levels occurs at both $\theta = 103.5^{\circ}$ and at its complementary angle, then equal power levels are delivered to each end of the dielectric, if the waves arrive in phase. By varying the relative phase between the incident waves, the power at either end can be varied by 12 dB or more.

The actual division of power between the two ends of the dielectric is affected by the waveguide terminations. (Measured data are presented later in this section.)

In the case of the dual-beam grating, where $\theta_1 = 76.5^{\circ}$ and $\theta_2 = 117.5^{\circ}$, energy incident at either of these angles is delivered primarily to the left (source) end of the dielectric. If incident radiation occurs at both angles

simultaneously, some power is reflected from the left end and delivered to the right. The power division between the two ends is a strong function of the relative phase of the two sources, but in general as the phase is varied from 0^{o} to 180^{o}, the power level at both ends goes up and down together. The phase setting for maximum power at the left end also produces maximum power at the right end. However, phase settings to produce minima at each end are different. The power levels delivered to each end are also affected by "source" and "load" impedance terminations.

The experimental arrangement used for the signal reception tests is shown schematically in Figure 18. The left end of the receiving system is arbitrarily called the "source" end, and the right end is referred to as the "load" end. The angle θ is referenced to 0^{o} at the load end.

Polystyrene waveguide was used for all tests. A thermistor power detector was connected to one end, and the crystal detector to the other (only one thermistor was available at the time of these tests). Tests used the single beam brass grating (ℓ = 2.2mm) and the dual beam brass grating (ℓ = 3.96mm). In some tests only one horn was used to radiate in at the desired angle, and the other horn was replaced with a matched termination.

Different types of terminations were used at the source and load to investigate the effects on received power levels. Open terminations, matched loads and terminations causing high VSWR's were used. Since the detectors represent matched loads, it was necessary to use 10 dB couplers for these tests. The high VSWR load was provided by a tunable short.

The test results are summarized in Tables 4 and 5. (During the course of these tests, the crystal failed and it was necessary to change crystals. The difference in the characteristics of the two was small, however.)

The test data indicate that best sensitivity occurs when matched loads are used at either end of the dielectric.

It should be noted that the diffraction system used as a receiver is highly insensitive to radiation impinging at angles other than those allowed by the grating equation.

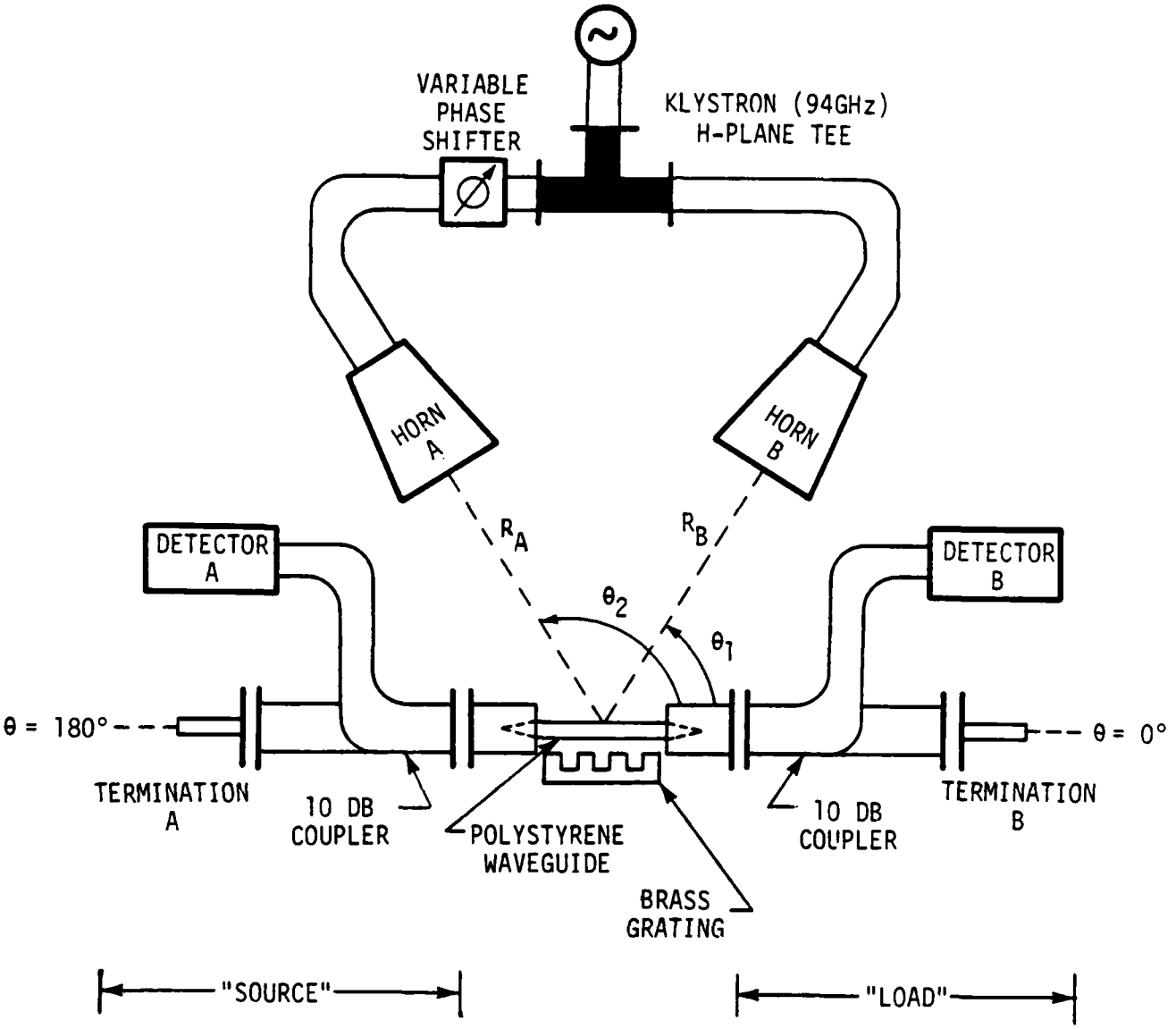

GRATING USED	R_A (Inches)	R_B (Inches)	θ_1 (Degrees)	θ_2 (Degrees)
SINGLE BEAM (ℓ = 2.2mm)	12 1/2	11	76.5	103.5
DUAL BEAM (ℓ = 3.96mm)	13 3/4	12	67.5	117.5

FIGURE 18. EXPERIMENTAL ARRANGEMENT USED FOR SIGNAL RECEPTION TESTS

TABLE 4.

TEST DATA SUMMARY SINGLE BEAM GRATING @ 94 GHz ℓ = 2.2mm, $\theta = 103.5^{o}$

PURPOSE OR DESCRIPTION	HORNS A	HORNS B	ANGLE(S) (note 1) θ_1 (deg)	ANGLE(S) (note 1) θ_2 (deg)	POWER RECEIVED (note 2) LEFT	POWER RECEIVED (note 2) RIGHT	TERMINATIONS LEFT	TERMINATIONS RIGHT	REMARKS (note 4)
SOURCE AT	OFF	ON	76.5^{o}	NA	-52.5dB	.22 mw	MATCHED	MATCHED	
θ_1 GIVES	↕	↕	↕	↕	-50 dB	.21 mw	↕	OPEN	
MAX POWER	↕	↕	↕	↕	-54 dB	.31 mw	↕	ADJ SHORT	MAX→P RIGHT
AT RIGHT END	↕	↕	↕	↕	-51.4dB	.23 mw	↕	ADJ SHORT	MAX→P LEFT
(see note 3)	↕	↕	↕	↕	-54.5dB	.36 mw	↕	ADJ SHORT	MAX→P RIGHT
	OFF	ON	76.5^{o}	NA	-52.6dB	.35 mw	MATCHED	ADJ SHORT	MAX→P LEFT
SOURCE AT	ON	OFF	NA	103.5^{o}	-44 dB	.046mw	MATCHED	ADJ SHORT	MAX→P LEFT
θ_2 GIVES	↕	↕	↕	↕	-47 dB	.039mw	↕	↕	MIN→P LEFT
MAX POWER	↕	↕	↕	↕	-43.8dB	.05 mw	↕	↕	MAX→P RIGHT
AT LEFT END	↕	↕	↕	↕	-45.3dB	.026mw	↕	ADJ SHORT	MIN→P RIGHT
	ON	OFF	NA	103.5^{o}	-42.5dB	.056mw	MATCHED	MATCHED	

See page 50 for notes.

TABLE 4. (Continued)

TEST DATA SUMMARY SINGLE BEAM GRATING @ 94 GHz ℓ = 2.2mm, θ = 103.5°

PURPOSE OR DESCRIPTION	HORNS A	HORNS B	ANGLE(S) (note 1) θ_1 (deg)	ANGLE(S) (note 1) θ_2 (deg)	POWER RECEIVED (note 2) LEFT	POWER RECEIVED (note 2) RIGHT	TERMINATIONS LEFT	TERMINATIONS RIGHT	REMARKS (note 4)
INSTALLED NEW	ON	OFF	NA	103.5°	.34 mw	-57 dB	MATCHED	MATCHED	
CRYSTAL	ON	OFF	NA	103.5°	.34 mw	-54.5dB	ADJ SHORT	MATCHED	MAX→P LEFT
REVERSED CRYSTAL & THERMISTOR	ON	OFF	NA	103.5°	.32 mw	-51.3dB	ADJ SHORT	MATCHED	MAX→P RIGHT
SOURCES AT θ_1 & θ_2	ON	ON	76.5°	103.5°	.42 mw	-44 dB	ADJ SHORT	MATCHED	ADJ ϕ &
WITH MISMATCH AT	OFF	ON	76.5°	--	.003mw	-52.4dB	ADJ SHORT	MATCHED	ADJ SHORT
LEFT GIVES MAX	ON	OFF	--	103.5°	.35 mw	-56.5dB	ADJ SHORT	MATCHED	FOR
PWR RIGHT									MAX→P LEFT
MATCHED TERM'S,	ON	ON	76.5°	103.5°	.44 mw	-53.8dB	MATCHED	MATCHED	
TWO SOURCES,	↕	↕	↕	↕	.29 mw	-48 dB	↕	↕	ADJ ϕ MAX→P RIGHT
VARIABLE PHASING	↕	↕	↕	↕	.47 mw	-49.5dB	↕	↕	ADJ ϕ MAX→P LEFT
	↕	↕	↕	↕	.22 mw	-58 dB	↕	↕	ADJ ϕ MIN→P LEFT
	ON	ON	76.5°	103.5°	.24 mw	-61.5dB	MATCHED	MATCHED	ADJ ϕ MIN→P RIGHT

See page 50 for notes.

Notes for TABLE 4.

(1) θ_1 is the radiation angle given by the grating equation for a source located at the right end (0° reference) of the dielectric waveguide. θ_2 is the value given by the grating equation for a source located at the left end (180° reference) of the dielectric waveguide.

(2) Values in dB denote the crystal detector output after amplification by the SWR meter. The correlation between the dB values and the actual CW power level is shown in Figure B-1, Appendix B.

(3) The grating was positioned longitudinally to maximize the power at the end of the waveguide indicated in REMARKS column. (See note 4 for abbreviations.)

(4)

Abbreviation or Symbol	Definition
P RIGHT, P LEFT	Power detected at right or left end of dielectric waveguide.
MAX→, MIN→	Parameter adjusted to maximize or minimize power detected at indicated end.
ADJ SHORT	Adjustable short was adjusted to obtain condition indicated in REMARKS column.
ADJ ϕ	The relative phase between power applied at the radiating horns was adjusted to obtain condition indicated in REMARKS column.

TABLE 5.

TEST DATA SUMMARY DUAL BEAM GRATING @ 94 GHz. ℓ = 3.96 mm, $\theta_1 = 67.5^o$, $\theta_2 = 117.5^o$*

PURPOSE OR DESCRIPTION	HORNS A	HORNS B	ANGLES* θ_1	ANGLES* θ_2	POWER RECEIVED LEFT	POWER RECEIVED RIGHT	TERMINATION LEFT	TERMINATION RIGHT	REMARKS
MATCHED TERM'S & PHASE ADJUSTED FOR MAXIMUM POWER	ON	ON	67.5^o	117.5^o	.145mw	-48.9dB	MATCHED	MATCHED	
	OFF	ON	67.5^o	--	.022mw	-59 dB	MATCHED	MATCHED	
	ON	OFF	--	117.5^o	.041mw	-56 dB	MATCHED	MATCHED	
ADJUSTED PHASE FOR MIN PWR LEFT	ON	ON	67.5^o	117.5^o	.004mw	-54.4dB	MATCHED	MATCHED	
	OFF	ON	67.5^o	--	.022mw	-59 dB	MATCHED	MATCHED	
	ON	OFF	--	117.5^o	.042mw	-57 dB	MATCHED	MATCHED	
ADJUSTED PHASE FOR MIN PWR RIGHT	ON	ON	67.5^o	117.5^o	.047mw	-64.4dB	MATCHED	MATCHED	
	OFF	ON	67.5^o	--	.022mw	-57 dB	MATCHED	MATCHED	
	ON	OFF	--	117.5^o	.041mw	-57 dB	MATCHED	MATCHED	
EFFECTS OF TERMINATION MISMATCHES AT RIGHT END	ON	ON	67.5^o	117.5^o	.144mw	--	MATCHED	MATCHED	
	ON	ON	67.5^o	117.5^o	.144mw	--	MATCHED	OPEN	
	ON	ON	67.5^o	117.5^o	.191mw	--	MATCHED	ADJ SHORT	SET FOR MAX
	ON	ON	67.5^o	117.5^o	.109mw	--	MATCHED	ADJ SHORT	SET FOR MIN

*Nominal values given by grating equation for source located at left end.

3.4 EXPERIMENTAL RESULTS FOR OTHER GRATINGS

Several types of materials were examined to investigate the effectiveness of periodic changes in dielectric as well as in conducting properties in achieving controlled radiation. The details of these experiments are described in the following paragraphs, along with the results of other experiments that did not result in controlled radiation.

3.4.1 Glass Slide Gratings

A series of gratings was constructed using quartz microscope slides arranged in a sandwich type structure. The edges of the slides were coated with materials of varying values of resistivity. Unless noted, all slides were 1 inch x 3 inch x 1 $\pm$ 0.1mm thick. Thus, on the average, the slide structures had a periodic spacing ℓ = 2.0mm. Ideally, this value would produce a beam at an angle $\theta = 112^{o}$ at 94 GHz.

The first grating tested used silver paint on the edges of alternate slides. (see Figure 19.) The average resistance of a silvered edge was 1.865Ω.

The pattern obtained when the edges were coated with alternating conducting layers of 2.25 MΩ/sq and 23.8Ω/sq is shown in Figure 20. The slides used for this grating had an average thickness of 0.94mm. Thus, the average period ℓ = 1.88mm, and the "ideal" beam angle would be 118.5^{o}, or 6.5^{o} greater than that predicted for the silvered paint grating angle.

A 'high resistance' grating using a coating of 4.04 MΩ/sq on the edges was fabricated. Alternate slides in this grating were uncoated. The radiation pattern is shown in Figure 21.

Additional samples were fabricated using a high resistivity coating (2.25 MΩ/sq) alternating with intermediate levels of resistivity of 129Ω/sq, 1.3KΩ/sq, and 32KΩ/sq. The peak beam angle and the radiated power level at the peak of the beam was measured for each type. To obtain a valid comparison with the brass structure, since the klystron's power output had become degraded, the brass structure was retested under the same conditions as the glass gratings. These results are summarized in Table 6.

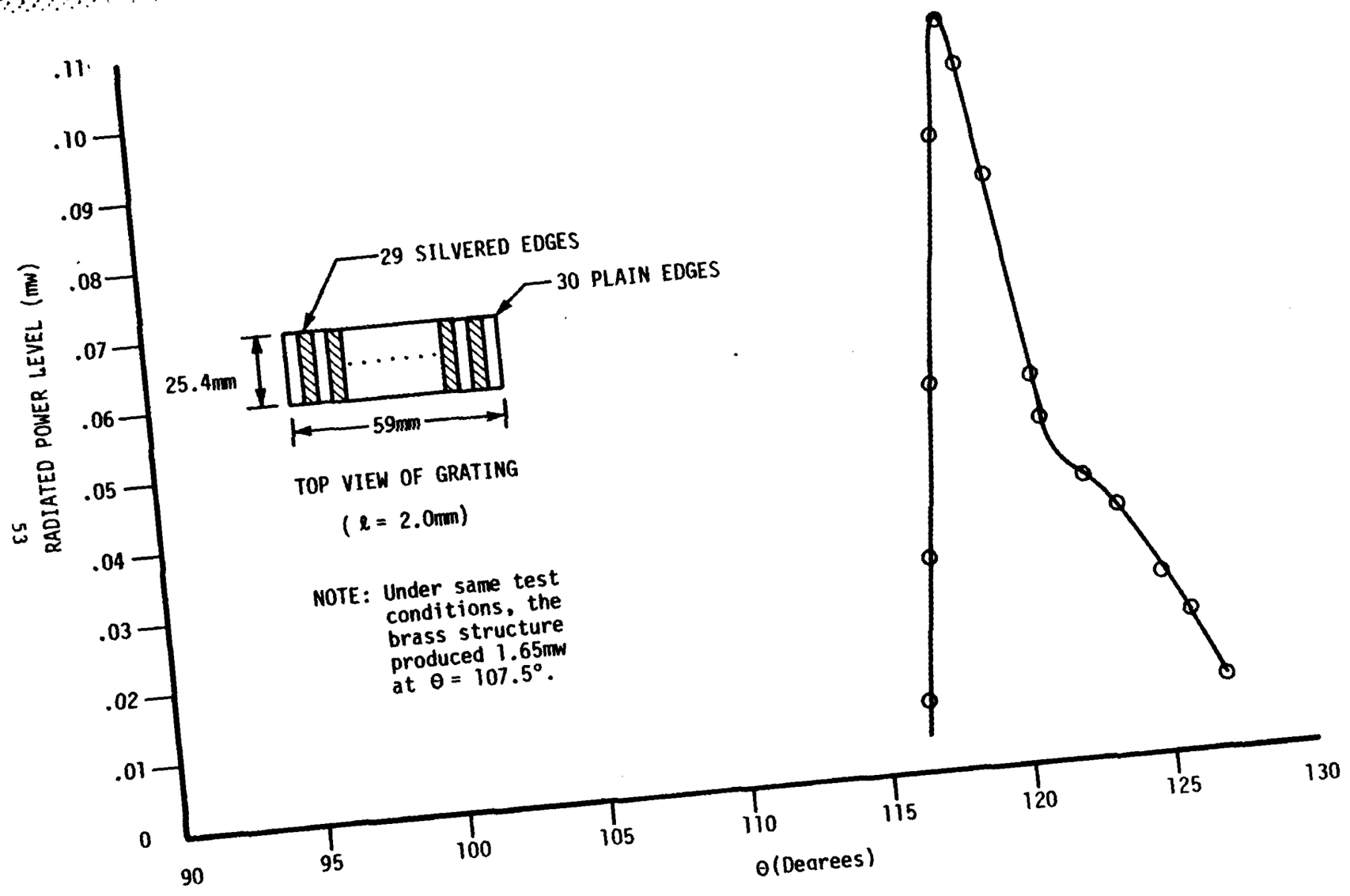

FIGURE 19. SILVER PAINT STRIPS ON GLASS

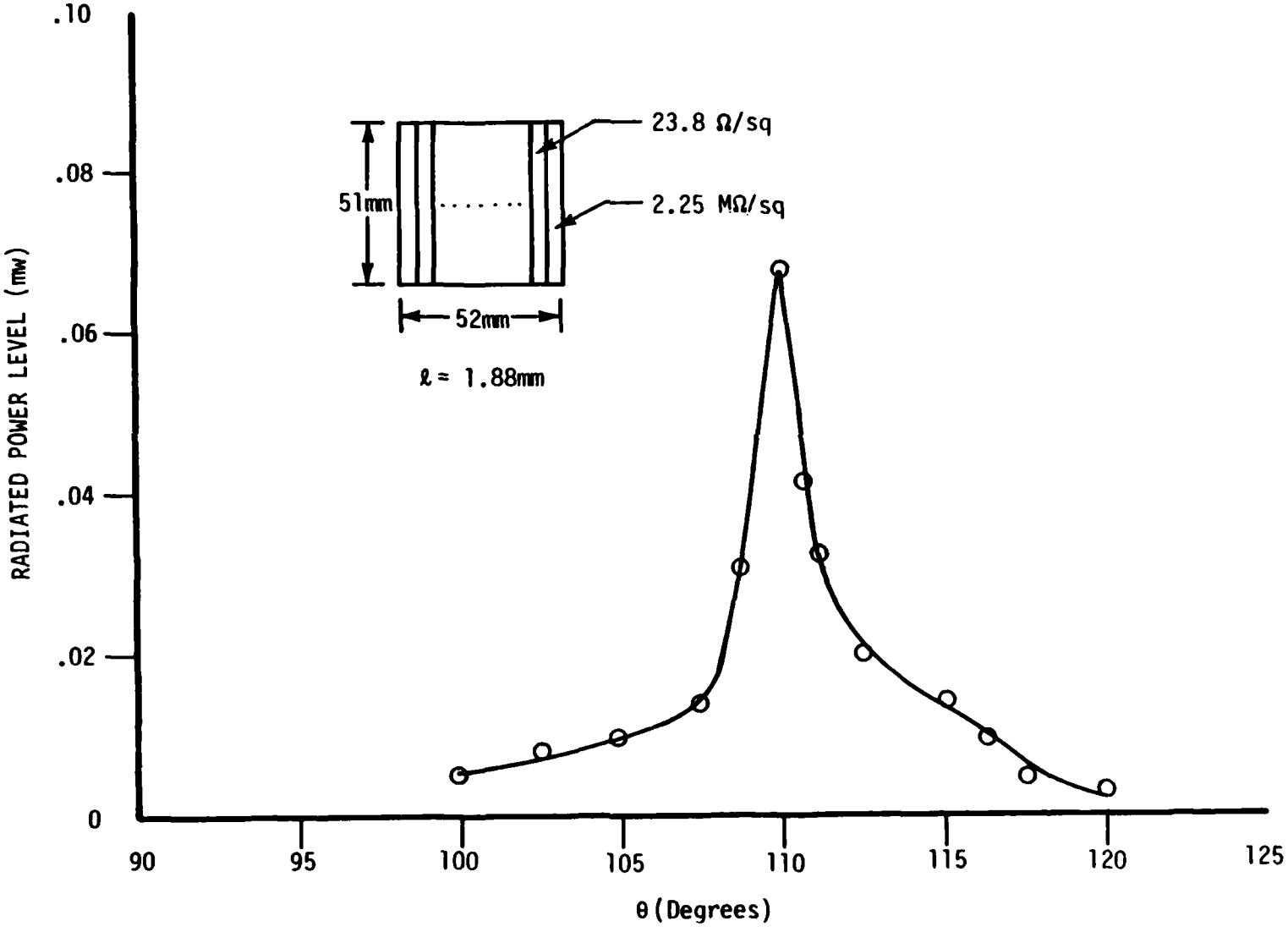

FIGURE 20 - ALTERNATING CONDUCTING FILMS (2.25 MΩ/sq & 23.8Ω/sq)

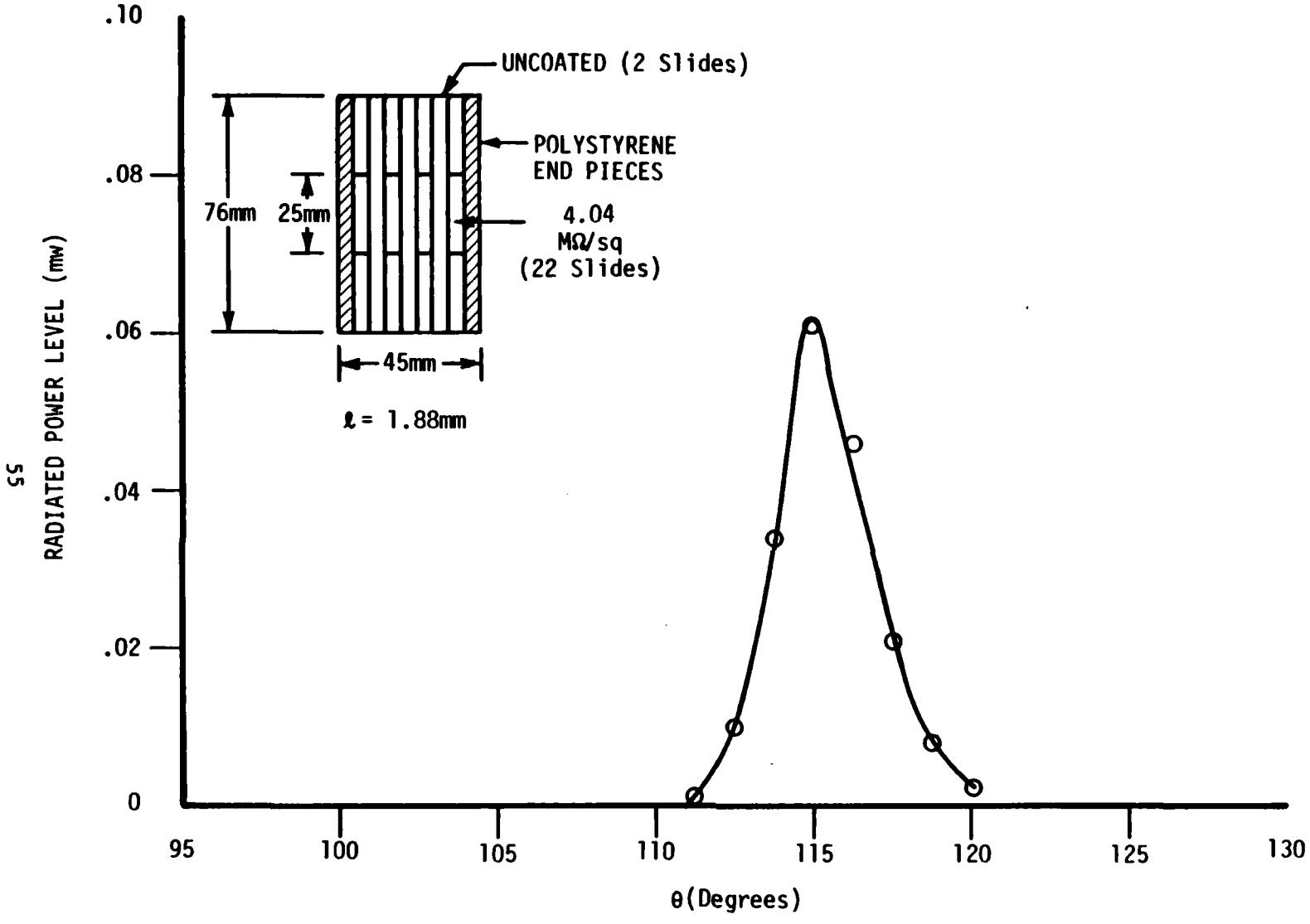

FIGURE 21. CONDUCTING FILM (4.04 MΩ/sq) ON GLASS

TABLE 6.

COMPARISON OF SELECTED GLASS GRATINGS WITH BRASS STRUCTURE

STRUCTURE	θ (deg)	P (mw)	RELATIVE POWER
BRASS	108.75	0.66	1.0
2.25MΩ/sq. & 23.8Ω/sq.	126.25	0.075	0.114
2.25MΩ/sq. & 129Ω/sq.	127.5	0.044	0.067
2.25MΩ/sq. & 1.3kΩ/sq.	126.875	0.0145	0.022
2.25MΩ/sq. & .32kΩ/sq.	126.25	0.028	0.042
ALUMINA TUBES	82.5	0.072	0.109

3.4.2 Alternating Dielectric Constant

Alumina tubes of approximately 2mm diameter were cut to a length of about 15mm and attached to a glass slide. The tubes were spaced at 3.2mm. Paraffin wax was used to fasten the tubes to the slide. The radiation pattern of this grating is plotted in Figure 22. (This grating is also included in Table 6 for comparison with the glass gratings.)

It was found that the level of the radiated power at the peak of the beam was strongly affected by the position of the grating along the length of the dielectric waveguide. The peak of the beam remains at the same angle, but the power level goes through large excursions. The variation is shown on Figure 23. A proposed explanation of this effect is given in Appendix A.

3.4.3 Copper Strips on Printed Circuit Board

A copper grating was placed on a printed circuit board (PCB) to investigate the interaction, if any, of periodic, high intensity dc electric fields with the RF energy in the dielectric. The PCB is depicted in Figure 24. The copper grating itself resulted in a radiated beam. The pattern is also shown in Figure 24. As with the alumina tube grating, the power level at the peak of the beam was sensitive to the lengthwise positioning of the PCB. This is shown in Figure 25. The application of high dc voltages to the grating strips did not produce any noticeable difference in the radiation pattern.

The data for the pattern of Figure 24 were obtained with the grating adjusted for the maximum received power at the horn, which was at an angle of 58°. This value does not agree with any values that can be calculated from the grating equation for values of $\ell = 1.6$ and 3.6, and any mode number n. It is noted that the maxima and minima of the power level shown in Figure 25 are separated by about 1.6mm. (The period is about 3.2 mm.) An explanation of this effect is given in Appendix A.

3.4.4 Ferrofluid

A ferrofluid is a magnetic fluid which responds to magnetic fields as well as Newtonian and gravitational force fields. A ferrofluid consists of a permanent, colloidal suspension of small particles

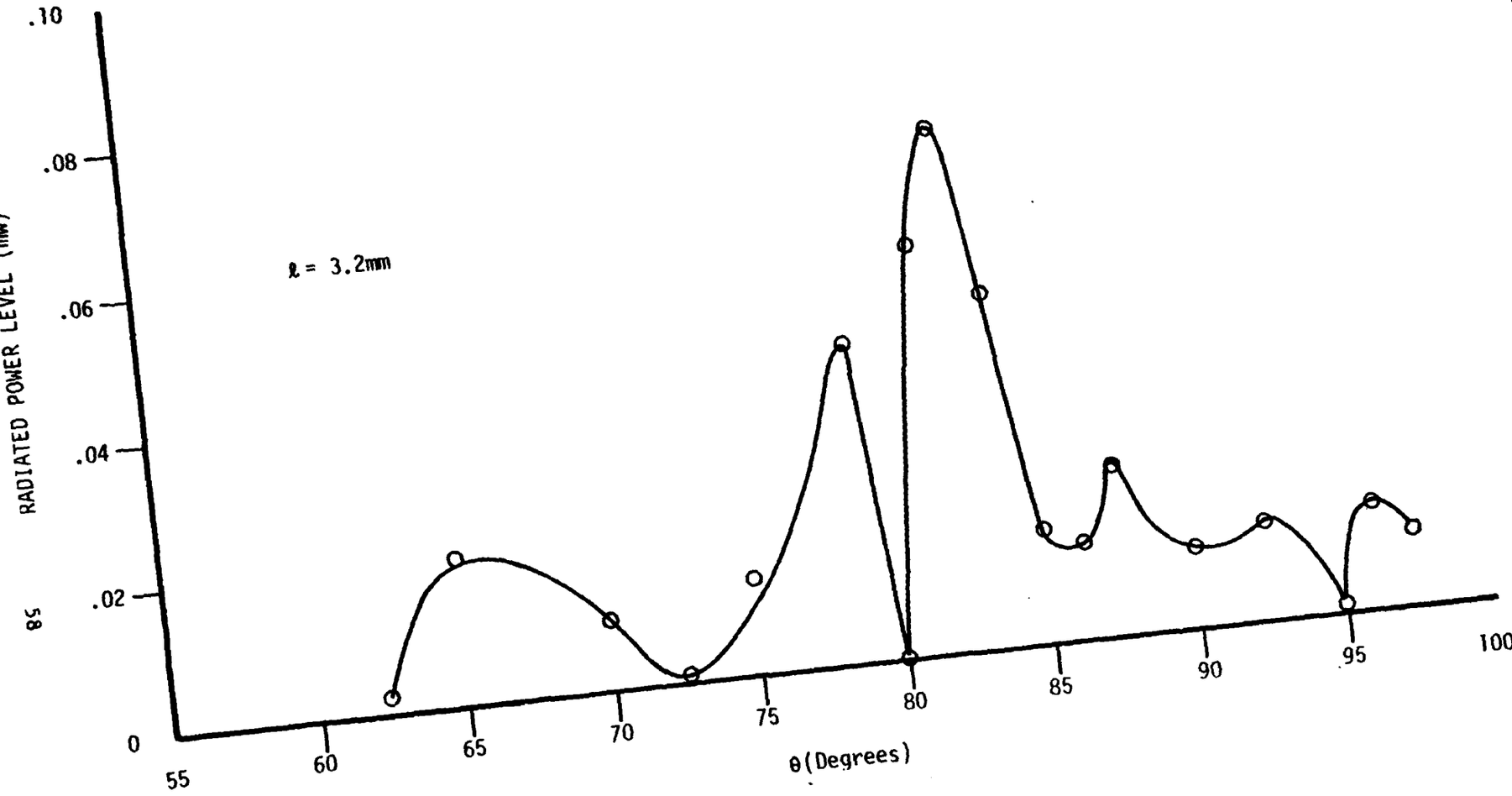

FIGURE 22. ALTERNATING DIELECTRIC CONSTANT
(ALUMINA TUBES ON GLASS SUBSTRATE)

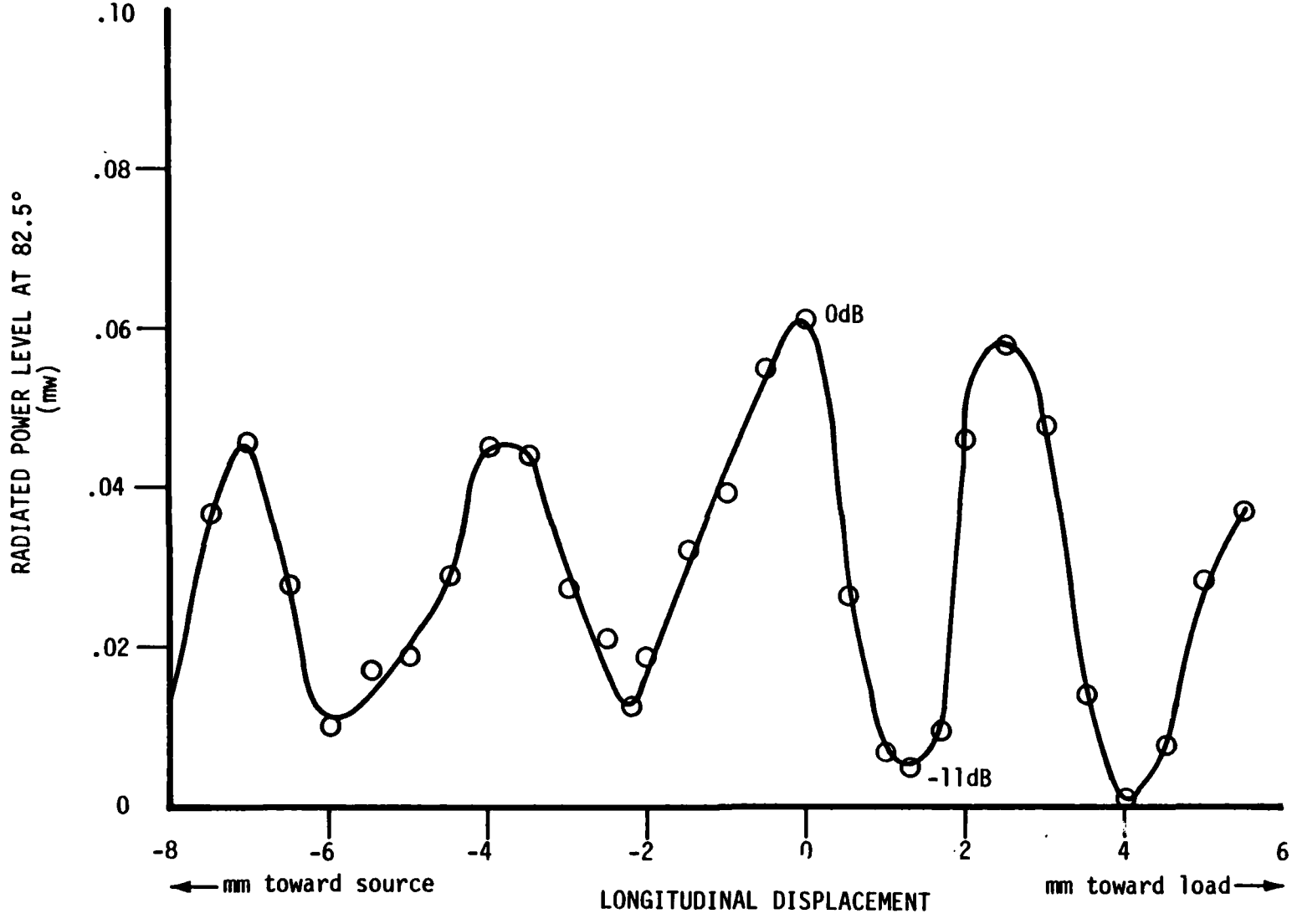

FIGURE 23. VARIATION OF PEAK POWER LEVEL WITH POSITION OF ALUMINA GRATING ALONG LENGTH OF DIELECTRIC WAVEGUIDE (AT $\theta = 82.5°$)

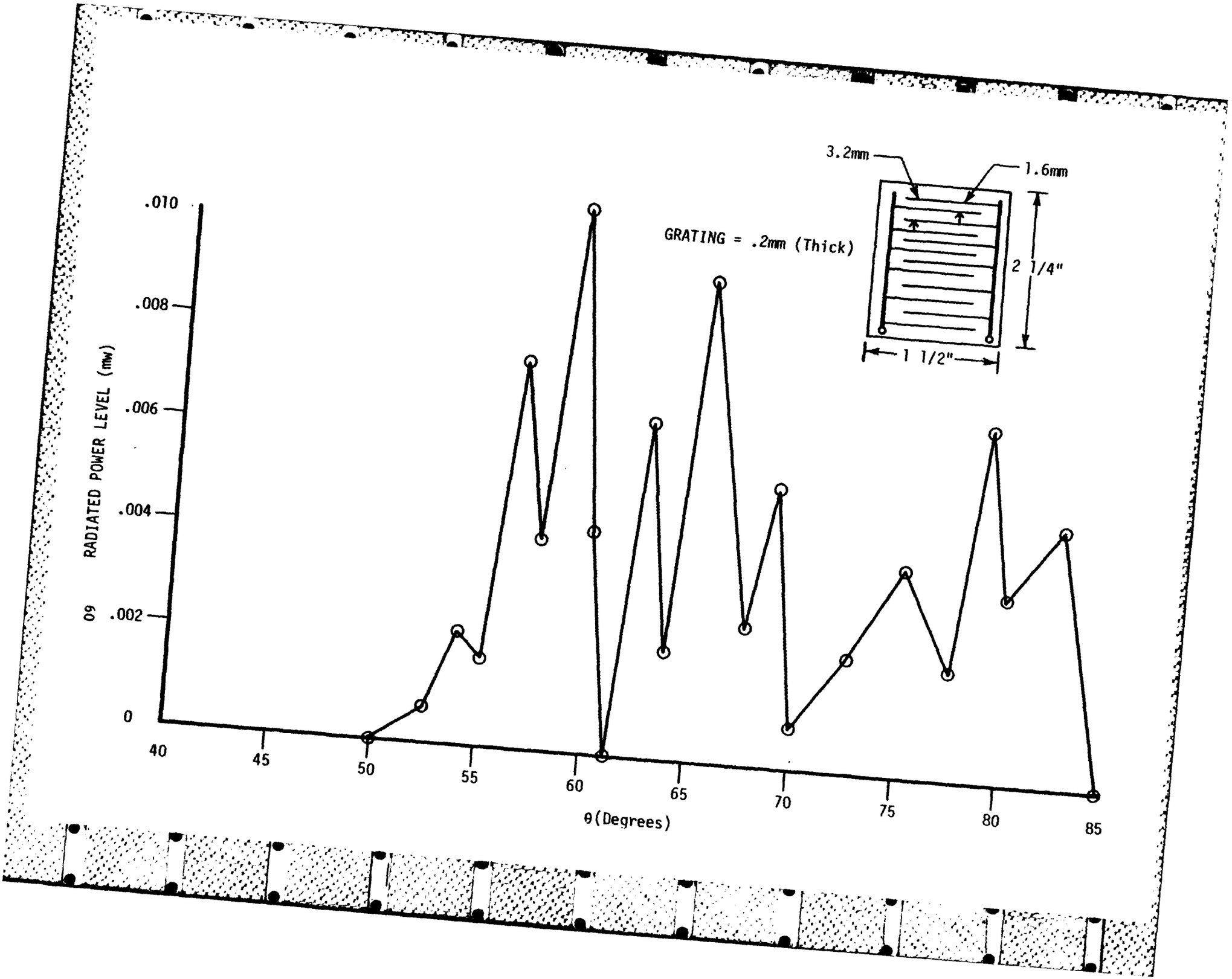
3.2mm
1.6mm
GRATING = .2mm (Thick)
2 1/4"
1 1/2"
.010
.008
.006
.004
.002
0
RADIATED POWER LEVEL (mw)
09
40
45
50
55
60
65
70
75
80
85
θ(Degrees)

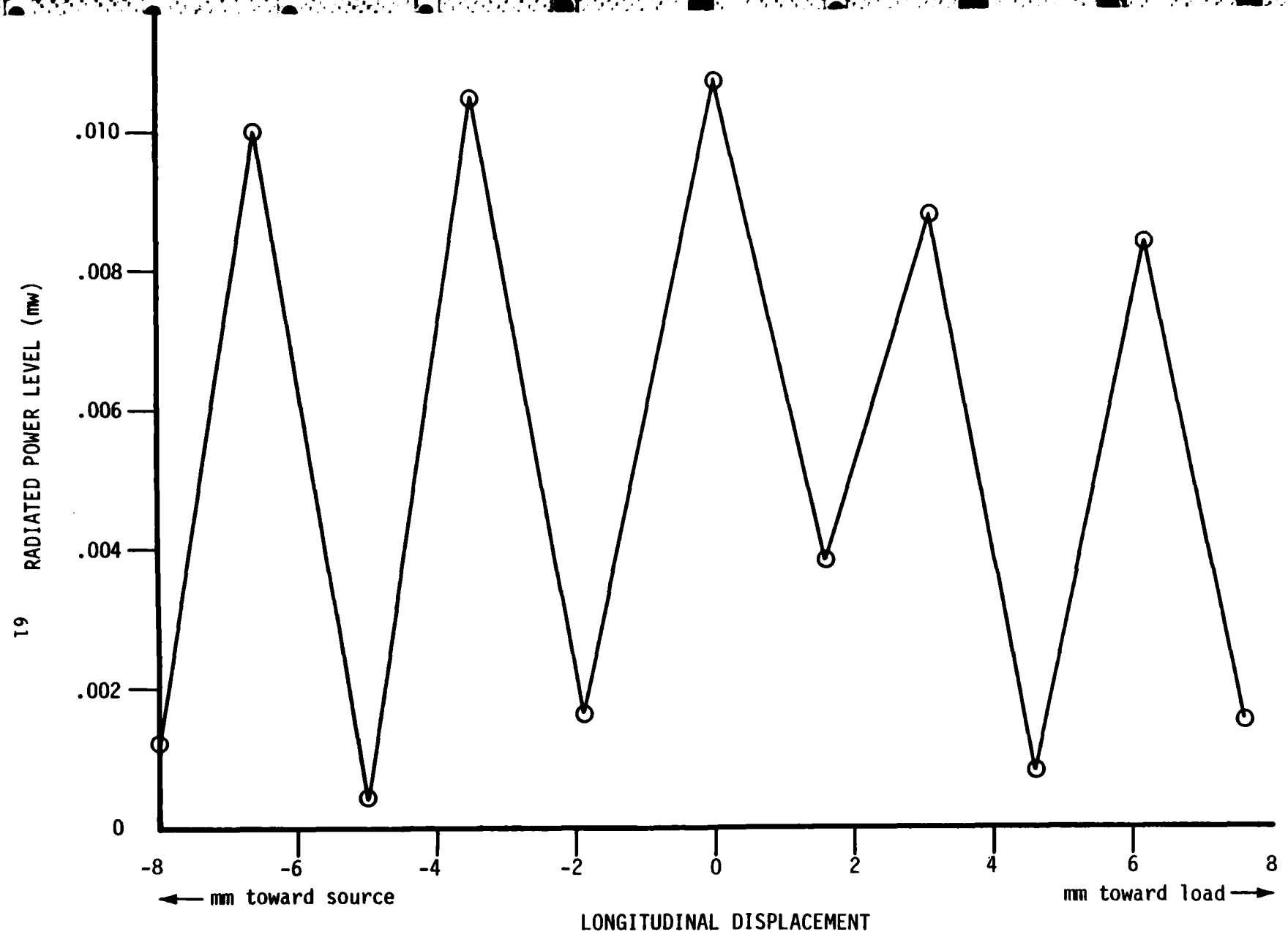

FIGURE 25. VARIATION OF PEAK POWER LEVEL WITH LENGTH-WISE POSITION OF COPPER STRIP/PCB GRATING (AT $\Theta = 58.75°$)

($\cong$ 0.01mm diameter) of magnetite (Fe_3O_4) in various carrier solvents. A stabilizer or surfactant is added to prevent agglomeration of the particles.

Ferrofluids are commercially available from Ferrofluidics Corporation in several forms within three basic categories, according to the manufacturer. They are :

(1) Diester Based--Used in heat transfer, sealing, lubricating and damping applications.

(2) Water Based--Used in medical, biological and various magnetic detection applications such as domain detection, magnetic tape detection and quality control of metal parts.

(3) Hydrocarbon Based--Used in densimetrics, magnetic detection of parts, special display effects, sealed environment and in research applications.

A standard product in the third category was selected for this experiment. The fluid is kerosene based. According to the manufacturer, who recommended this type (EMG-901), its properties are best suited to the generation of periodic surface waves. The fluid viscosity is less than 10 centipoise, and its magnetic saturation occurs at a magnetic flux density of 600 Gauss.

Several approaches were tried in an attempt to produce a uniform pattern of surface waves in the fluid at a spacing of 2 to 3mm. These methods included a motor driven actuator "beating" against the fluid, sound waves, electromagnets and permanent magnets. The tests using electomagnets revealed that the required coils would be excessively large to generate the required fields. Construction of such an electromagnet was considered outside the scope of this project.

Some limited success was achieved with a large permanent magnet. A sketch of the experimental setup is shown in Figure 26. The radiation pattern is given in Figure 27. It is apparent that the pattern is irregular. This is due to irregularities in the periodicity of the ripples in the ferrofluid.

This experiment served to demonstrate that a reaction occurs between the RF in the dielectric and the ferrofluid surface ripples. It seems possible that by devising more sophisticated methods of controlling the magnetic fluid, one could achieve controlled radiation. It might be that a combination of applied magnetic fields in conjunction with physical movement or shock waves in the fluid would achieve the desired result.

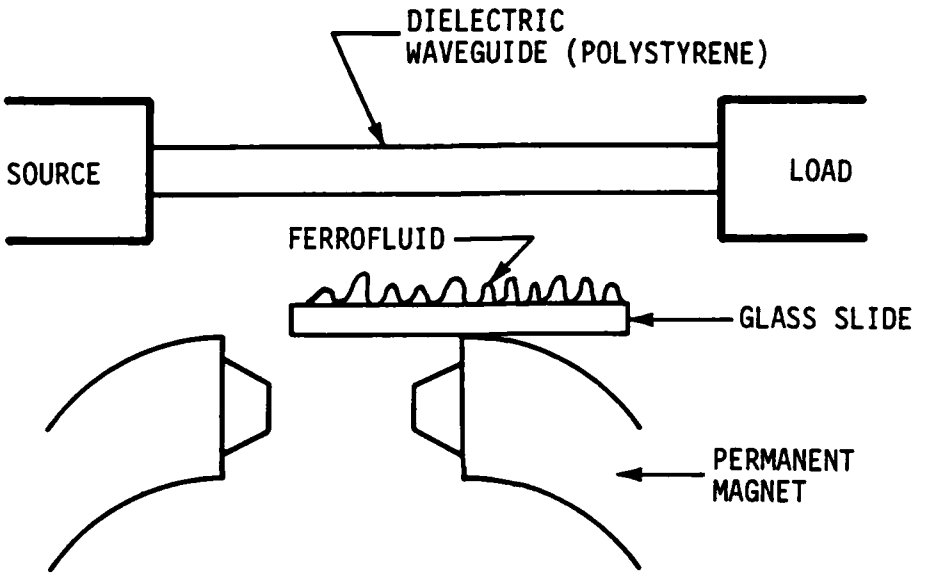

FIGURE 26. EXPERIMENTAL SETUP USING FERROFLUID

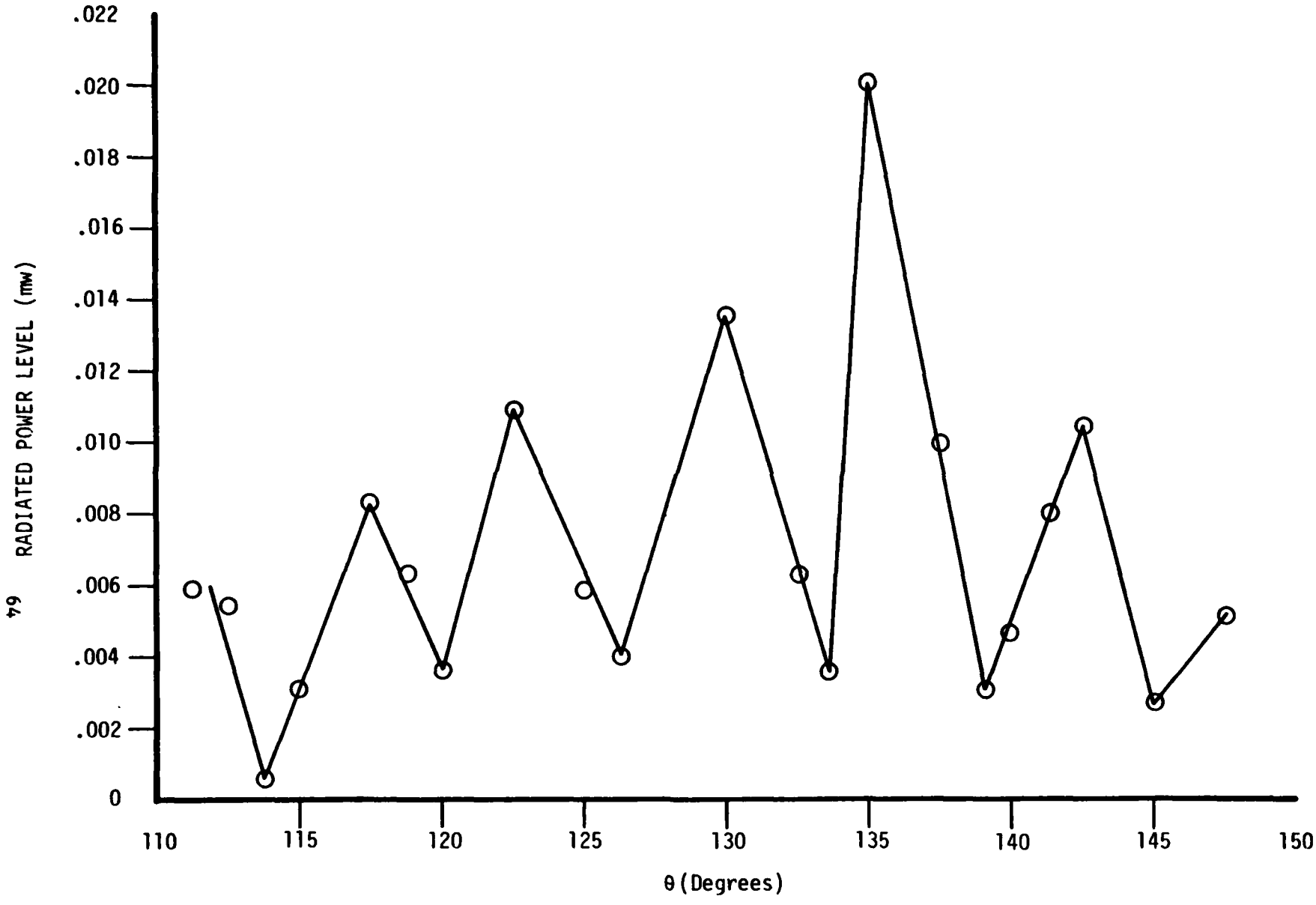

FIGURE 27. FERROFLUID GRATING

3.4.5 Spring

One of the simplest methods of achieving beam-steering by varying the period of a grating is to use a spring for the grating. Ideally, a spring for this purpose would have a rectangular or square cross-section so that a maximum portion of the "reflecting" surface would be parallel to the waveguide. Such springs may be constructed although they are quite expensive and not readily available. Therefore, springs of circular cross-section were used in these experiments. Several different diameters were tried. It was thought initially that a spring of large diameter, such as 1/2 to 1 inch, would present the least amount of curvature under the dielectric and would, therefore, be most efficient. However, it was found extremely difficult to maintain a reasonably uniform pitch over a usable length of the spring. Best overall performance was obtained with a flexible spring having a diameter of 5.5mm (.21 inch) and having 32 coils. The diameter of the wire was 0.5mm. It was found that the efficiency of the spring was increased significantly by using a conducting rod as the "core" of the spring. A brass rod of 5mm diameter was used for this purpose.

The spring was adjusted for a spacing d = 2.2mm and the radiation pattern was measured. The results are shown in Figure 28, normalized to the gain at beam maximum (the "gain" of the spring was about 5 dB below that of the brass structure).

The length of the spring was varied from a minimum of 45.3mm to a maximum of 99mm, in steps of about 2.5mm, to steer the beam from 166° to 80°. The variation of pointing angle with spacing is shown in Figure 29a. The measured values show good agreement with theory for $c/V_g = 1.22$, $n = -1$ and $\lambda = 3.19$ mm.

It was found that best efficiency was obtained if the brass rod was of length comparable to the length of the spring. Three different rod lengths were used in the course of these tests.

The 3 dB beamwidth was measured at 5 positions. The values are given in Table 7 and Figure 29b.

3.4.6 Photoconductive Gratings of CdS

One method of achieving a periodic, electrically controllable grating is to use conductive strips on the surface of a photoconducting slab. The conductivity might be spatially controlled by a scanning laser beam.

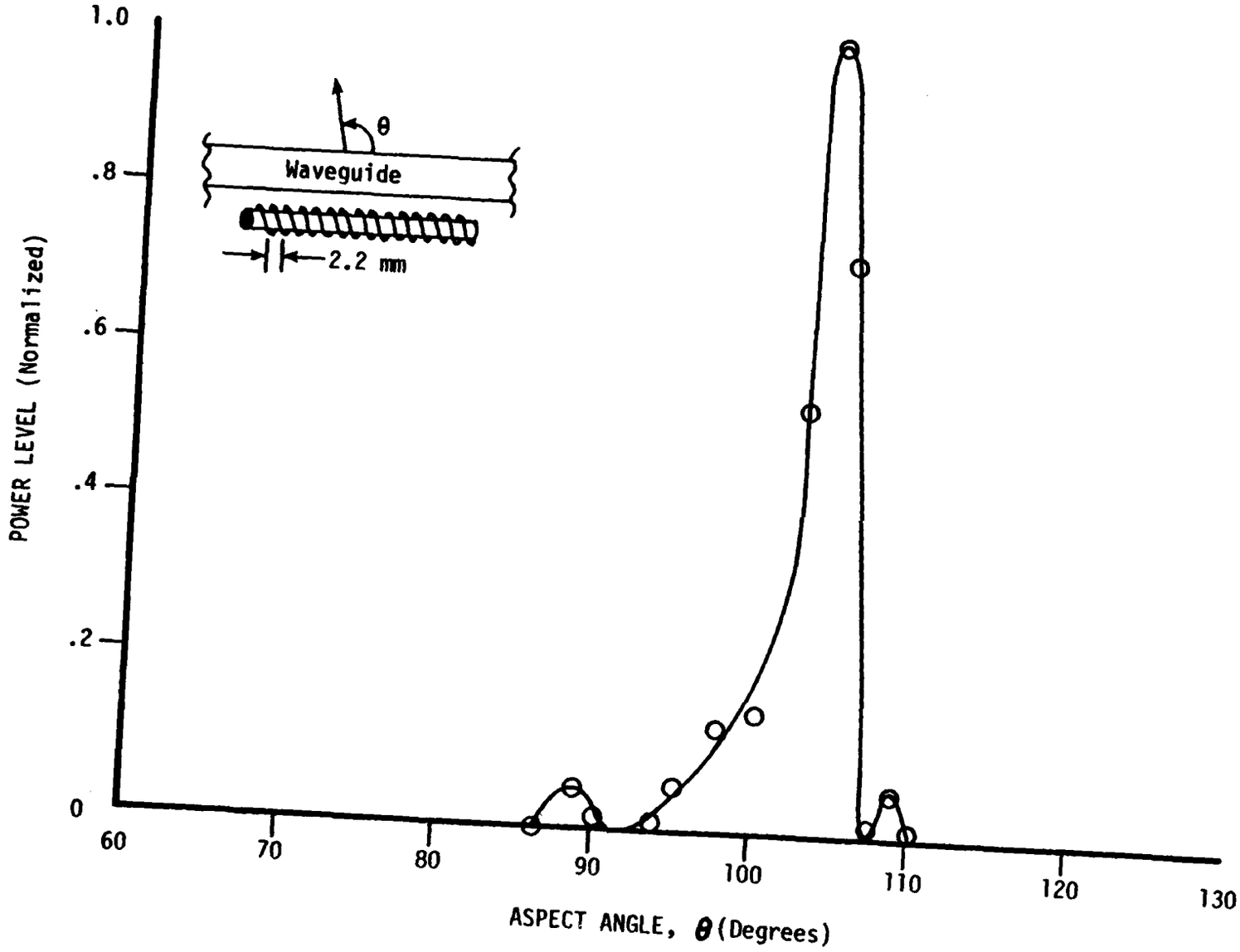

FIGURE 28. RADIATION PATTERN FOR 2.2mm SPACING

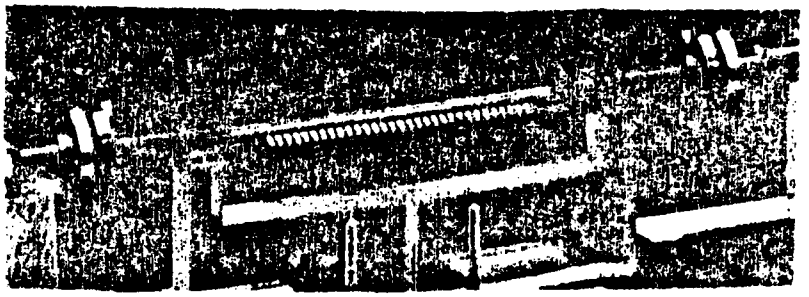

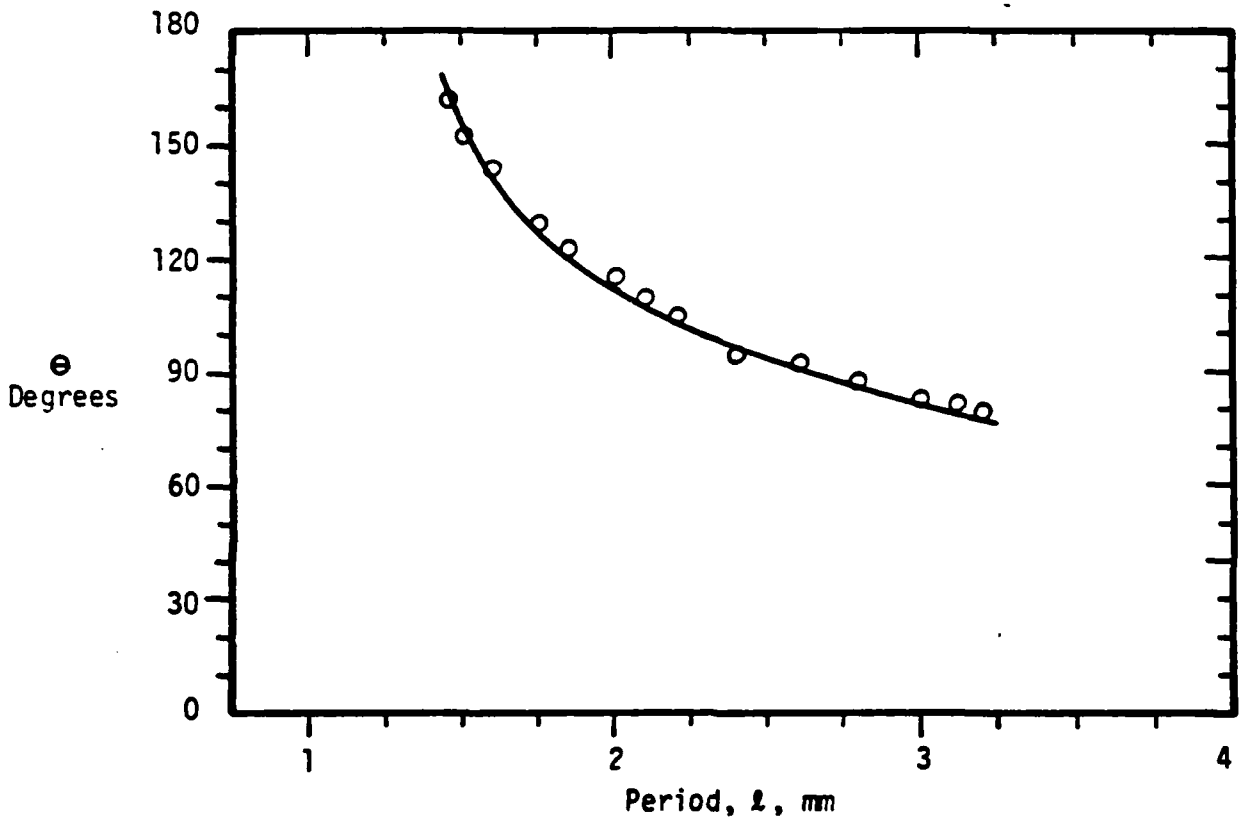

FIGURE 29a. BEAM STEERING ANGLE VERSUS SPRING COIL SPACING

TABLE 7.

HALF-POWER BEAMWIDTH AT SELECTED BEAM ANGLES
(SPRING GRATING)

BEAM ANGLE	BEAMWIDTH
80.6°	1.98°
103.0°	2.75°
121.3°	3.90°
138.8°	5.30°
159.7°	5.35°

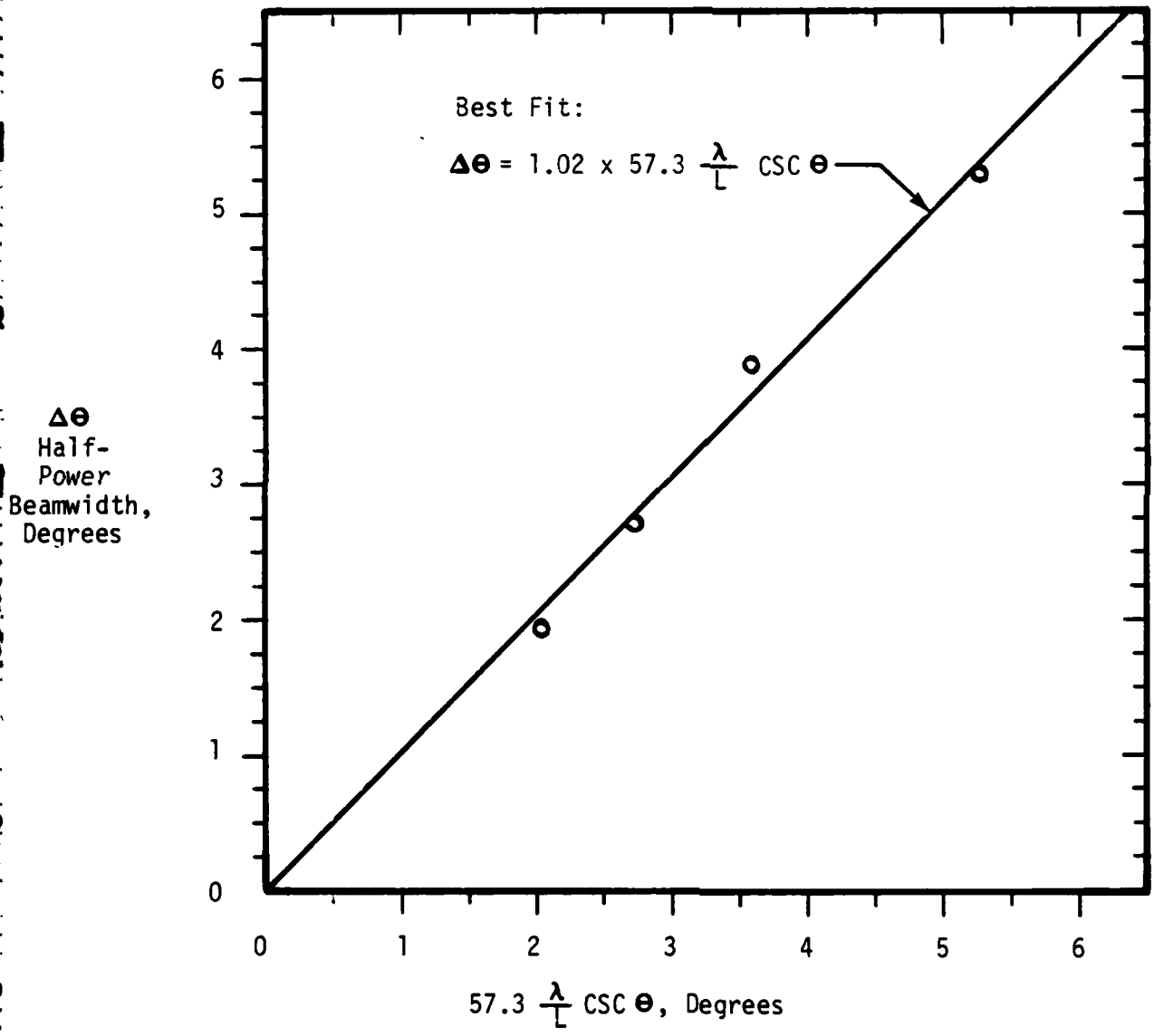

FIGURE 29b. HALF-POWER BEAMWIDTH VERSUS EFFECTIVE NORMALIZED LENGTH OF SPRING

Several attempts were made to obtain controlled radiation through the interaction of the 94GHz wave with conducting strips on the surface of cadmium sulfide slabs of different resistivities.

A mask of black, opaque tape was constructed with a period the same as that of the brass grating--i.e., 2.2mm. All slabs used were 2mm thick by 5mm wide by 20mm in length.

The CdS slabs had the characteristics listed in Table 8. The "low resistivity" sample has such a low value in the dark (1Ω-cm) that changes in its value with light are negligible. This slab was not expected to produce a beam, and such was the case.

The high resistivity sample was expected to produce a beam, but none was observed. Experimental evidence, and discussions with the manufacturer (Cleveland Crystals), indicate that the incident light diffuses throughout the slab. This is caused by surface and bulk scattering sites. Hence the entire slab "turns on," rather than just the un-masked portions.

During the course of these tests, it was observed that the placement of the slab under the dielectric waveguide results in a reduction in the power transmitted to the load detector through the polystyrene waveguide. This effect occurred whether the slab was illuminated or not. It was thought that the photoconductive slab was capturing the power from the polystyrene, because the slab has a much higher dielectric constant. It was found that a slab of silicon had the same result.

Three steps were taken to investigate this effect. These were:

(1) Obtain a dielectric waveguide having a much higher dielectric constant. Silicon was used for this test.

(2) Place a conductive pattern directly on the surface of a silicon slab (for use as a grating) to see if a beam can be observed with the polystyrene waveguide.

Each of these tests is discussed below.

3.4.7 Silicon Waveguide

Several pieces of undoped silicon ($n \cong 10^{10}$/cc) cut to a size of 10cm x 1mm x 1mm were obtained from Eagle-Picher Corporation. A brass structure was machined with a period of 1.2mm. This value was chosen to produce a beam at about 90° (according to Klohn[12], λ_g for silicon is about

TABLE 8.

CADMIUM SULFIDE SLABS

TYPE	CARRIER CONCENTRATION (n/cc) DARK	LIGHT	ρ (Ω-cm) DARK	LIGHT
LOW RESISTIVITY (c-axis $\perp$ Bar Length)	$\cong 10^{16}$	$10^{16} + 10^{10} \cong 10^{16}$	1Ω-cm	1Ω-cm
HIGH RESISTIVITY (c-axis $\parallel$ Bar Length)	$\leq 10^{10}$	NOT SPECIFIED	$\geq 4 \times 10^{9}$	10^{5}

1.2mm). The notch depth in the grating was made the same as the brass structure for polystyrene. The silicon proved extremely difficult to work with, not only in matching it to the metal waveguide but also in minimizing leakage radiation around the waveguide-silicon junction. In the absence of a grating, the power transmitted through the silicon to the load was very low compared to the polystyrene, and was of the order of 2 to 10 μ watts. The radiated beam, with the brass grating in place, was at an angle of 116°. This indicates a value for λ_g of 1.44mm. The power level was extremely weak, being near the noise level. Insufficient power was radiated to allow a meaningful measurement of the radiation pattern. However, it was observed that the polarization of the radiated beam was 90° from that of the radiation when polystyrene is used. It was concluded that the RF energy is too tightly bound to the silicon for this material to be suitable for diffraction electronics using a "detached" grating.

Klohn[12], et. al., reported work with silicon waveguide whereby conducting strips were attached directly to the silicon. They reported controlled radiation, but did not present any data on power levels, efficiencies, etc. In Klohn's work, beam steering is achieved either by frequency shifting, or by changing the dielectric constant of the silicon waveguide and, hence, λ_g. The change in dielectric constant is effected by bringing conducting plates or PIN diodes in close proximity to the dielectric. This approach is fundamentally different from the diffraction electronics work of this project.

3.4.8 Silicon Slab Grating

A grating was formed by placing strips of self-adhesive, conducting lead foil on the surface of a slab of "pure" silicon ($n \cong 10^{10/cc}$) obtained from Eagle-Picher Corporation. The slab dimensions were .04 inch thick (1mm) x 0.25 inch (6.4mm) wide x 2.5 inches (64mm) long. The strips were arranged as shown in Figure 30. The grating was placed under the polystyrene and several beams were formed.

The tilt and separation were adjusted to maximize the power in the "strongest" beam, which appeared at 94°. The formation of several beams was due to the irregular spacing. The principal beams and power levels are listed in Table 9. If the power levels shown are added up, the total is about .09/mw. This is about the same as that achieved with the lead foil grating on a glass slide.

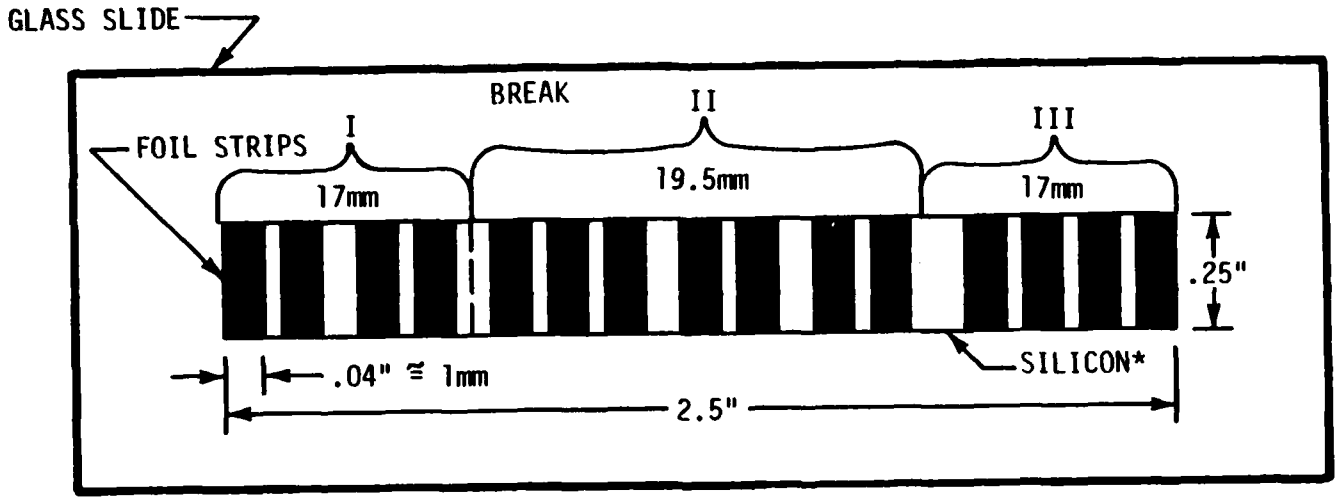

* Paraffin wax used to attach silicon. The slab was in two pieces, broken at the dotted line.

FIGURE 30. FOIL STRIPS ON SILICON SLAB

TABLE 9.

BEAM POWER LEVELS AND ANGLE θ
FOR FOIL ON SILICON

ANGLE (degrees)	POWER LEVEL (milliwatts)
94.0°	.024 mw
92.5°	.007 mw
89.5°	.018 mw
87.5°	.002 mw
82.0°	.0175mw
78.8°	.014 mw
64.0°	.008 mw

The effect of the silicon on power transmitted to the load was measured for 4 cases: (1) No Grating, (2) Plain Silicon Slab, (3) Slab with Foil Strips, and (4) Brass Structure. The values are summarized in Table 10.

The data shown in Tables 9 and 10 would seem to indicate that a "semiconductor grating"--i.e., conductive strips on the surface of a semiconductor such as silicon, would produce radiation but the efficiency would be extremely low. However, it is believed that the low amount of radiation at a given angle is primarily caused by the irregular spacing and the formation of many beams. Analogous experiments with laser excitation of silicon are given in section 3.9.

TABLE 10.

COMPARISON OF LOAD POWER LEVELS
WITH SILICON SLABS OR BRASS GRATING
LOCATED BENEATH POLYSTYRENE WAVEGUIDE

GRATING	LOAD POWER (mw)	RADIATION (DOMINANT BEAM)	
		θ (deg)	P (mw)
NONE	85	--	--
BRASS	0.8	105	.6
PLAIN SILICON SLAB	1.0	--	--
FOIL STRIPS ON SILICON SLAB	0.3	94	.024

3.5 ZnO VARISTOR STUDIES

3.5.1 Introduction

The objective of this task was to fabricate a periodic linear array of ZnO-based varistor elements which could be biased to provide either a highly conductive state or a resistive state. The linear array thus formed could then be used to diffract incident mm-waves. The diffraction angle could be adjusted by turning on or turning off the ZnO varistor elements to form new periodic array configurations. In this way, a solid state steerable beam antenna or detector could be produced. The results obtained to date indicate that thin film ZnO-based varistors can be fabricated, but the devices fabricated to date have not had the desired high degree of non-linearity in their I-V characteristic.

3.5.2 Device Fabrication

Bulk ZnO-based varistors are fabricated by sintering approximately 95 mole % ZnO with a variety of dopants such as Bi_2O_3, Al_2O_3, MgO, etc. The sintering step normally takes place at temperatures in excess of 1200 C. In the present effort, the fabrication of thin film ZnO-based varistor devices was carried out by evaporating Zn and Bi in the presence of an oxygen plasma. The desired reaction between Zn, Bi, and oxygen to form thin film Bi_2O_3 doped ZnO varistors was successfully carried out. However, the I-V characteristics of the resulting devices were not as non-linear as desired.

A dual-source electron beam evaporation system was used to prepare the coatings. A schematic diagram of the system is shown in Figure 31. Oxygen was admitted to the differentially pumped upper chamber through an electronic mass flow controller. A capacitance manometer was used to monitor the system pressure. Table 11 summarizes the coating deposition conditions. The output from an audio-frequency generator operating at 100 KHz was applied to the substrates. The 100 KHz substrate bias established an oxygen plasma which was required to obtain appreciable reaction between the evaporant and the background gases. The maximum ZnO deposition rate, which was determined by the reaction kinetics between the atomic oxygen plasma and the Zn vapor, was found to be 0.12 μm/min. Zn deposition rates of up to 7 μm/min. had excess metal in them. Coatings with excess metal

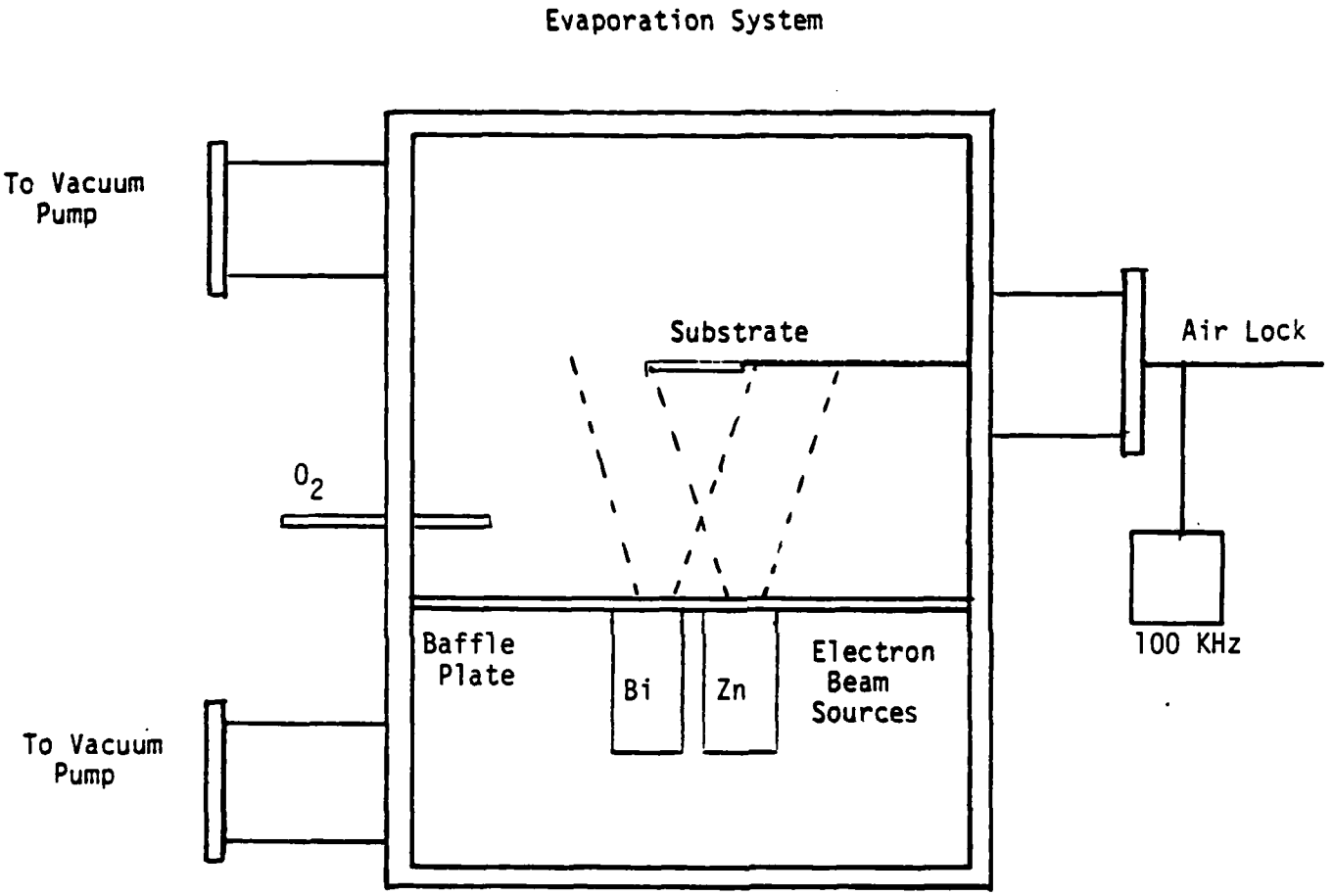

FIGURE 31. SCHEMATIC DIAGRAM OF THE ELECTRON BEAM EVAPORATION SYSTEM

TABLE 11.

SAMPLE PREPARATION CONDITIONS

PARAMETERS	VALUES
OXYGEN PRESSURE	2.7×10^{-3} torr
OXYGEN FLOW	170 sccm
Zn POWER	800 watts
Bi POWER	200 watts
DEPOSITION TIME	2.5 minutes
SUBSTRATE POWER	12.8 watts/cm^2
AIR OXIDIZED	460 C, 45 minutes

were oxidized by heating the coatings in air to 500 C. Since thick coatings were believed to be required, high coating rates were used and all samples were given a 500 C oxidation treatment after deposition. A metal contact mask was fabricated which provided for 10 strips of zinc oxide 1 cm x 0.2 cm spaced 0.2 cm apart to be formed on glass slides. These coatings on glass were then placed in an air furnace at 400 to 500 C and oxidized. Following this step, leads were attached with conductive epoxy and connected to test equipment. During the coating trials, the substrates were placed midway between the Zn and Bi sources so that the amount of Bi incorporated in the film varied from one end to the other. Bismuth and zinc contents were subsequently measured using the EDAX attachment on an SEM.

The I-V characteristics of the deposited coatings were measured with the circuit shown in Figure 32. The electrical circuit for this test consisted of a 0.2 μF capacitor which could be charged to voltage levels as high as 1000 volts and switched across the fabricated device. Voltage across and current through the device were recorded on a storage oscilloscope.

3.5.3 Results

The amount of Bi incorporated in the coating has a significant effect on the I-V characteristics of the Bi_2O_3 doped ZnO coatings. Figure 33 shows the I-V curves for several thin film Bi_2O_3 doped ZnO samples as well as for a commercially available varistor. The trend in the thin film devices is for the non-linearity to increase with decreasing bismuth content.

Scanning electron micrographs of the deposited coatings revealed a granular coating microstructure with particulate sizes of approximately 10 μm. A fibrous structure was also detected in the samples with lower bismuth content. A typical SEM micrograph of a ZnO varistor film is shown in Figure 34.

3.5.4 Conclusions

We conclude from this limited study that non-linear I-V characteristics can be obtained in thin film Bi_2O_3 doped ZnO varistors. However, additional work is needed to obtain devices with characteristics which are practical for beam steerable device fabrication.

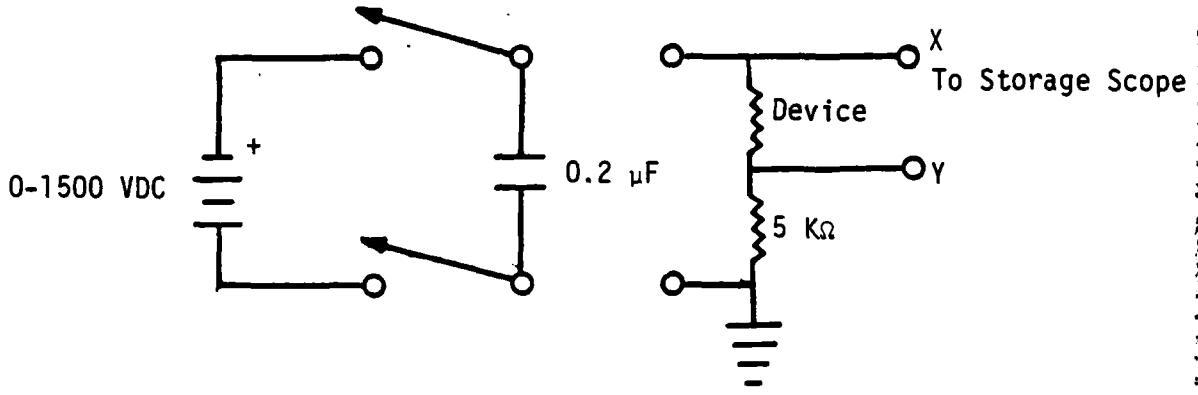

FIGURE 32. ELECTRICAL CIRCUIT FOR OBTAINING I-V CURVES FOR THIN FILM ZnO VARISTORS

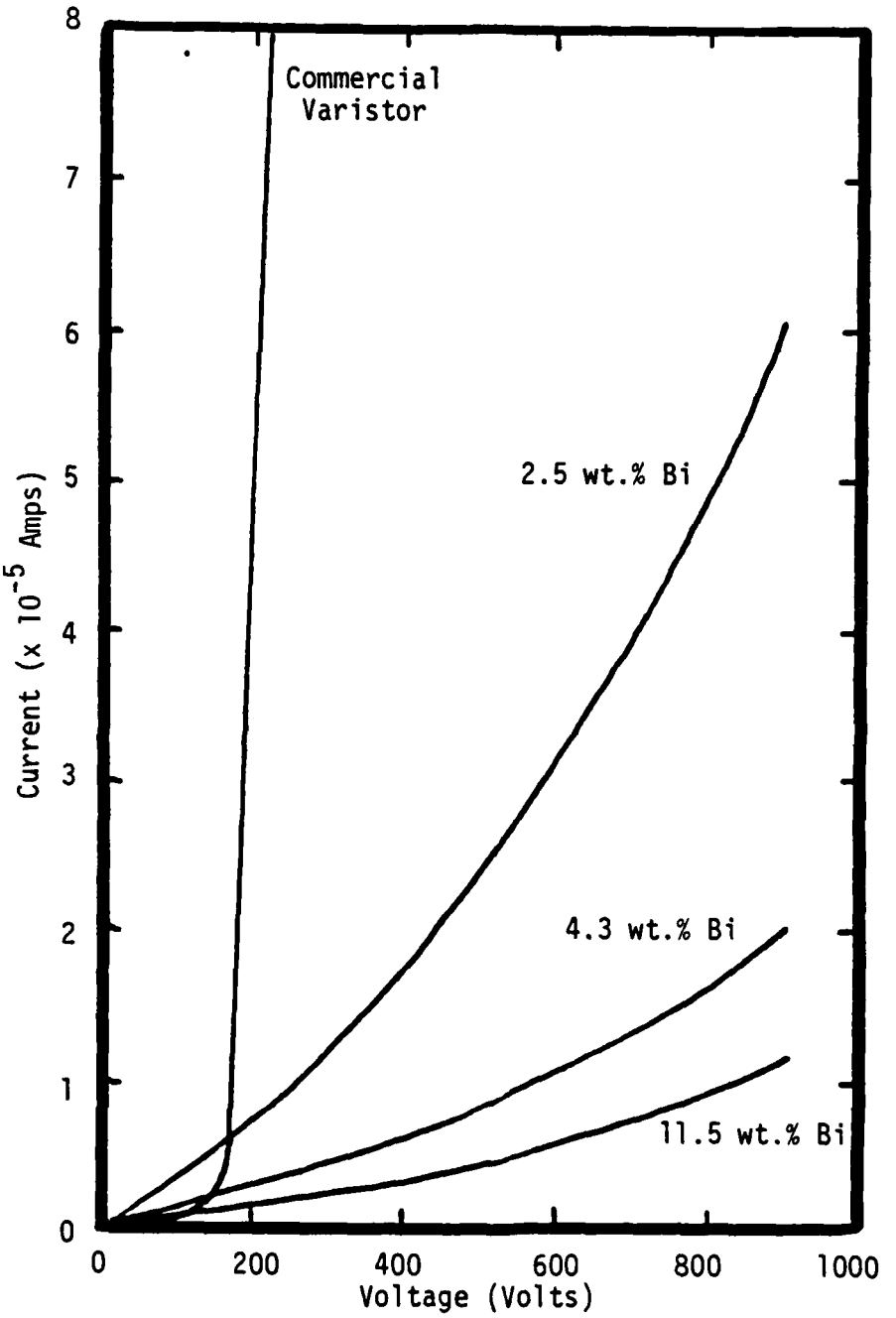

FIGURE 33. I-V CHARACTERISTICS FOR THIN FILM Bi_2O_3 DOPED ZnO VARISTORS

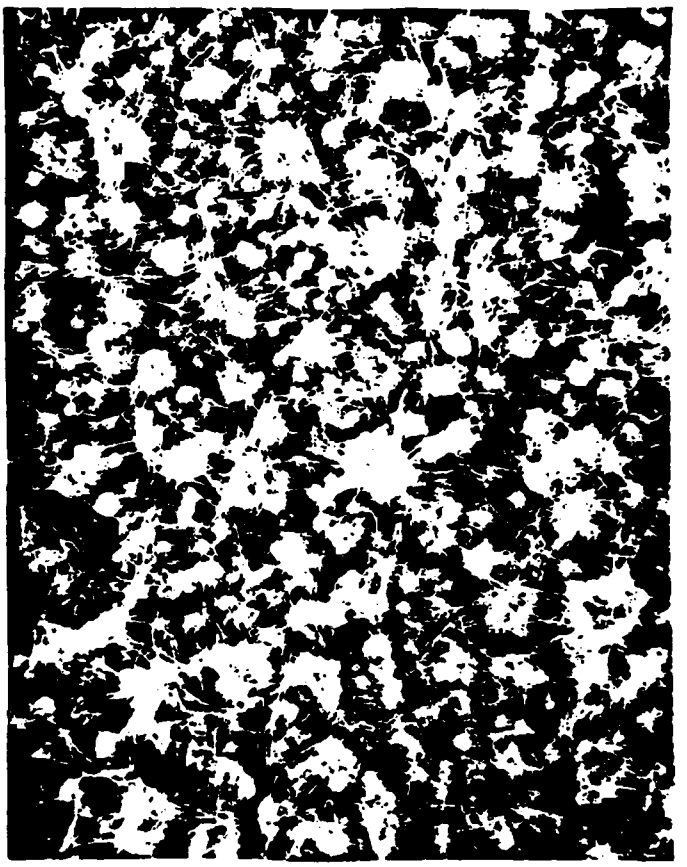

1200X

FIGURE 34. SCANNING ELECTRON MICROGRAPH OF A ZnO COATING DOPED WITH 2.5 WT.% Bi

3.6 MILLIMETER WAVE DIFFRACTION USING ACTIVE ACOUSTIC WAVES

3.6.1 Introduction

A conductivity grating can be generated by applying a Surface Acoustic Wave (SAW) to a semiconductor material in the presence of a large DC voltage. The large DC voltage (>1000 volts), which is applied across the semiconductor material parallel to the acoustic path, allows the electrons to randomly drift between the electrodes. These mobile carriers in the semiconductor are coupled to the surface acoustic wave through the associated electric fields. As the SAW travels across the surface of the semiconductor, it orients the randomly drifting electrons into a grating of high and low conductivity regions that are spaced at a distance equal to the acoustic wavelength. Researchers in the Soviet Union[13] as well as in the United States[14] have used this basic principle in the generation of surface acoustic wave amplifiers and sources.

A variety of semiconductor materials have been considered in the generation of "active" SAW devices. These materials include cadmium sulfide(CdS) and indium antimonide (InSb). In most cases the semiconductor is evaporated on high piezoelectric material, like lithium niobate ($LiNbO_3$). However, since CdS is both piezoelectric and semiconductor it was theorized that it could be used without a separate piezoelectric substrate.

3.6.2 Experiments

A SAW transducer was fabricated on a piece of CdS using standard photolithography. The transducer was designed to launch a 1 millimeter acoustic wave corresponding to the desired diffraction grating spacing for the silicon waveguide.

A narrow pulse was applied to the input SAW transducer in order to measure the acoustic velocity in the CdS and to study the effect of the DC voltage on the output amplitude.

The acoustic velocity in the CdS was measured to be 2125 meters per second. A typical SAW has a velocity of 3500 meters per second. This reduced velocity could imply a shallow bulk or even a pure bulk acoustic wave.

As predicted, the output of the SAW device was very dependent on the applied DC voltage. However, the results were not completely encouraging. The insertion loss of the SAW device was very high.

A variable DC supply was used to control the amount of random electron drift in the semiconductor while monitoring the output acoustic signal. The output power doubles as the DC voltage reaches 1500 volts over a 1 cm active region. It was also observed that adding additional light to the CdS crystal further increases the acoustic power out of the device. This is due primarily to the increased conductivity of the semiconductor and thus increased electron drift.

After verifying the concept of the active SAW device, the CdS crystal was placed below the silicon waveguide. The silicon waveguide was selected because the CdS tends to draw the power out of the polystyrene waveguide due to its high dielectric constant. Since silicon has a higher dielectric constant than CdS the millimeter wave remained in the waveguide.

A variety of acoustic frequencies and power levels were applied to the CdS crystal. However, the semiconductor device was never able to diffract the millimeter waves out of the waveguide.

3.6.3 Problems

In principle, it is still believed that an active SAW device can be used to diffract millimeter waves out of a waveguide. However, before this concept can be realized a variety of questions need to be addressed. The most important question is how the acoustic energy can be coupled into the semiconductor material with the proper power levels and frequencies to achieve the required conductivity grating. A bulk wave device probably lends itself to more efficient coupling at these wavelengths.

In addition, what materials could be used to enhance the conductivity grating? One logical choice would be InSb since many Soviet and U.S. researchers have shown it to be the most promising active SAW material. The InSb would be applied to a highly piezoelectric material, such as $LiNbO_3$.

A final problem which must be overcome is the question of system grounding. The high voltage DC supply that was used to supply the DC bias for the semiconductor had a ground that was hard to isolate from the RF signals. Even when an isolating AC supply was used to isolate the high voltage supply from the RF components, the high voltage found grounding paths which caused the electrons to drift in directions other than parallel to the acoustic path. This reduces the effectiveness of the randomly drifting electrons. This problem would be reduced if a semiconductor film was applied to an insulating piezoelectric crystal. In this case the electrons would only flow in the semiconductor film and would be unable to interact with the

RF components, i.e. the SAW transducers attached to the piezoelectric. In any case, care would be required in the layout of the high voltage electrodes and the acoustic transducers.

3.7 BULK ACOUSTIC WAVE DEVICES

Two experimenta were performed to determine if an adjustable grating for the beam steerable antenna could be generated using bulk acoustic wave devices. Earlier experiments showed that the millimeter wave beam could be diffracted with either a conductivity grating or a dielectric grating. It was hypothesized that a conductivity grating could be generated in a piezoelectric semiconductor, such as Gallium Arsenide (GaAs), by launching a strong bulk acoustic wave in the material with a wavelength equal to required grating spacing. If this worked, then simply adjusting the acoustic frequency would change the grating spacing and would steer the millimeter wave.

It was also hypothesized that a strong bulk acoustic wave in a piezoelectric material, such as lithium niobate or quartz, would generate a dielectric grading that would steer the antenna. Both of these experiments are described in the following sections.

3.7.1 Semiconductor Grating

The experimental device that was used to generate the conductivity grating in the GaAs is shown in Figure 35. The device consists of a 2" x 1/4" x 1/8" rod of GaAs, electrodes on the ends of the rod to produce a large DC electric field, a glass buffer layer for isolation between the electrodes and the piezoelectric transducers, and two PZT-4 piezoelectric transducers for generating the bulk acoustic waves.

The semiconductor GaAs was chosen as the material because it is both a piezoelectric and a semiconductor. Therefore, an acoustic wave that travels through the material generates a sinusoidal varying electric field at acoustic wavelength.

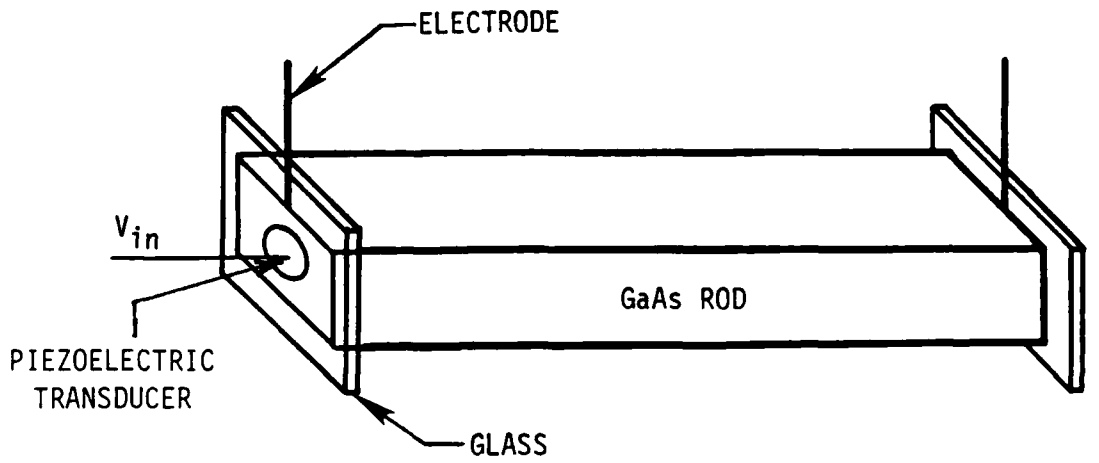

FIGURE 35. SEMI-CONDUCTOR GRATING

To aid in the generation of the conductivity grating, a large DC voltage (>1000 volts) was placed on the electrodes which generated a large DC electric field across the rod. When the electric field E is applied across the semiconductor, each electron experiences a net force of -qE from the field. Although the field has little effect on the random motion of a single electron, when averaged over all of the electrons, a net motion is observed towards the positive electrode.

Adding the electromagnetic acoustic wave in the semiconductor material again has little effect on the individual electrons. However, when allof the electrons are considered, the electrons would tend to cluster on the positive crests of the electromagnetic wave. Figure 36 shows conceptually how the conductivity grating was generated.

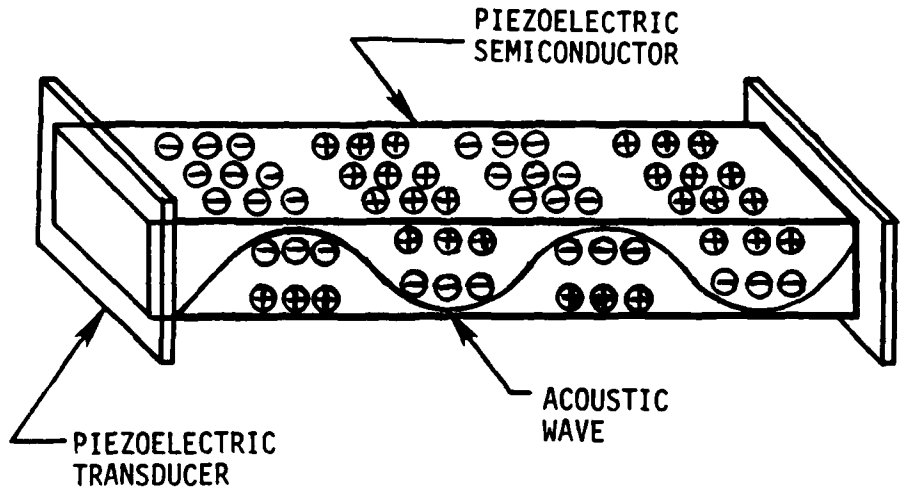

FIGURE 36. CONCEPTUAL DRAWING OF CONDUCTIVITY GRATING

3.7.2 Experimental Results

The acoustic velocity of the GaAs was measured by impulsing the input transducer and observing the output. The delay for the 2" rod was measured as ∿10 μsec. The velocity if therefore

$$\upsilon = \frac{L}{D} = \frac{2" \times 2.54 \text{ cm/inch}}{} = 5.08 \times 10^3 \text{ m/sec.}$$

The velocity of a compressional wave is 5.15×10^3 m/sec. Therefore, it was assumed that the piezoelectric transducers were generating compressional waves. The GaAs rods had many resonant modes due to the size and shape of the rod and piezoelectric transducers. One of the resonant modes had a frequency f_o = 1.877 MHz. The acoustic wavelength Λ at that frequency is equal to

$$\Lambda = \frac{\upsilon_a}{f_o} = \frac{5150 \text{ m/sec}}{1.877 \text{ MHz}} = 2.74 \text{ mm.}$$

This acoustic wavelength could create a grating with the same period which is similar in size to the metallic structures that were fabricated in the early phases of this project.

Substituting this grating period into the diffraction equation gives a predicted diffraction angle θ of:

$$\theta = \cos^{-1}\left(\frac{c}{v_g} - m\frac{\lambda}{\ell}\right)$$

where c is the velocity of light, v_g is the velocity of propagation in the waveguide, m is the mode number, λ is the wavelength of the 94 GHz millimeter wave, and ℓ is the grating period.

$$\theta = \cos^{-1}\left(1.22 - m\frac{3.2\ \text{mm}}{2.74\ \text{mm}}\right)$$

For m = 1

$$\theta_1 = \cos^{-1}(0.052) = 87^\circ .$$

The rod was placed under the dielectric waveguide in the configuration shown in Figure 37. The klystron was modulated at 1000 Hz and a spectrum analyzer was used to detect the modulation frequency on the crystal. To determine if the received signal was from diffraction of the acoustic waves or just due to leakage, the acoustic source was turned on and off while monitoring the received signal.

The position of the horn was swept over the entire arc in an effort to search for a diffracted wave. The bulk acoustic wave device was unsuccessful in creating a conductivity grating with the appropriate characteristics for steering the millimeter waves.

Another frequency that resonated in the rod was 950 KHz. The acoustic wavelength at that frequency is given by

$$\Lambda = \frac{v_a}{f_o} = \frac{5150\ \text{m/sec}}{950\ \text{KH}_z} = 5.4\ \text{mm}.$$

This grating period leads to 3 diffracted modes

$$m = 1 \qquad \theta_1 = 50.9^\circ$$
$$m = 2 \qquad \theta_2 = 87.7^\circ$$
$$m = 3 \qquad \theta_3 = 123.4^\circ \quad .$$

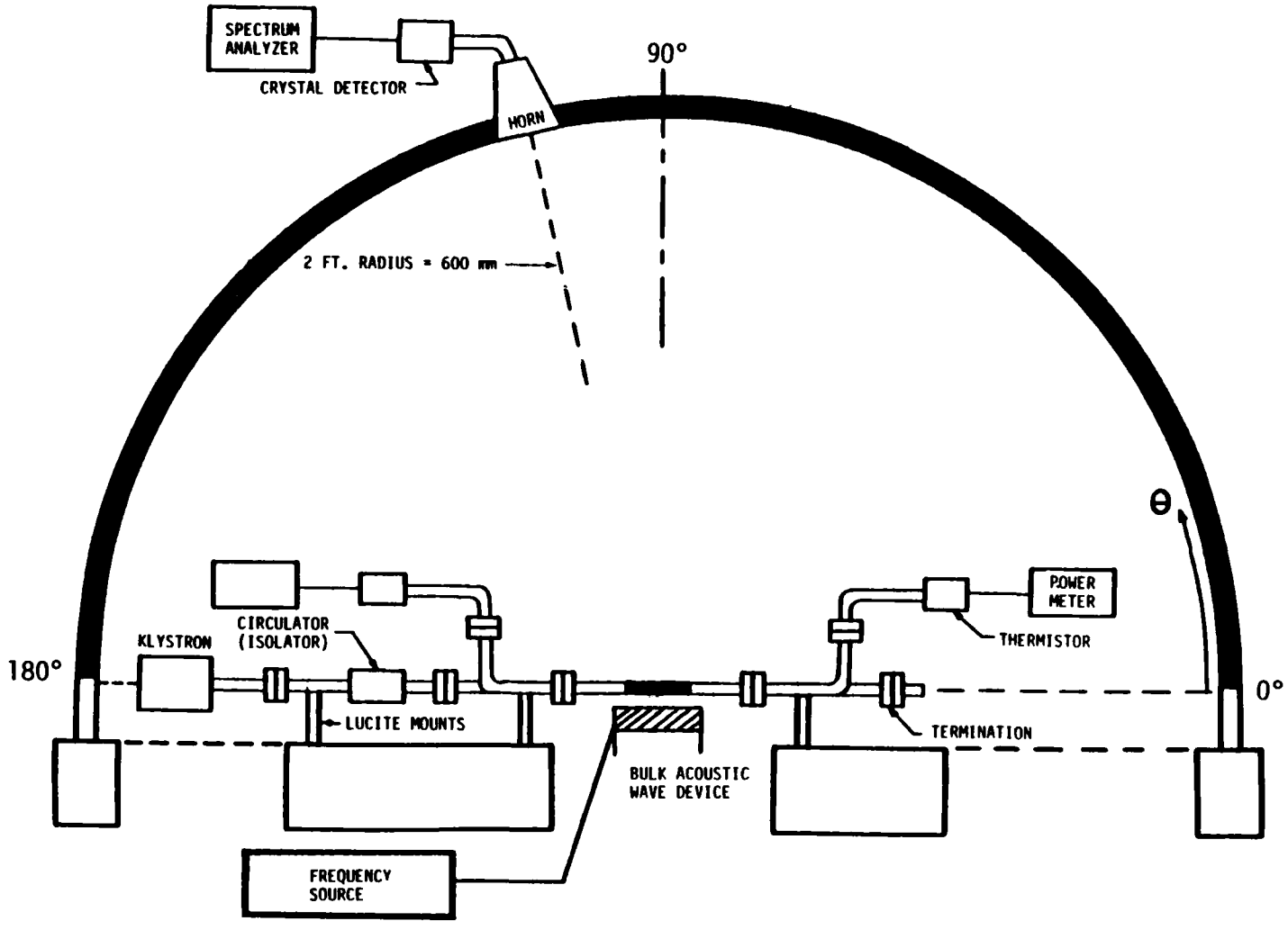

FIGURE 37. BULK ACOUSTIC WAVE PERIODIC STRUCTURE

Again, the horn was swept over the arc. No diffracted signals that could be attributed to the acoustic wave, were received.

Another frequency that resonated in the rod was f_o = 500 KHz. The acoustic wavelength was

$$\theta = \frac{\upsilon_a}{f_o} = \frac{5150 \text{ m/sec}}{500 \text{ KHz}} = 10.3 \text{ mm}$$

which leads to the following diffracted modes:

$$\begin{aligned} m &= 1 \quad \theta_1 = 24.58^\circ \\ m &= 2 \quad \theta_2 = 53.22^\circ \\ m &= 3 \quad \theta_3 = 73.26^\circ \\ m &= 4 \quad \theta_4 = 91.3^\circ \\ m &= 5 \quad \theta_5 = 109.5^\circ \\ m &= 6 \quad \theta_6 = 130^\circ \\ m &= 7 \quad \theta_7 = 163^\circ \quad . \end{aligned}$$

The horn on the arc was again swept over the arc. No diffracted signals were received.

3.7.3 Dielectric Grating

The experimental device for generating a dielectric grating in Lithium Niobate is shown in Figure 38. It consists of a 72 mm x 3 mm x 3 mm rod of Lithium Niobate with PZT-4 bulk wave transducers on each end. It was known from experiments in the first phase of this project that a millimeter wave beam could be formed by placing a dielectric grating under the dielectric waveguide. To further verify this assumption a group of clear glass slides were stacked, as shown in Figure 38 and placed under the waveguide. The period of the grating was approximately 2 millimeters. This corresponds to a diffraction angle given by

$$\theta = \cos^{-1}\left[1.22 - \frac{3.2}{2}\right] = 112^\circ \quad .$$

A beam was measured using the receiving antenna on the arc. The peak signal, which was located at $\theta = 121^\circ$, had an amplitude of 0.022 mW.

AD-A150 876 MILLIMETER-WAVE DIFFRACTION DEVICES AND MATERIALS(U) 2/2
BATTELLE COLUMBUS LABS OH M R SEILER ET AL. 28 DEC 84
AFOSR-TR-85-0131 F49620-82-C-0099

UNCLASSIFIED F/G 20/8 NL

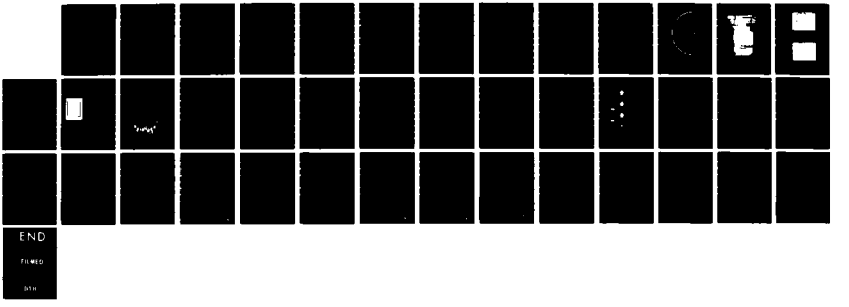

END

FILMED

DTIC

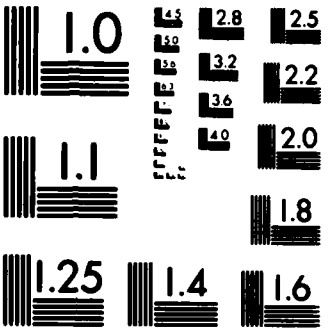

MICROCOPY RESOLUTION TEST CHART
NATIONAL BUREAU OF STANDARDS-1963-A

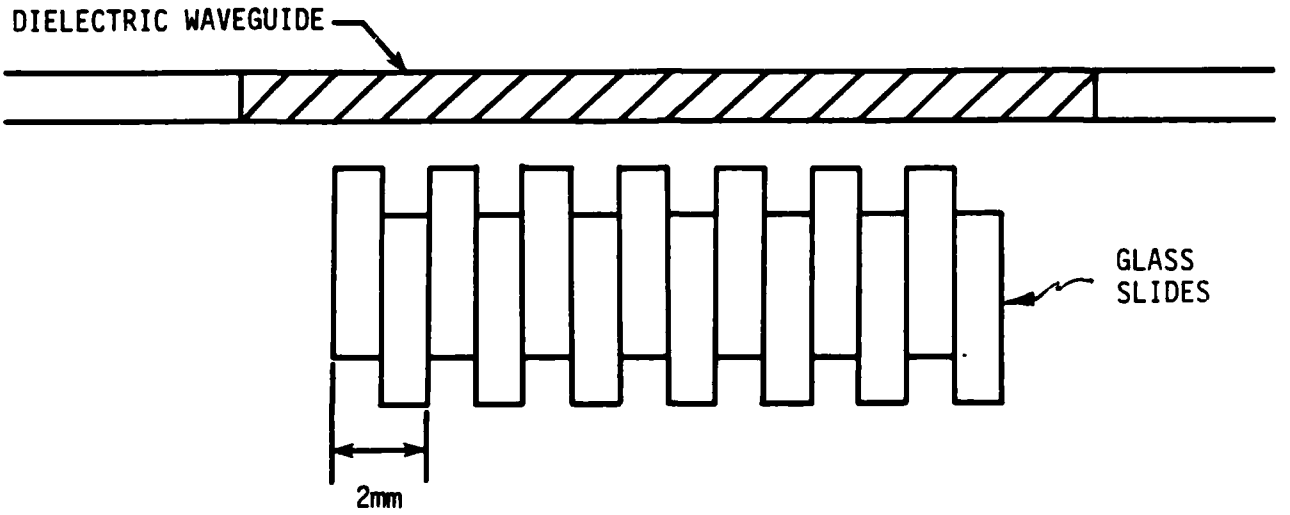

FIGURE 38. DIELECTRIC GRATING

The signal fell by 6 dB (to 0.005 mW) at 125° and 118.5° and the power was consistently lower at all other angles.

The acoustic velocity in the Lithium Niobate was measured by impulsing the input transducer and observing the delay on the output transducer. The delay in the 72 millimeter crystal was 22 microseconds. The velocity was, therefore,

$$v_a = \frac{\ell}{t_d} = \frac{72 \text{ mm}}{11 \text{ } \mu\text{sec}} = 6545 \text{ m/sec} \quad .$$

The crystal had many resonant frequencies in which a strong acoustic wave would propagate down the rod. One of the resonant frequencies was 3854 kHz which led to an acoustic wavelength of

$$\Lambda = \frac{v_a}{f} = \frac{6545 \text{ m/sec}}{2854 \text{ kHz}} = 2.29 \text{ mm} \quad .$$

This wavelength would correspond to a diffraction angle of 99.5°. An experimental arrangement similar to that used with the GaAs device was used to attempt to observe the diffracted beam, however, no diffraction was observed.

3.8 FERRITE EXPERIMENTS

The following pages describe a series of experiments with a ferrite material purchased from AMPEX. Specifically it is their Type 0, low power, square-loop lithium ferrite, Part No. 3.5000 A. As received, it was in slabs 2.5 cm wide x 14 cm long x 0.07 cm thick. Specifications were:

$4\pi M_s$ = 5000 gauss
ε_r = 14.5
$\tan\delta_\varepsilon$ = $\leq 1 \times 10^{-3}$
T_c = 400°C
H_c = 1.0 oersted
B_r = 3200 gauss

3.8.1 Ferrite Waveguide

A waveguide for the 94 GHz experiment was fabricated from the ferrite. Its dimensions were 0.5 mm x 0.8 mm x 10 cm. When used with a 2 mm period brass grating (Figure 39) the dominant radiation lobe occurred at 104.2° in the X-Z plane. Smaller lobes were also observed, as shown in Table 12.

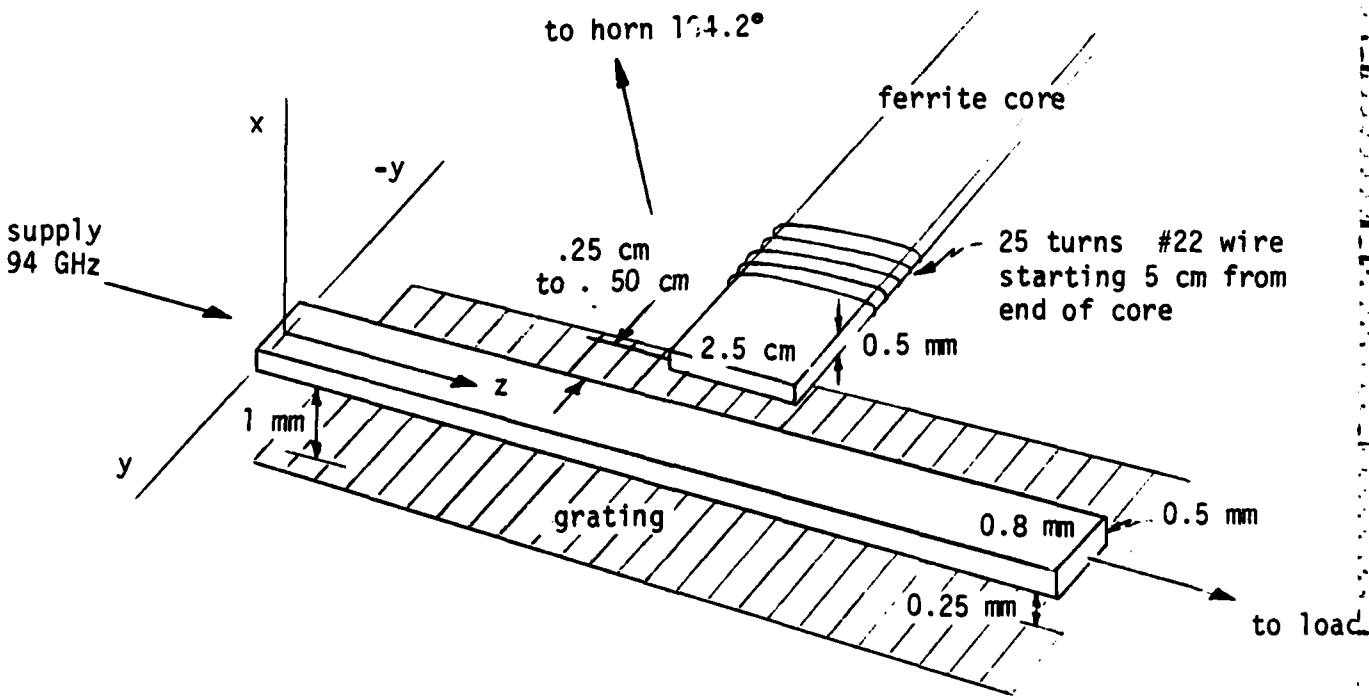

FIGURE 39. FERRITE WAVEGUIDE CONFIGURATION

TABLE 12. OBSERVED RADIATION LOBES WITH FERRITE WAVEGUIDE AND 2 MM GRATING

Lobe Location, degrees	Observed Peak Power, m watt
104.2	0.12
114.5	0.06
128.6	0.03
132.4	0.09

An electromagnet was fabricated using the same ferrite material as the core. The core was 14-1/2 cm long x 1 cm wide x 0.5 mm thick and placed as shown in Figure 39, 0.25 to 0.50 cm from the waveguide. The results were as shown in Table 13. The changes in received power at the horn were negligible and no alteration in the radiation angle was observed.

The intent of the experiment was to show if beam steering would be achieved by altering the propagation velocity, V_g, in the ferrite guide. That is, in the basic diffraction equation we would be altering c/V_g rather than λ/ℓ. In an attempt to obtain improved results a number of configurations were used. Results are summarized in Table 14. Figure 40 illustrates the configurations.

TABLE 13. RESULTS OF ELECTROMAGNET-FERRITE WAVEGUIDE TESTS

Radiation Angle = 104.2°

	Received Power at Horn	Reflected Power Toward Source	Load Power
H field off	0.10 mw	0.18 mw	0.19 mw
H field on (200 milliamps to coil)	0.11 mw	0.17 mw	0.18 mw

TABLE 14. SUMMARY OF ELECTROMAGNET TESTS ON FERRITE WAVEGUIDE

Experiment Designation Fig. 40	Electromagnet Configuration		Received Power at Horn, mW	Maximum Radiation Angle, degrees	Reflected Power toward Source, mW	Load Power, mW
B	Two electromagnets, oriented N-S on opposite sides of waveguide, 25 turns each	H "off"	.10	104.2	.18	.19
		H "on" 200 ma	.07	104.2	.23	.17
C	Same as B except 75 turns each	H "off"	.11	104.2	.18	.16
		H "on" 200 ma	.09	104.3	.21	.14
D	Same as C except magnets opposing, N-N.	H "off"	.11	104.2	.17	.16
		H "on" 200 ma	.13	104.6	.19	.11
E	Magnets on same side of guide	H "off"	.11	104.2	.17	.16
		H "on" 200 ma	.17	105.7	.11	.08

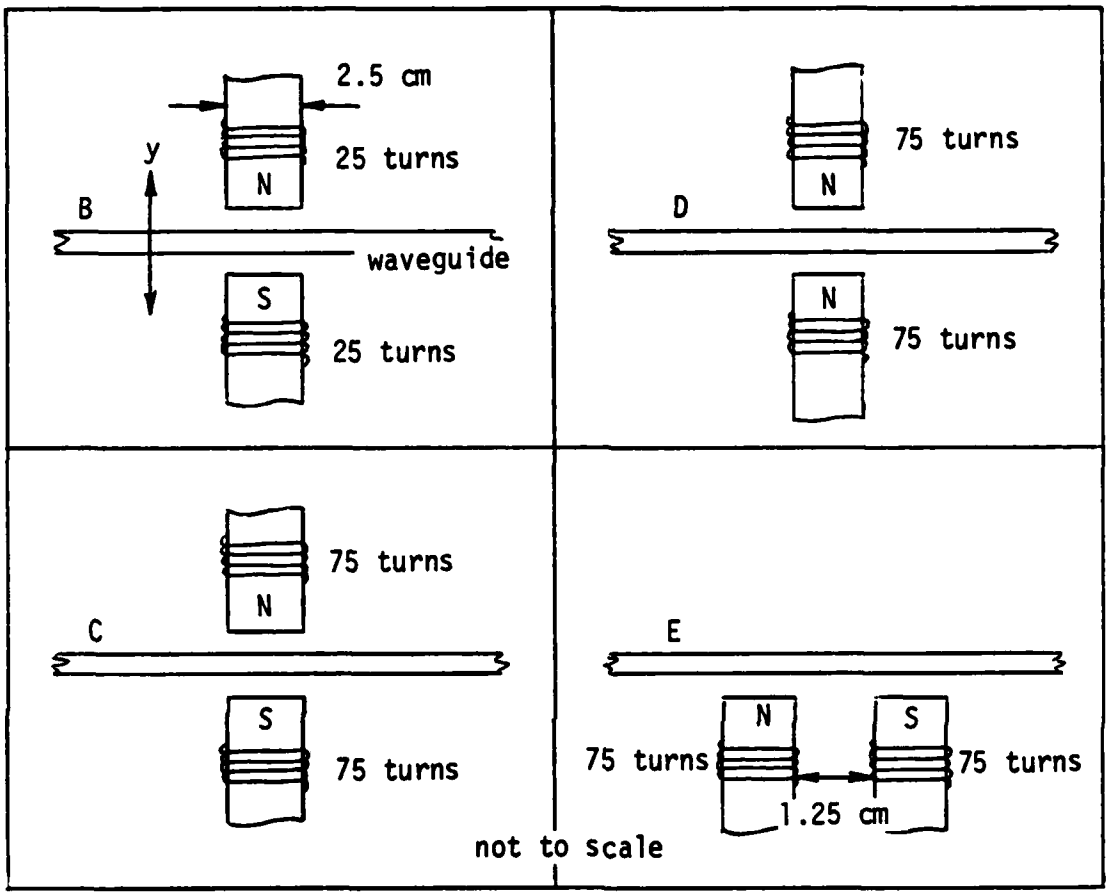

FIGURE 40. CONFIGURATION OF THE ELECTROMAGNETS

The conclusions are that a longitudinal B field (Configuration E) produces the greatest effect on radiation angle and radiated power. However, the magnitude of the steering effect is still small (104.2 to 105.7°).

Another series of tests was also conducted with a permanent horseshoe magnet oriented along the Y direction of the waveguide. The effect was to decrease the radiated power, increase the reflected power, and to also decrease the load power as the magnet was applied. Various permanent magnet field strengths did not change the above trends.

In order to utilize the longitudinal field effect, another configuration was tested which used a co-axial helix wound on 0.010 inch clear acrylic sheet. The diameter of the coil was 4 inches and its length was 10 inches, as shown in Figure 41. With 1.5 amperes applied to the coil there was some small beam steering effect, as shown in Table 15.

It is concluded from these ferrite waveguide tests that a longitudinal H-field will cause a relatively weak effect on the permeability of the ferrite, change the propagation velocity, and hence produce a slight change in the radiation angle. However, there are additional problems created by the changing VSWR of the waveguide. Considerable effort would need to be expended in order to improve the performance, and even then it is doubtful that a highly useful antenna could be achieved by this technique.

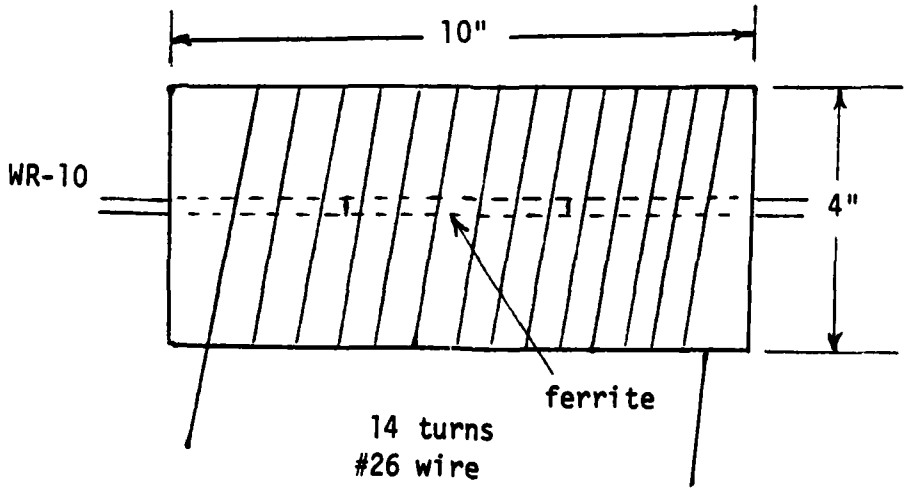

FIGURE 41. HELICAL COIL, COAXIAL WITH WAVEGUIDE

TABLE 15. BEAM EFFECTS WITH COAXIAL H-FIELD

	Received Beam Power mW	Radiation Angle degrees	Reflected Power mW	Local Power mW
H-field "off"	.084	109.5	.20	.042
H-field "on"	.087	108.5	.23	.048

Above tests were with a 2 mm brass grating.

3.9 LASER EXCITED GRATING EXPERIMENTS

3.9.1 Silicon Grating

A number of experiments were conducted with a laser excited photoconductor grating to achieve a periodic structure. The basic experiment is described in Figures 42 and 43 where the laser is illuminating a silicon film placed either above or below the dielectric waveguide.

A 1.06 micrometer Nd:YAG laser creates 10 pulses per second, each approximately 300 picoseconds to 3 nanoseconds in duration. The beam is "spoiled" so as to fill a reflecting mirror that is 2.5 inches in diameter. The beam then was passed through a 400 mm focal length cylindrical lens so that a rectangular area 6 mm by 63 mm was illuminated near the polystyrene waveguide. A fused silica microscope slide was coated on one side with an amorphous silicon film of 1 micrometer thickness. This film was deposited by physical vapor deposition (PVD) in the Battelle laboratory. The silicon also has a grown SiO protective passivation layer of approximately 0.2 micrometer thickness. The silicon film is placed within the evanescent mode coupling distance from the waveguide--a nominal distance of 1 to 5 mm. The illuminated side of the microscope slide was prepared with a periodic mask to create a 2 mm periodicity. A photograph of the grating is shown in Figure 44.

In operation, the 94 GHz klystron is first turned on without the laser illumination. The thickness of the microscope slide is sufficient to ensure that no radiated beam is formed from the periodic mask. (Such radiation had previously been seen from masks placed too close to the waveguide.) Figure 45 shows the noise level spectrum from the crystal detector/horn receiver on the arc. With laser illumination at a prf of 10 Hz a spatial conductivity variation is created on the silicon film. When the silicon film is placed above the waveguide, the resultant beam occurred at an angle of 76 degrees*. The spectral analysis of the crystal detector output is shown in Figure 46. The signal also contains harmonics.

---

*This angle is different than previous grating results for the same 2 mm spacing. When the grating is placed below the waveguide the beam occurs at 103 degrees.

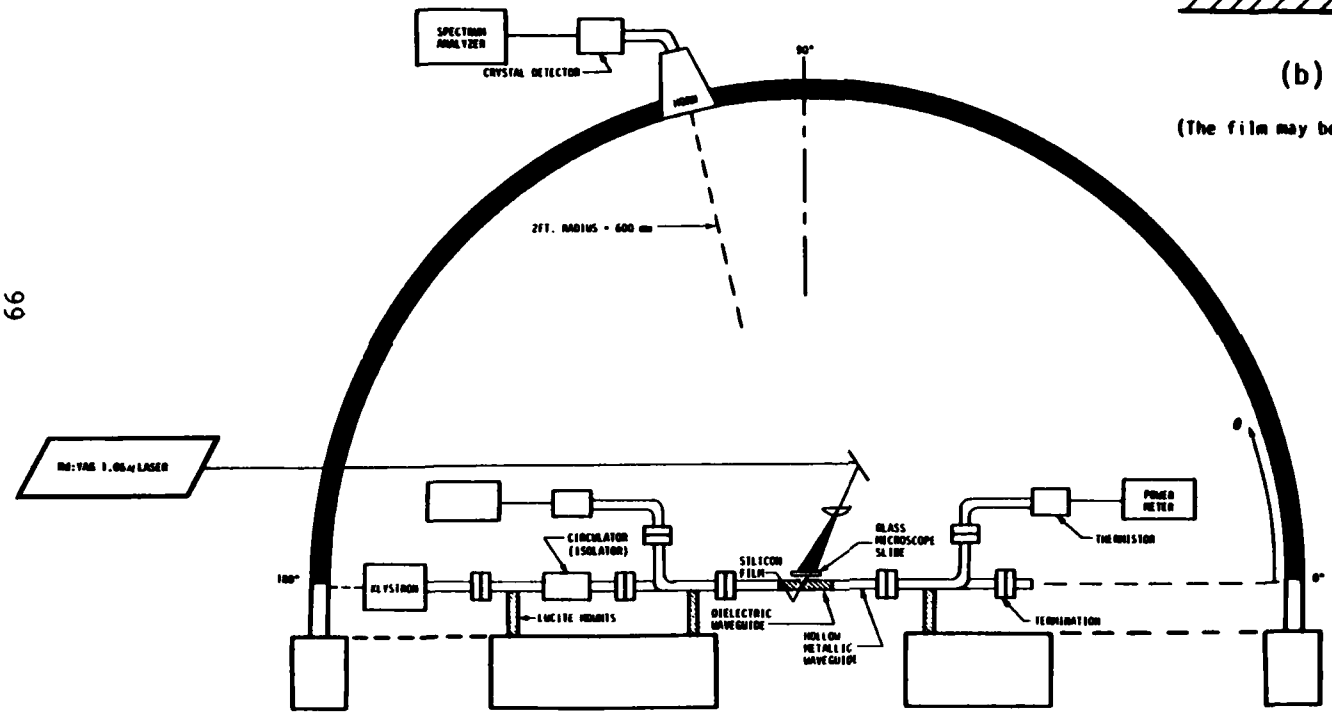

(a) OVERVIEW OF EXPERIMENT

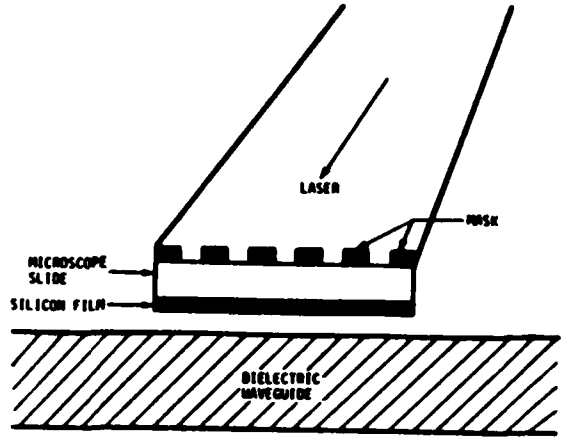

(b) SEMICONDUCTOR FILM

(The film may be placed on either side of the waveguide)

FIGURE 42. BASIC ARRANGEMENT FOR LASER EXCITED PHOTOCONDUCTIVE GRATING EXPERIMENT

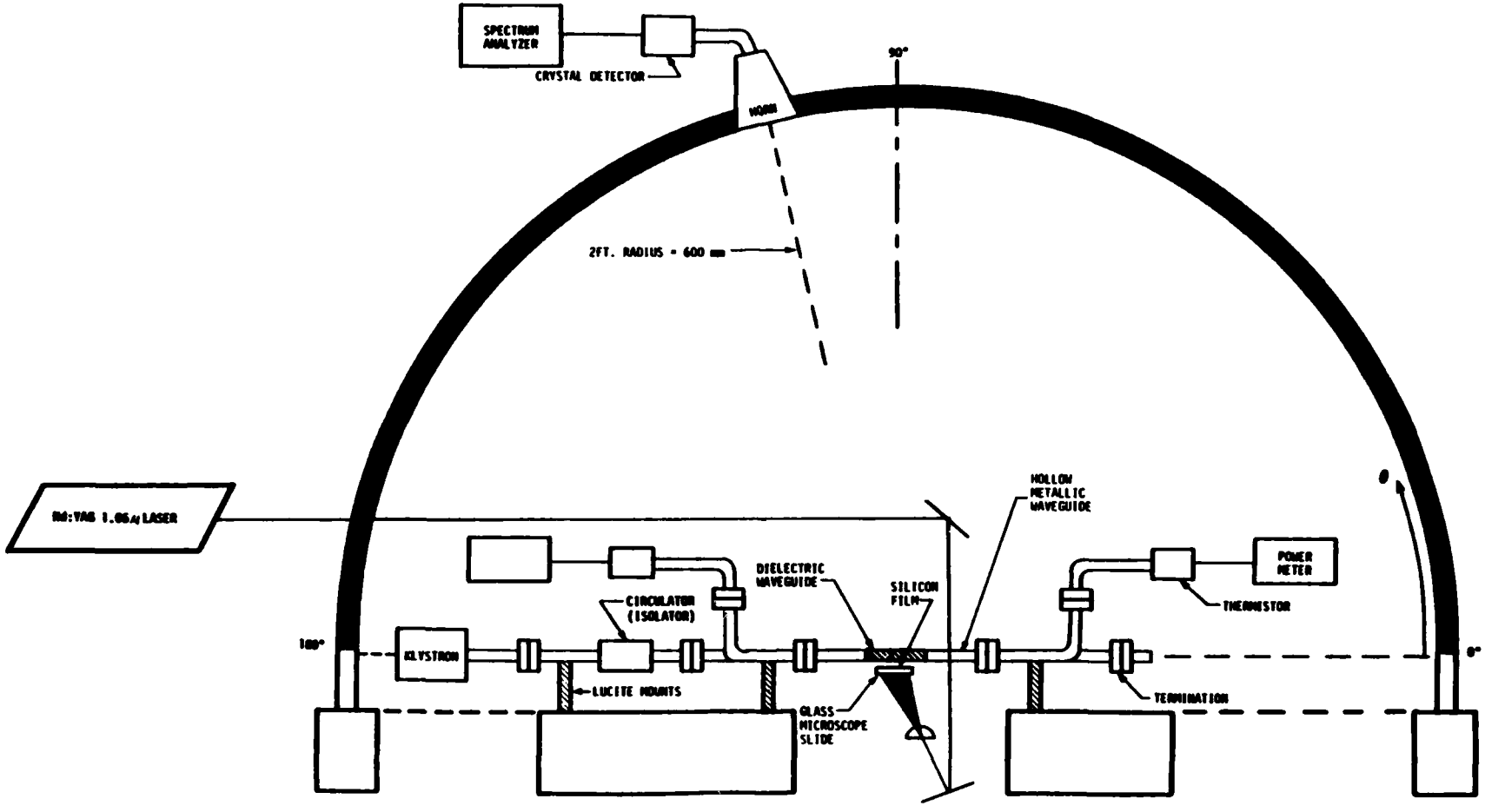

FIGURE 43. LASER EXCITED PHOTOCONDUCTIVE GRATING EXPERIMENT (UNDERSIDE ILLUMINATED)

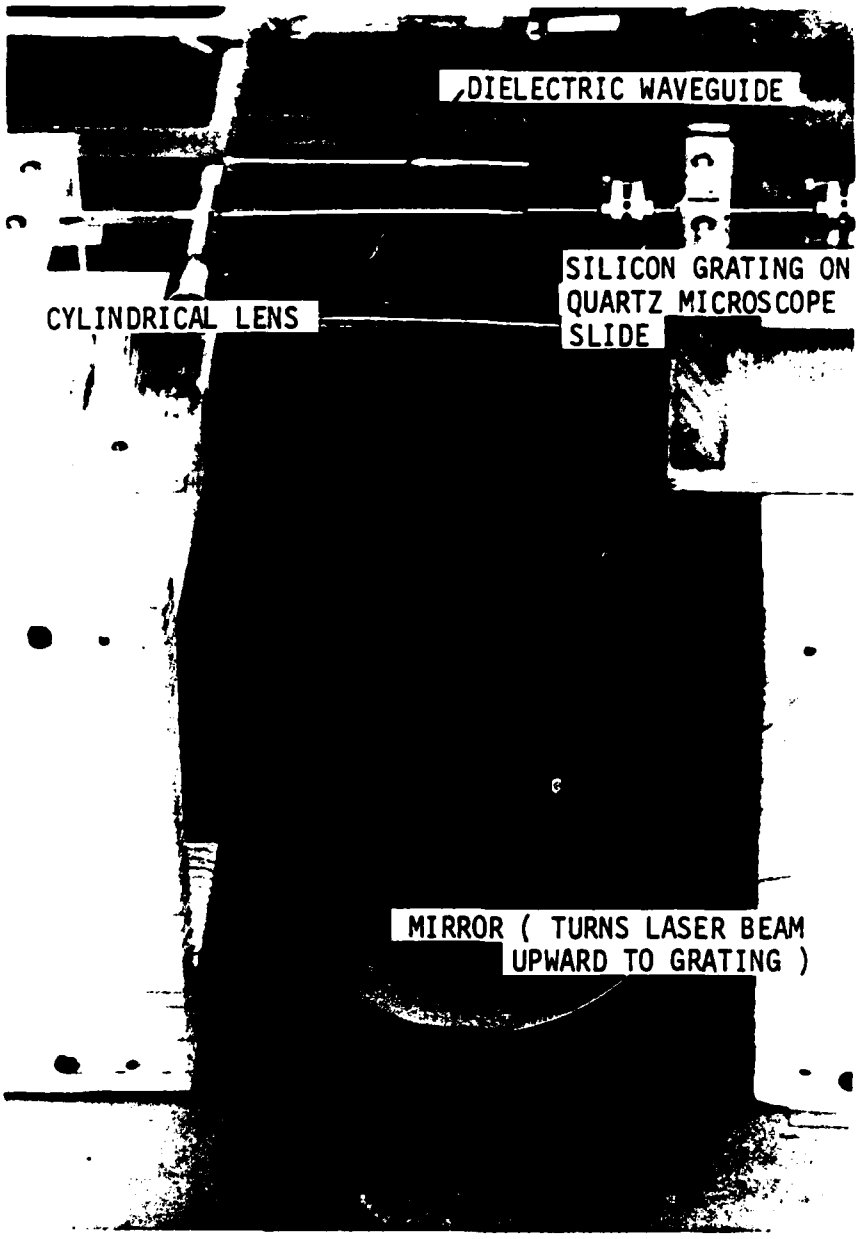

FIGURE 44. PHOTOCONDUCTIVE GRATING

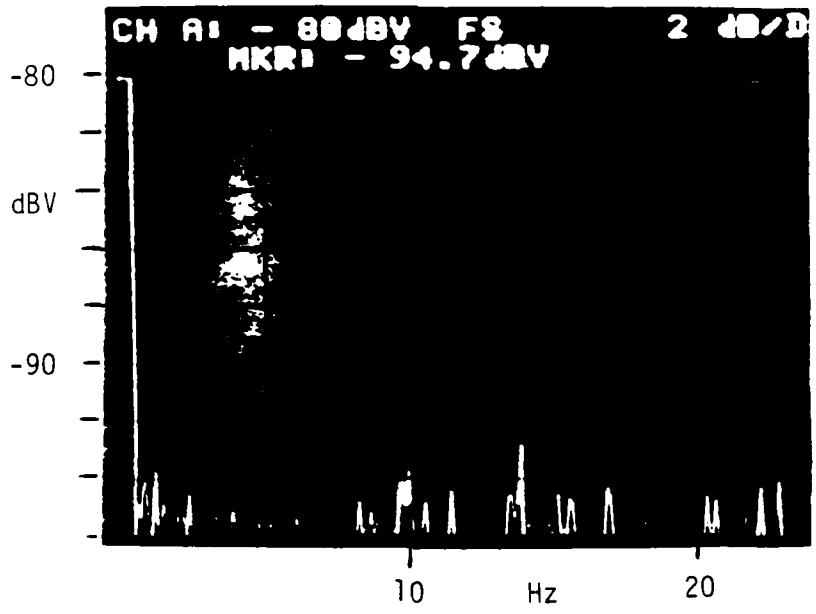

FIGURE 45. POWER DENSITY SPECTRUM WITH LASER ILLUMINATION

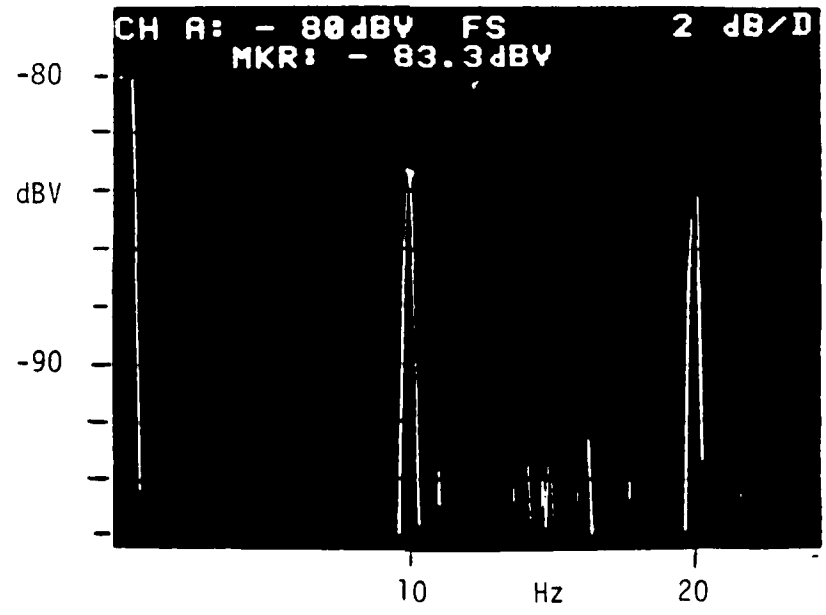

FIGURE 46. POWER DENSITY SPECTRUM WITH LASER ILLUMINATION OF SEMICONDUCTOR

(Only the 20 Hz harmonic component is shown.) The 10 Hz component shows a voltage ratio of 10. Figure 47 gives the transient waveform of two pulses from the 94 GHz crystal detector and makes a comparison with the laser pulse. The laser pulse is approximately 3 nanoseconds duration while the crystal response shows a pulse on the order of 1 microsecond duration. The experiment was repeated at a later date after disassembly and subsequent use of the laser for other experiments. The crystal response in the second experiment is shown in Figure 48. The second spurious laser pulse after 45 microseconds is less distinct.

An extended time trace of the system noise is shown in Figure 49. (Note the voltage scale change.) The relative magnitude of signal and noise is not inconsistent with the spectral data of Figures 45 and 46.

The photoconductive response of the silicon was measured with the same laser pulse excitation. Results are shown in Figure 50. It is concluded that the 94 GHz response is characteristic of the photoconductive lifetime of silicon and a thermal process is not being observed.

By monitoring the waveguide power to the load before and after laser illumination, the total radiated power was noted. (No increase in reflected power from the antenna toward the source was observed.) This radiated power is only about 4% of the total waveguide power. An efficient antenna would radiate more than 50% of the applied power.

Other details of the experiment are given in Table 16. No parameters have as yet been optimized. It is suspected that the photoconductive film needs to be thicker—it is semi-transparent to the eye but a spectral transmission has not been measured. It would be desirable to frequency double the 1.06 micrometer radiation to determine if improved response is obtained. Neither 1.06 nor 0.53 micrometer radiation is optimum for silicon, however.

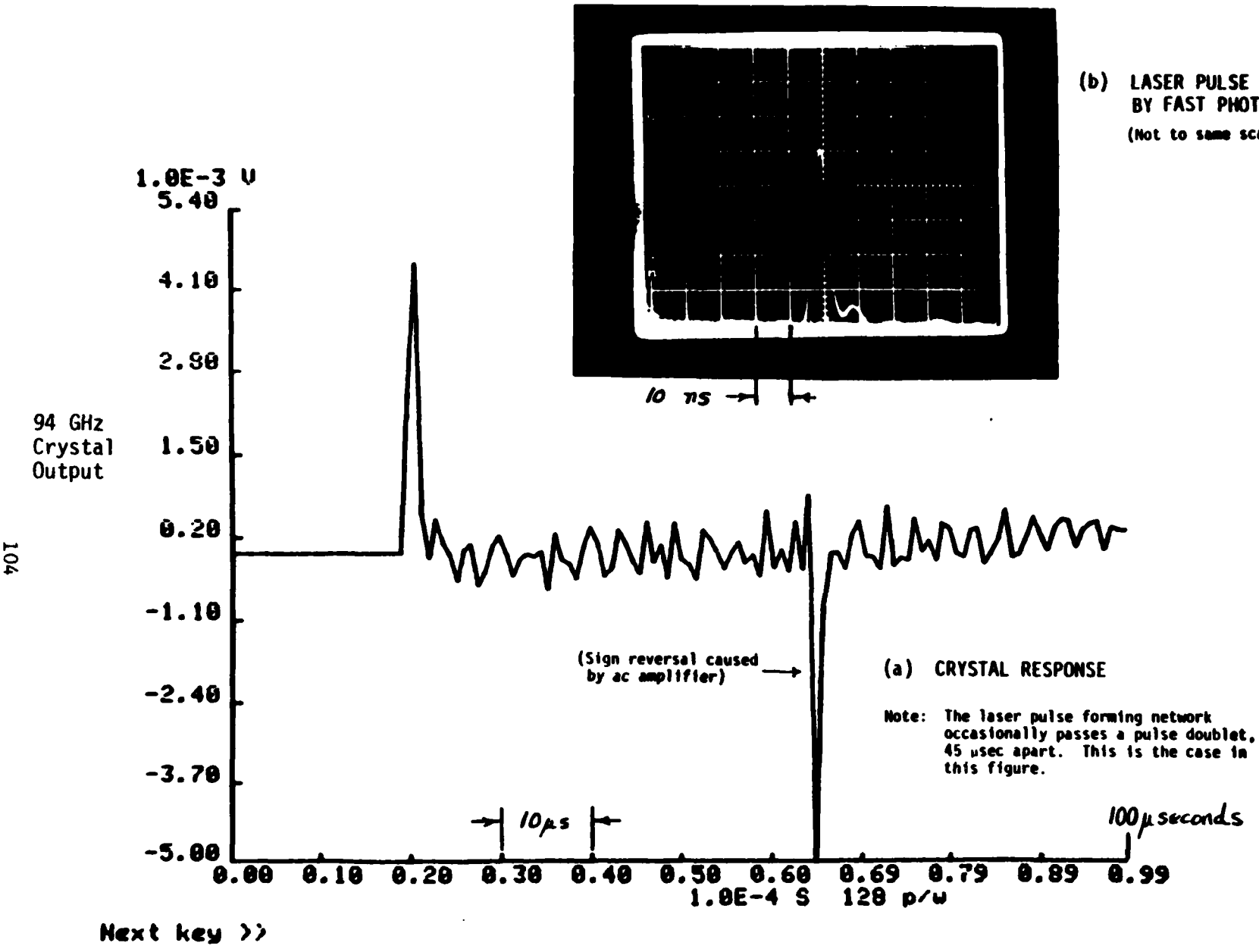

FIGURE 47. RF CRYSTAL TRANSIENT RESPONSE TO LASER-PULSED GRATING

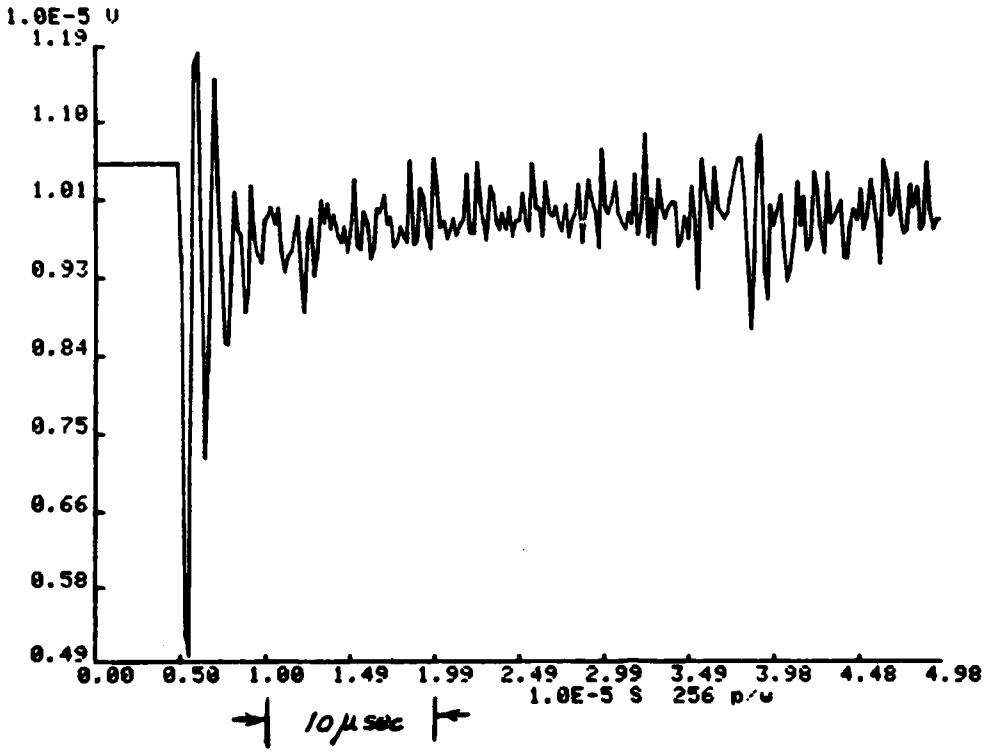

FIGURE 48. 94 GHz CRYSTAL RESPONSE
(2nd EXPERIMENT)

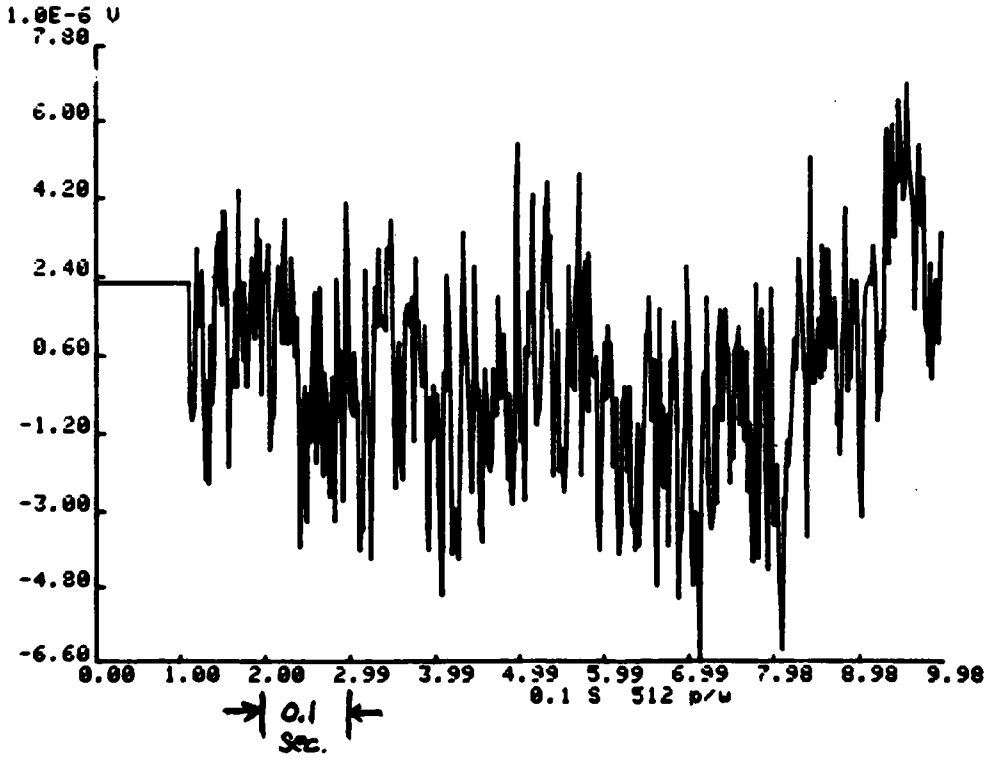

FIGURE 49. SYSTEM NOISE

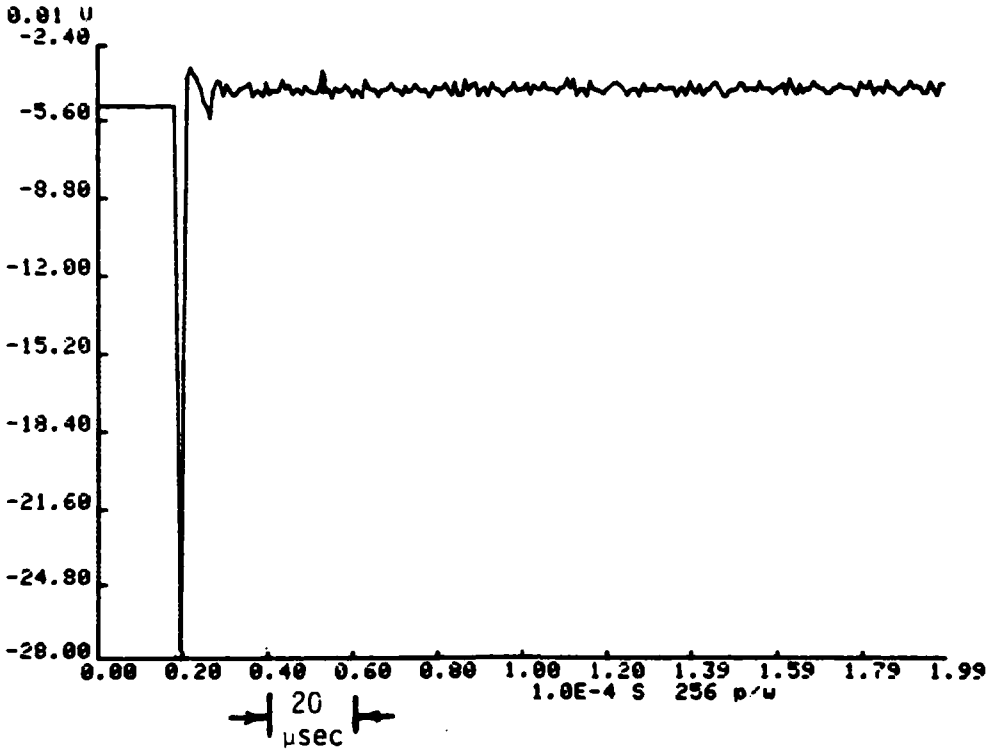

FIGURE 50. PHOTOCONDUCTIVE RESPONSE OF SILICON

TABLE 16. PARAMETERS OF THE LASER ILLUMINATED PERIODIC STRUCTURE

Laser: 1.06μ, Nd:YAG	Output: 16 mj per pulse 10 pulses per second 3 nanoseconds per pulse
Illumination on Photo-conductive Layer:	Total: 0.54 mj/cm^2 per pulse Per 1 x 3 mm area: ~20 μjoules per pulse
Silicon:	n-type, amorphous, 1 micrometer thick Approximately resistivity: 2000-3000 Ωcm
Grating:	Period = 2.0 mm Total illuminated area, 6 x 63 mm

3.9.2 GaAs Grating

Bulk single crystal samples of GaAs, purchased from COMINCO, were used in experiments where periodic illumination was achieved by irradiating the crystal surface through masks placed directly on the GaAs. Since the material thickness was so large compared with the absorption depth, the samples had to be illuminated through the polystyrene waveguide. This caused severe heating effects in the waveguide and thermally induced effects in the radiation field.

These experiments do not rule out GaAs for consideration. Future experiments should resort to thin films with excitation through the substrate--much like the silicon experiments.

3.9.3 Future Designs

The required laser flux on the photoconductive layer will depend upon material parameters as well as the desired conductivity modulation. A limited number of tests with varying conductivity films has given some guidelines. These previous results* show that two criteria appear to be important to achieve a conductivity grating that will form a useful millimeter-wave beam. These are:

(1) The dark conductivity, or minimum conductivity, should be of the order of 10^{-2} ohm^{-1} cm^{-1}

(2) The maximum conductivity should be at least 10^3 to 10^5 times greater.

In other words it would <u>not</u> be productive to achieve a grating or periodic structure that alternated between 10^{-6} ohm^{-1} cm^{-1} and 10^{-2} ohm^{-1} cm^{-1}.

The conductivity modulation is dependent upon the effective number of injected carriers. Approximately, for pulse widths small in comparison with the excess carrier lifetime,

---

*See Section 3.4.1 of this report. The dark resistivity should be $\rho = t \times S$ where S = ohms/sq and t = thickness. With $S \approx 2 \times 10^6$ and $t = 10^{-4}$ cm, $\rho = 200$ ohm-cm.

Δn = change in carrier concentration in a layer of thickness equal to $1/\alpha$, cm.

$$= \frac{P\eta\alpha\delta}{hf}, \text{ cm}^{-3},$$

where

P = laser flux density, watts/cm^2

h = Planck's constant = 6.6×10^{-34} joule-sec

f = frequency of laser, Hz

η = quantum efficiency

α = absorption coefficient at frequency f, cm^{-1}

δ = pulse width, seconds.

From earlier experiments it is desired that $n \geq 1000\ n$, where n is the dark carrier concentration. For optimized material α may be on the order of 10^4 cm^{-1} (absorption depth of one micrometer). Hence

$$P\delta \geq \frac{hf\ 1000\ n}{\eta\alpha} = \frac{6.6 \times 10^{-34} \times 5 \times 10^{14} \times 1000\ n}{0.5 \times 10^4}$$

$$\geq 6.6 \times 10^{-19}\ n \quad \text{joules/cm}^2 \quad (\delta << \tau)$$

The above relationship illustrates that moderately low carrier concentration material* with sufficient lifetime (τ) is needed to keep the required energy density at attainable levels. For example, GaAs with $n \approx 10^{14}$ carriers/cm^3 would give

$$P\delta \approx 6.6 \times 10^{-5} \text{ joules/cm}^2 = 6.6 \times 10^{-7} \text{ joules/mm}^2.$$

An illuminated strip 1 mm by 3 mm would then require about 2 microjoules per pulse. This is a reasonably attainable goal with commercially available laser diodes. Typically pulse outputs are 2-10 watts/pulse, for 1 microsecond pulse widths in some of the higher power diodes. The photoconductor needs to have a photoconductive decay time, τ, that is appreciably longer than the laser pulse width for maximum sensitivity. On the other hand , for applications requiring very short pulse widths, the time constant needs to be very small. In this latter case, the antenna efficiency may also be lower.

---

*Remembering that the initial conductivity cannot be too low.

3.10 BEAM STEERING CONCEPTS

Various concepts were investigated for beam steering control of diffraction grating antennas. Three of the concepts described in this section deal with the control of laser illumination on photoconductive gratings. Two other concepts are also briefly described which may be used to control beam steering with conductive and dielectric gratings.

3.10.1 Digital Control of Laser-Excited Gratings

In order to laser illuminate the grating target, three methods were investigated. These are the simultaneous, scanning, and parallel methods as illustrated in Figures 51, 52, and 53, respectively. In the simultaneous system, a laser beam is broken up by a grating, or some other beam splitter, and then directed onto the target. In the scanning system, a single laser beam is deflected and modulated on and off in such a way as to produce the desired pattern of lines on the target. In the parallel system, a large number of sources are directed onto the target and individual sources commanded to turn on or off in order to generate the desired pattern. A discussion of the relative merits of each system follows. For comparison between the different methods, one hundred lines were assumed with an energy to be delivered to the target of 2 μjoules per line.

3.10.1.1 Simultaneous System

The laser beam in the simultaneous system must illuminate all the lines on the target simultaneously. This produces the requirement that the power of the laser be at least equal to the sum of the individual line powers plus the loss present in the beam splitter. Assuming a beam splitter with a 50% efficiency, the power required in the main beam for various beam pulse lengths is:

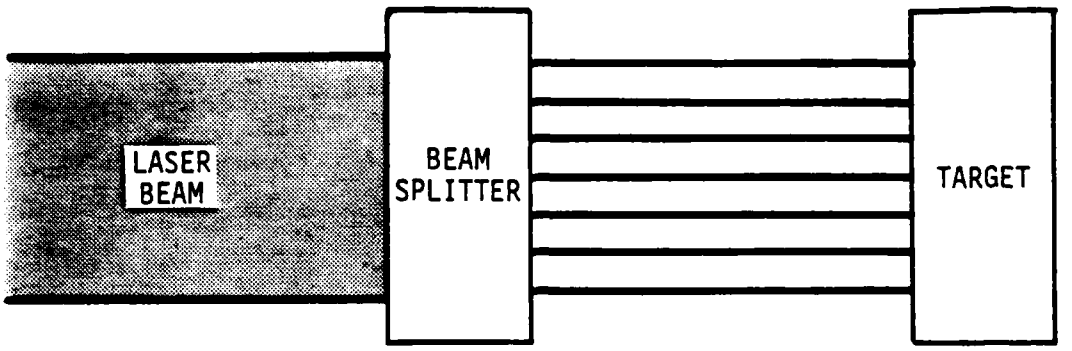

FIGURE 51. SIMULTANEOUS SYSTEM

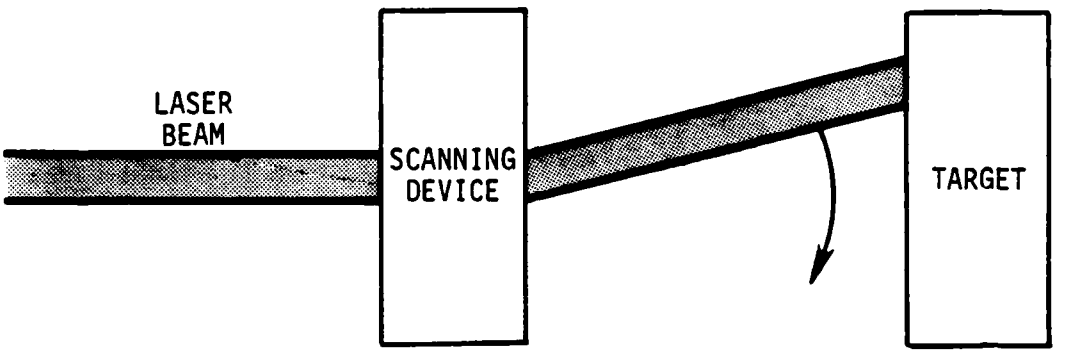

FIGURE 52. SCANNING SYSTEM

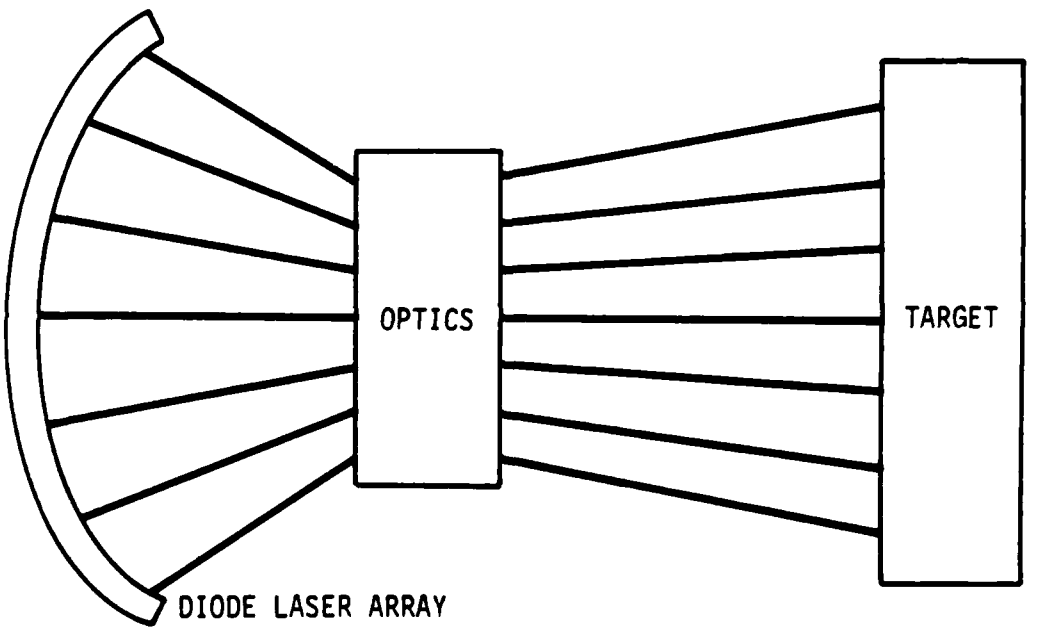

FIGURE 53. PARALLEL SYSTEM

Pulse Lengths (μsec)	Beam Power (watts)
1	400
10	40
100	4
1000	0.4

Some of the problems associated with the simultaneous system are creating a uniform enough grating for accurate placement of lines on the target and keeping the amplitude variation between lines at a minimum. Also the changing of patterns would be rather slow, possibly requiring a manual set up between each test.

3.10.1.2 Scanning System

The scanning system beam power requirements are a function of the time constant of the target. In order for the target to "see" all the lines simultaneously, the beam must scan all the lines in less than the time constant of the target. For this comparison, one-half the time constant of the target was used with a scanning system efficiency of 50%. For the various target time constants the associated laser power levels are:

Target Time Constant (μsec)	Beam Power (watts)
1	800
10	80
100	8
1000	0.8

Although the placement of the lines is much more accurate with this system as compared to the simultaneous system, and the changing of patterns would be much quicker, the regulation of line amplitude would be much harder due to inaccuracies generated in the scanning system.

3.10.1.3 Parallel System

The last system evaluated was the parallel system. In this system an array of focused laser diodes is aimed at the target and diodes are turned on or off in order to generate the desired pattern on the target. The power

required for each diode, as determined by the pulse width capability of the diode, is listed below:

Pulse Length (μsec)	Beam Power (watts)
10	200
100	20
1000	2

Many laser diodes are available in the 100 μsec, 200 watt range. Since the diodes may be pre-focused and controlled by a computer, a quick and easy method would exist to change the desired pattern at will without the disadvantages that exist in the other systems.

3.10.1.4 Preferred Concept

Because of its inherent advantages, the parallel laser diode system was chosen. A block diagram of the proposed system is shown in Figure 54. An HP9836 computer is used to set up the various patterns required on the target. These patterns are sent through a parallel interface (98622A) to a series of registers which hold the information until the command is received from the computer to fire the lasers. The firing trigger pulse is generated by a 10 μsec one shot to achieve uniformity in trigger specifications. The trigger pulses are transferred through opto-isolators to the laser diode drive circuitry which is shown in Figure 55. The opto-isolators are provided to protect the digital equipment from transients produced by the high voltage and current circuitry used to drive the laser diode. The output of the opto-isolator turns on transistor Q3 which acts as a current amplifier. Capacitor C2 then discharges through Q3 and thus fires the SCR (Q2). Q2, in turn provides a discharge path for capacitor C1 which holds the calibrated amount of stored energy for the laser diode. Transistor Q1 and its associated components are provided as a fast charging circuit for the energy storage capacitor C1. This should provide for a repetition rate of at least 1 kHz. The drive circuitry can be adjusted to vary the output power of the laser diode by varying the 0 to +350 V supply. The current through (and therefore, the power generated by) the laser diode can be monitored at a test point provided for this purpose as shown on the diagram. A slightly more complicated circuit is

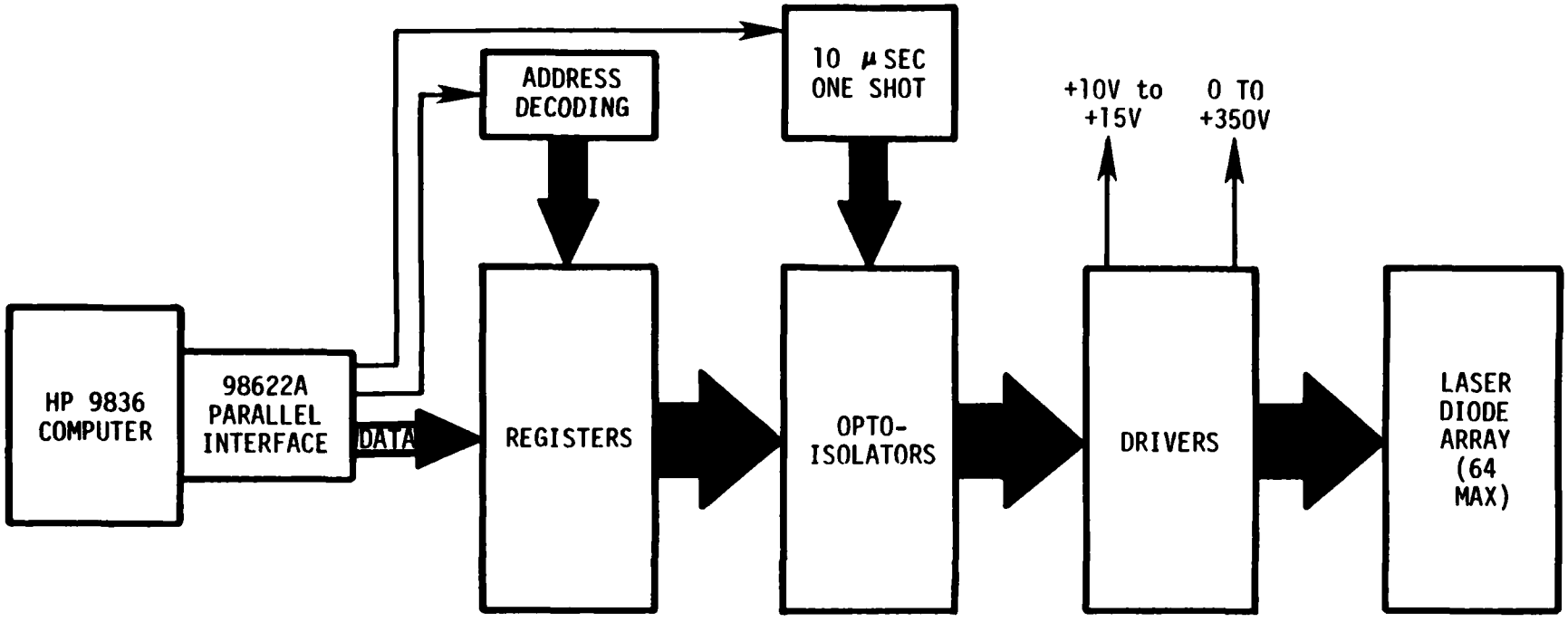

FIGURE 54. DRIVE SYSTEM BLOCK DIAGRAM

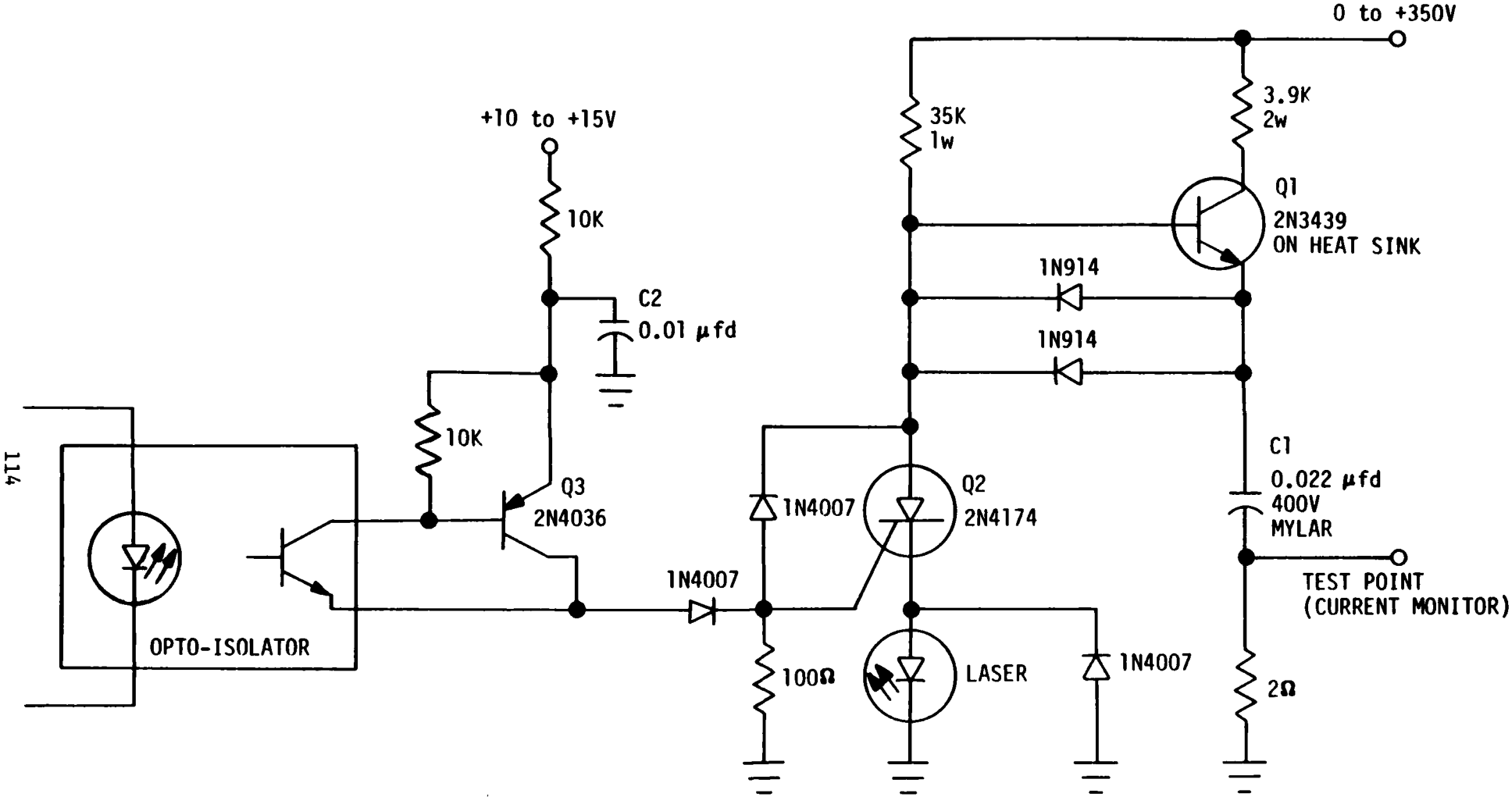

FIGURE 55. SINGLE LASER DRIVE CIRCUIT

available which would allow for the individual adjustment of each laser diode's output power. It was felt, however, that the added complexity was not called for at this time. If during the course of the experiment it is demonstrated that this circuit is necessary, then it could easily be added at that time.

It should be noted that the HP9836 computer cannot only generate the patterns desired but can also be made to collect the data generated, thus automating the entire procedure.

The above design was not tested during the current program. The design is presented instead to suggest future systems design using photoconductive gratings.

3.10.2 Control of Conductive and Dielectric Gratings

This concept is based on the use of conductive ink printed on tape or the use of perforated tape to accomplish beam steering as shown in Figure 56. In the case of the printed ink, the ink is applied to a moving tape in the form of periodic lines to form an alternating high and low conductivity grating. These lines, controlled by a computer, are written at the spacing ℓ. The beam radiation angle θ, will vary with ℓ as

$$\text{Cos } \theta = \frac{c}{V_g} - \frac{\lambda}{\ell} \quad ,$$

an equation previously explained in this report. The tape is traveling at high speed so that the beam may be rapidly steered as the spacing ℓ is changed. High speed jet printers can write approximately 10,000 lines/sec, so if 50 lines are used to set the beam angle, roughly 10,000/50 = 200 changes in the beam angle could be accomplished per second. The tape speed would need to be on the order of 20 meters/sec if the line spacing were 2 mm.

An alternative method is to form an alternating high and low dielectric constant by using perforated tape, as shown in Figure 56.

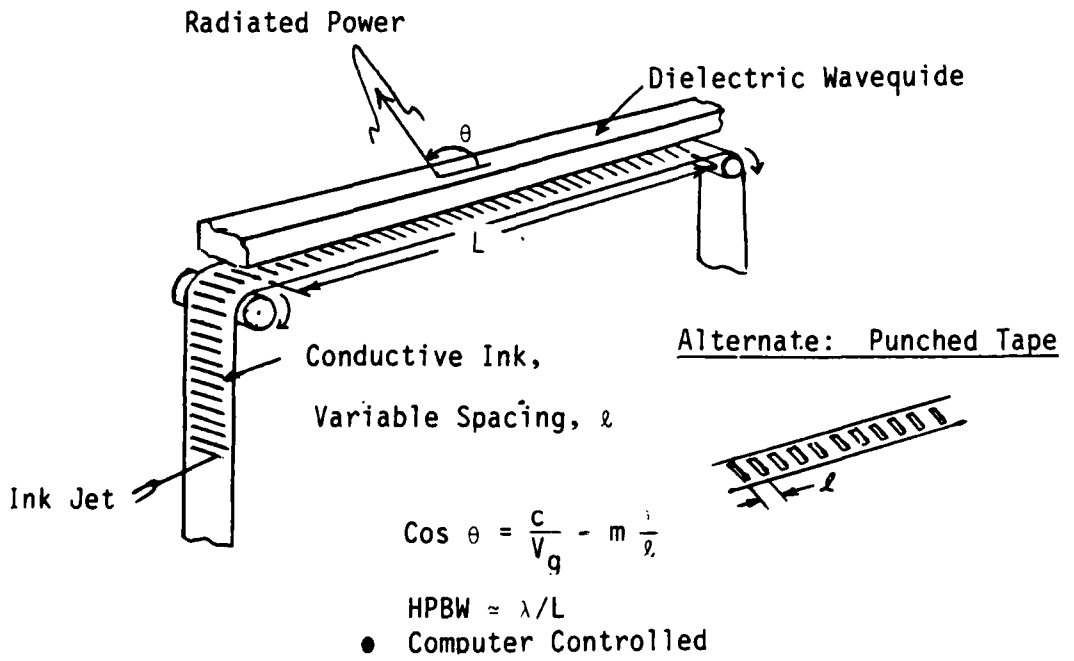

FIGURE 56. BEAM STEERING BY PRINTED/PUNCHED TAPE

3.11 SIGNAL PROCESSING CONCEPTS

3.11.1 Microwave Grating Logic

Soviet authors have suggested that the diffraction electronics antenna may have computer applications (Reference 15). Figures 57 and 58 show the logic diagrams associated with the Soviet paper.

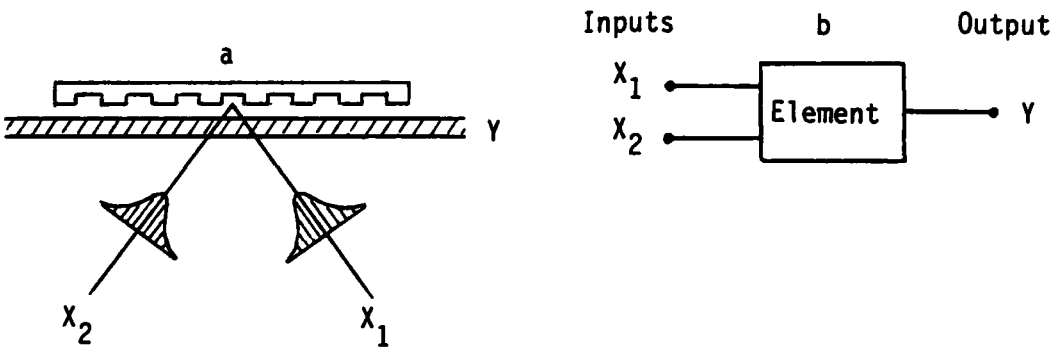

FIGURE 57. BASIC COMPUTER APPLICATION

OPERATION	OUTPUT-SIGNAL LEVEL					SYSTEM PARAMETERS
	X_1	0	1	0	1	
	X_2	0	0	1	1	
Constant (zero)		0	0	0	0	$\alpha^{(1)}$, $\alpha^{(2)}$ - not resonant
Exclusive or (inequality)		0	1	1	0	$\alpha^{(1)}$, $\alpha^{(2)}$ - resonant $\psi_2 - \psi_1 = \pi$
Repeat		0	1	0	1	$\alpha^{(1)}$ - resonant $\alpha^{(2)}$ - not resonant
Repeat		0	0	1	1	$\alpha^{(1)}$ - not resonant $\alpha^{(2)}$ - resonant
Disjunction or logical addition (or)		0	1	1	1	$\alpha^{(1)}$, $\alpha^{(2)}$ - resonant $\psi_1 - \psi_2 = 0$

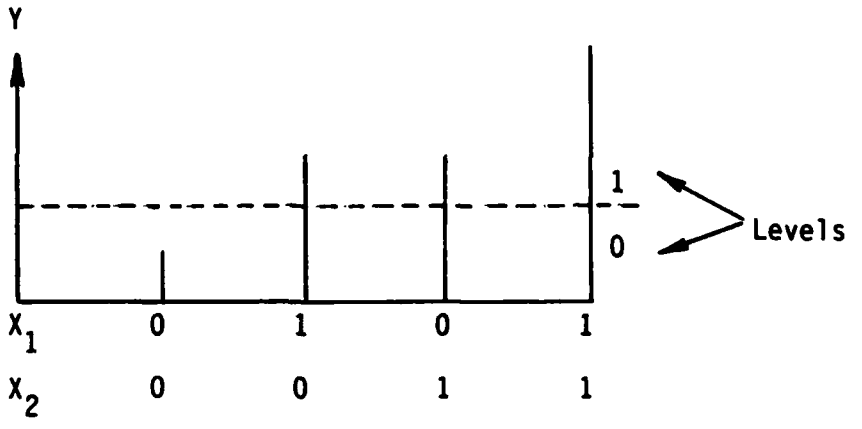

FIGURE 58. COMPUTER FUNCTIONS

Although this method does appear to have some advantages for signal pre-processing, there are, however, some severe limitations to this concept when viewed as an alternative to the use of hardware logic and general purpose computers. This technology appears, on the surface, to be able to do general logical operations. However, on closer examination it will be shown that it fails. A simple example should prove this. Let the first signal, with its respective phase angles, be given by:

Signal	———	0	1	0	1
Phase	———		0		0

Let the second signal be given by:

Signal	———	0	0	1	1
Phase	———			π	π

Now let us take the EXCLUSIVE OR of the two signals. This can be shown to be:

Signal-1	0	1	0	1
Phase		0		0
+				
Signal-2	0	0	1	1
Phase			π	π

Combined Signal Phase ——— 0 1 1 0

0 π

The output signal appears to be what we want. However, the phase of the different parts (i.e., the ones) of the output signal are not the same. Since phase is critical to this type of processing this output will not combine in following stages as one would at first expect. As the length of the "words" gets longer and the number of stages increases the problem will become more and more complicated.

Another problem with this kind of technology is the necessity of assuring that all input signals have precisely the same power levels in order for the different functions to perform as desired. In the uncontrolled environment of a RADAR receiver this would be near impossible.

To sum up; this kind of technology would probably best be suited in controlled situations where the power levels and phase of the signals could be rigidly controlled and where only very simple logical operations are involved.

4.0 CONCLUSIONS

This two-year study has sorted through a number of potential phenomena that could be used for diffraction antennas. Many of the methods that were explored led to poor antenna efficiency, difficulties in obtaining uniform periodicity in the grating, or other interactions that were undesirable. There were two techniques that arose, however, which show definite promise. These are: (1) the coil-spring grating and (2) the laser-excited photoconductive grating. Their characteristics are distinctly different from one another, although they both use the same diffraction-electronics concept.

The coiled spring diffraction antenna offers a very low-cost beam-steerable method for millimeter waves. The scanning rates will generally be low--perhaps a few radians per second. The uses for such a device lie in low-cost millimeter-wave communications antennas and in relatively low scan-rate seekers. The results of the current program are nearly optimum, although some improvement in antenna efficiency could be obtained if coils were used that presented a straight edge adjacent to the dielectric waveguide.

The laser-excited antenna is the one method studied during the program that offers potentially rapid beam steering. It also has the unique feature that the antenna is created only at the instant of radiation or reception. Nothing about the antenna was optimized during the program. The items remaining to be optimized include (1) the choice of semiconductor along with its initial dark conductivity and thickness, and (2) the excitation wavelength for the laser. Currently a silicon film about 1 to 2 microns thick with dark resistivity near 100 ohm-cm appears near optimum. GaAs laser diodes also appear as appropriate illuminators.

It is concluded that a third concept is suited for further development. This is the conductive ink-jet printer or perforated tape device. Although not tested in a prototype configuration, the concept is based upon experimental results with printed conductive strips on circuit board and on results with periodic dielectric constant variation. These approaches, though the use of high-speed printers and tape devices,

should offer computer-compatible devices with scanning rates of several hundred radians/second.

5.0 PUBLICATIONS/REPORTS OF INVENTION

The following Reports of Invention (ROI) have been filed at Battelle:

Date	Title	Inventors
16 July 1981	Electronically Steered Millimeter-Wave Antenna	M. R. Seiler
2 March 1983	Beam Steerable Antenna	M. R. Seiler Lt. Col. H. Winson
9 March 1983	Beam Steerable Antenna	M. R. Seiler B. M. Mathena C. E. Wickersham T. M. Miller
28 March 1983	Ferrofluidic Millimeter-Wave Beam Steering Antenna	M. R. Seiler T. M. Miller Lt. Col. H. Winsor
30 March 1983	Photoconductive *Antenna Modulator*	M. R. Seiler
3 May 1983	Addendum to ROI of 2 March 1983	
21 August 1984	Millimeter-Wave Beam Steering Antenna (Using Conductive Ink Tape or Perforated Tape)	M. R. Seiler
21 December 1984	Millimeter-Wave Beam Steering by Laser Excited Photoconductive Gratings	M. R. Seiler

A paper entitled "Millimeter-Wave Beam Steering Using Diffraction Electronics", by Milton R. Seiler and Bill M. Mathena was published in IEEE Transactions on Antennas and Propagation, Vol AP-32, No. 9, September 1984.

Plans have been made to submit a paper in 1985 on laser-excited photoconductive antenna techniques to IEEE Transactions on Antennas and Propagation.

6.0 PERSONNEL

The following personnel participated in the activities of this research:

Milton R. Seiler	Principal Investigator.
Bill M. Mathena	Principal Research Scientist. Experimental set-up and measurements on all types of gratings, and analysis of Marcatili's equations. (Presently employed by Rockwell International, Inc.)
Richard Ridgway	Research Scientist. Bulk acoustic wave studies.
Charles Wickersham	Principal Research Scientist, ZnO study.
Kenneth Walcott	Researcher. Photoconductive studies.
George Falkenbach	Researcher. Ferrofluid studies.
Timothy Miller	Technician. Various experimental measurements
Everett Clutter	Technician. Fabricated and assembled test set-up.
Brad Chapman	Technician. Laser experimental measurements.
James Robbins	Researcher. Signal processing.
Robert Strohl	Researcher. System applications.

Data pertaining to the work described herein is documented in Laboratory Record Books No. 38337, 38567, and 42005.

7.0 REFERENCES

1. Andrenko, S. d., Devyatkov, Acad. N. D., and Shestopalov, V. P., "Millimeter Field Band Antenna Arrays", Dokl. Akad. Nauk SSSR, Vol 240, pp 1340-1343 (June 1978).

2. Andrenko, S. D., Belyaev, V. G., Devyatkov, Acad. N. E., and Shestopalov, V. P., "Diffraction Input of Energy to a Dielectric Waveguide", Dokl. Akad. Nauk SSSR, Vol 247, pp 73-76 (July 1979).

3. Andrenko, S. D., Usikov, A. Ya., and Shestopalov, V. P., "A New Method for Wavefront Reconstruction", Dokl. Akad. Nauk SSSR, Vol 244, pp 83-85 (January 1979).

4. Shestopalov, V. P., "Problems of Diffraction Electronics", Visnyk Akademiyi Nauk Ukrayins'koyi RSR, No. 10, pp 28-40 (1975).

5. Slater, J. C., "MICROWAVE ELECTRONICS", D. Van Nostrand Co., p 1970 (1950).

6. Zucker, F. J., "Surface-and Leaky-Wave Antennas", Chap 16 in ANTENNA ENGINEERING HANDBOOK, Jasik, H., editor, First edition, McGraw-Hill Book Co., pp 16-1 thru 16-57, (1969). In particular, see pp 16-34 for discussion of a "stretch" array investigated by Sletten, C. J. and Holt, F. S. in 1958.

7. Harrington, R., TIME HARMONIC ELECTROMAGNETIC FIELDS, McGraw-Hill Book Co., p 188 (1961).

8. op. cit., Figure 4-22, p 183.

9. Marcatili, E. A. J., Bell System Technology Journel, Vol 48, No. 7, pp 2071-2102, (September 1969).

10. Ramo, Simon and Whinnery, John R., Fields and Waves in Modern Radio, Second Edition, John Wiley and Sons, Inc., New York, pp 388-390 (1953).

11. Handbook of Chemistry, 7th Edition, Handbook Publishers, Sandusky, Ohio, p 121 (1949).

12. Klohn, K. L., Horn, R. E. and Jacobs, H., "Silicon Waveguide Frequency Scanning Linear Array Antenna", IEEE Trans., Vol MTT-26, No. 10, p 764 (October 1978).

13. Gulyaev, Yu. V., Kotelyanskii, I. M., Krikunov, A. I., Medved, A. V. and Mishkinis, R. A., "Integrated Acoustoelectric SAW Source" Pis'ma zh. Tekh. Fiz. Vol 6, pp 49-52 (January 1980).

14. Coldren, L. A. and Kino, G. S., "The InSb on a Piezoelectric Rayleigh Wave Amplifier", IEEE Trans. ED, Vol ED-21, No. 7, p 421 (July 1974).

15. Andrenko, S. D., and Shestopalov, V. P., Dokl. Akad. Nauk SSSR, Vol 248, pp 1070-1073 (October 1979).

APPENDIX A

EXPLANATION OF EFFECTS OF LONGITUDINAL GRATING MOTION

APPENDIX A

EXPLANATION OF EFFECTS OF LONGITUDINAL GRATING MOTION

As previously discussed in Section VI and shown on Figures 23 and 25, there is an effect created by the longitudinal motion of the grating. This has occurred predominantly with gratings that are relatively poor in radiation efficiency. For example, the effect is essentially undetectable with an efficient metallic block grating. It is also noted that the period of the cyclic behavior is that of the grating--within experimental error.

If we consider that standing wave pattern is created in the waveguide by the incident wave in the + x direction and the reflected wave in the - x direction (as shown in Figure 8 of Section V), then we have a standing-wave envelope in the waveguide of period $\lambda g/2$. The amplitude of the standing-wave, $V_{max}-V_{min}$, is dependent upon the relative magnitude of the wave reflected from the dielectric--metal waveguide junction. This reflected wave in turn is strongest for structures that are poor radiators (a perfect radiator would have no reflected wave--all of the incident wave would be radiated).

When this standing-wave is in close proximity with a grating structure, the coupling between the standing-wave and the grating is strongest at the maxima of the standing-wave. Hence the instantaneous radiated power from the grating--waveguide structure may be represented qualitatively by a convolution of the following form:

P_r = Relative power radiated

$$= \int_0^L r' \underbrace{\cos\left(\frac{4\pi x}{\lambda g}\right)}_{\text{standing wave}} \underbrace{\cos\left[\frac{4\pi x}{\lambda g} - \frac{2\pi x^1}{\ell}\right]}_{\text{relative coupling}} dx$$

where L = total length of grating $>> \ell$

ℓ = grating period

x^1 = longitudinal displacement of grating

r' = relative amplitude of reflected wave.

The above integral reduces to

$$P_r = \text{constant} \cdot \cos \frac{2\pi x^1}{\ell}$$

which is periodic in displacement with period ℓ. It follows that no longitudinal effects will occur if $r' = o$, which is the case when all of the waveguide power is radiated.

APPENDIX B

CRYSTAL DETECTOR CALIBRATION

APPENDIX B

CRYSTAL DETECTOR CALIBRATION

Figure B-1 gives the crystal detector calibration, dB versus actual cw power. The value in DB denotes crystal detector output after amplification by the SWR meter.

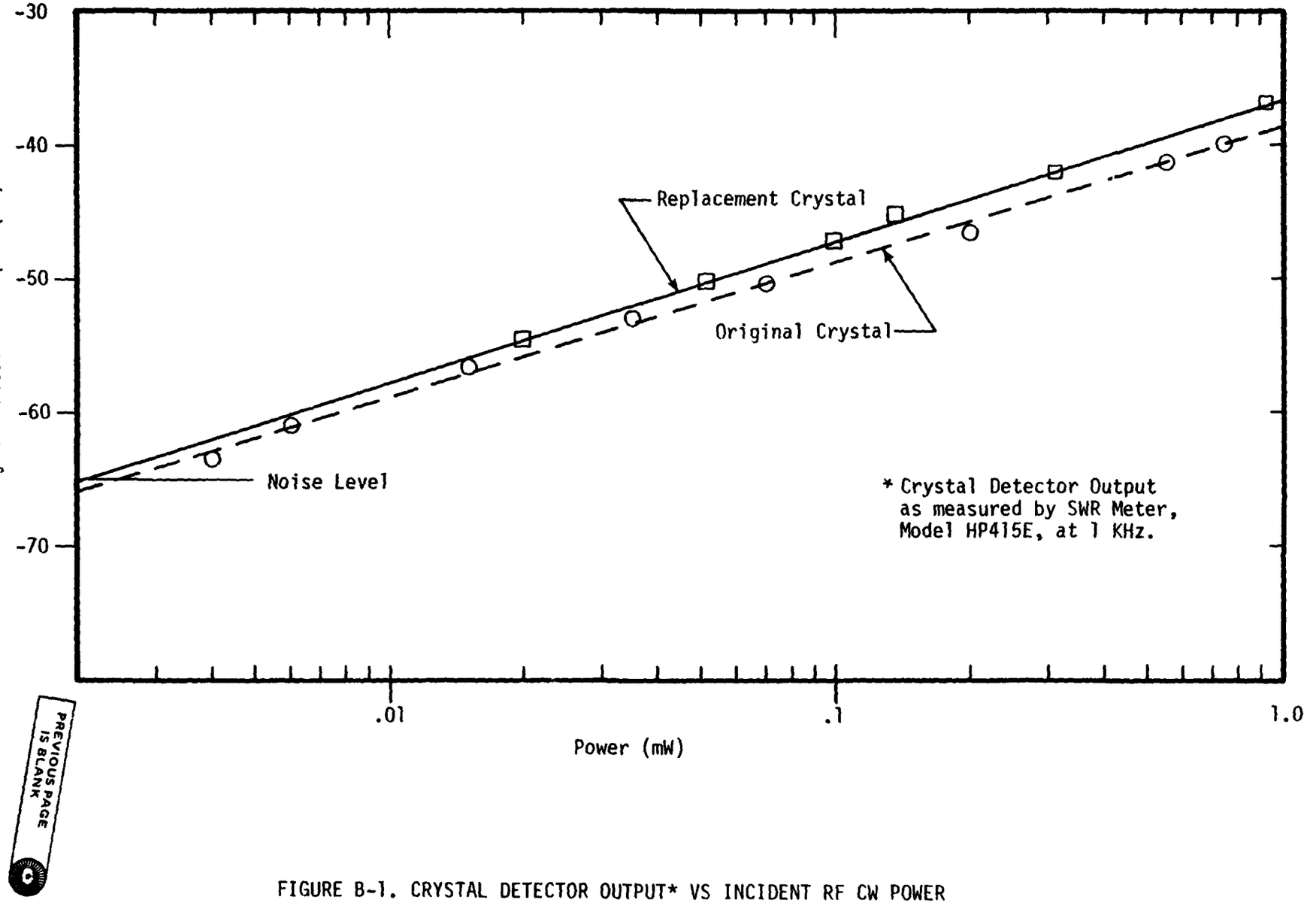

FIGURE B-1. CRYSTAL DETECTOR OUTPUT* VS INCIDENT RF CW POWER

END

FILMED

3-85

DTIC